

**ISTANBUL TECHNICAL UNIVERSITY ★ ENERGY INSTITUTE**

**ENERGY AND EXERGY-BASED THERMODYNAMIC ANALYSIS OF  
THE SCIMITAR ENGINE AT MACH 5.0**



**M.Sc. THESIS**

**Muhammed Bişar UCA**

**Energy Science and Technology Division**

**Energy Science and Technology Programme**

**JUNE 2017**



**ISTANBUL TECHNICAL UNIVERSITY ★ ENERGY INSTITUTE**

**ENERGY AND EXERGY-BASED THERMODYNAMIC ANALYSIS OF  
THE SCIMITAR ENGINE AT MACH 5.0**



**M.Sc. THESIS**

**Muhammed Bişar UCA  
(301141019)**

**Energy Science and Technology Division**

**Energy Science and Technology Programme**

**Thesis Advisor: Prof. Dr. Ahmet DURMAYAZ**

**JUNE 2017**



**İSTANBUL TEKNİK ÜNİVERSİTESİ ★ ENERJİ ENSTİTÜSÜ**

**SCIMITAR MOTORUNUN 5.0 MACH HIZDA ENERJİ VE EKSERJİ ESASLI  
TERMODİNAMİK ANALİZİ**

**YÜKSEK LİSANS TEZİ**

**Muhammed Bişar UCA  
(301141019)**

**Enerji Bilim ve Teknoloji Anabilim Dalı**

**Enerji Bilim ve Teknoloji Programı**

**Tez Danışmanı: Prof. Dr. Ahmet DURMAYAZ**

**HAZİRAN 2017**



Muhammed Bişar UCA, an M.Sc. student of ITU Energy Institute student ID 301141019 successfully defended the thesis entitled “ENERGY AND EXERGY-BASED THERMODYNAMIC ANALYSIS OF THE SCIMITAR ENGINE AT MACH 5.0”, which he prepared after fulfilling the requirements specified in the associated legislations, in the presence of the jury whose signatures are below.

**Thesis Advisor :**    **Prof. Dr. Ahmet DURMAYAZ**    .....

İstanbul Technical University

**Jury Members :**    **Prof. Dr. Mustafa ÖZDEMİR**    .....

İstanbul Technical University

**Prof. Dr. Z. Düriye BİLGE**    .....

Yıldız Technical University

**Date of Submission : 5 May 2017**

**Date of Defense : 6 June 2017**







*To my mother, father and brother,*



## **FOREWORD**

This thesis concentrates on the thermodynamic analysis of the Scimitar Engine at Mach 5.0 cruise conditions. A thermodynamic model for the engine is constructed, thermodynamic properties at various positions and some important performance parameters of the Scimitar Engine at Mach 5.0 are calculated.

Firstly, I would like to express my deepest appreciation to Prof. Dr. Ahmet DURMAYAZ for his invaluable contributions, support and advices during my M.Sc. study. His expertise, understanding, generous guidance and patience for me made this work possible.

I am indebted to Dr. Tayfun TANBAY who contributed with his knowledge and supported me during the challenging stages of my thesis.

I am also thankful to M.Sc. Mert ÇOLAKOĞLU who shared his knowledge with me during the initial phases of the thesis.

Finally, I would like to thank my parents and brother who invaluable supported me. Their support made this study meaningful.

June 2017

Muhammed Bişar UCA  
(Mechanical Engineer)



## TABLE OF CONTENTS

	<u>Page</u>
<b>FOREWORD</b> .....	<b>ix</b>
<b>TABLE OF CONTENTS</b> .....	<b>xi</b>
<b>ABBREVIATIONS</b> .....	<b>xiii</b>
<b>LIST OF SYMBOLS</b> .....	<b>xv</b>
<b>LIST OF TABLES</b> .....	<b>xix</b>
<b>LIST OF FIGURES</b> .....	<b>xxi</b>
<b>SUMMARY</b> .....	<b>xxiii</b>
<b>ÖZET</b> .....	<b>xxvii</b>
<b>1. INTRODUCTION</b> .....	<b>1</b>
1.1 Purpose of Thesis .....	1
1.2 Literature Review .....	1
<b>2. THERMODYNAMICS BACKGROUND</b> .....	<b>9</b>
2.1 Purpose .....	9
2.2 Stagnation Properties.....	9
2.3 Speed of Sound and Mach Number.....	11
2.4 Convergent-Divergent Nozzle.....	12
2.5 Entropy .....	13
2.6 Exergy .....	14
2.7 Gas Mixtures .....	15
2.8 Brayton, Gas Turbine Engine and Jet Engine Cycles .....	18
<b>3. TURBOFAN, RAMJET, TURBOROCKET AND SCIMITAR ENGINES</b> ...	<b>21</b>
3.1 Purpose .....	21
3.2 Turbofans .....	21
3.3 Ramjets.....	23
3.4 Turbo-rockets.....	25
3.5 Scimitar Engine; Design Features and Operating Principles .....	26
3.5.1 Precooler of the scimitar engine.....	28
3.5.2 Operating principles of the scimitar engine .....	29
3.5.3 Scimitar engine in atr mode at mach 5.0 .....	32
3.5.4 $T$ - $s$ diagram and processes in atr mode of the propellant fluid of the scimitar engine at mach 5.0.....	34
3.5.5 Helium cycle of the scimitar engine .....	35
<b>4. THEORETICAL MODEL OF THE SCIMITAR ENGINE</b> .....	<b>39</b>
4.1 Assumptions for the Scimitar Engine Model .....	39
4.2 Thermodynamic Relations Derived for the Scimitar Engine Subcomponents. 40	
4.2.1 Intake.....	40
4.2.2 Air compressor .....	48
4.2.3 Precooler .....	50
4.2.4 Hydrogen line.....	52
4.2.5 Preburner .....	55

4.2.6 Heat exchanger 3 .....	58
4.2.7 Combustion chamber .....	59
4.2.8 Convergent-divergent nozzle .....	61
4.2.9 Helium turbine.....	65
4.2.10 Low-temperature regenerator .....	67
4.2.11 High-temperature regenerator .....	70
4.3 Global Rate of Energy Balance for the Scimitar engine at Mach 5.0 .....	73
4.4 Global Rate of Exergy Balance for the Scimitar Engine at Mach 5.0.....	79
4.5 Performance Parameters .....	85
4.5.1 Uninstalled thrust ( $F_u$ ) .....	85
4.5.2 Thrust specific fuel consumption ( $TSFC$ ).....	86
4.5.3 Specific thrust ( $F_s$ ).....	87
4.5.4 Propulsive power.....	87
4.5.5 Net production of propellant kinetic power and the kinetic power loss....	87
4.5.6 Propulsive efficiency ( $\eta_p$ ) .....	88
4.5.7 Thermal efficiency ( $\eta_{th}$ ).....	89
4.5.8 Overall efficiency ( $\eta_o$ ) .....	90
4.5.9 Coefficient of ecological performance ( $CEP$ ).....	90
4.5.10 Exergetic sustainability index ( $\Theta_{exs}$ ).....	90
4.5.11 Exergy destruction factor ( $f_{exd}$ ) .....	91
4.5.12 Exergy efficiency ( $\eta_{ex}$ ).....	91
<b>5. RESULTS AND DISCUSSIONS .....</b>	<b>93</b>
5.1 Data Obtained from Literature for the Thesis .....	93
5.2 Results of the Thesis.....	94
5.3 Discussions .....	95
<b>6. CONCLUSIONS AND RECOMMENDATIONS .....</b>	<b>105</b>
6.1 Conclusions of this Study .....	105
6.2 Recommendations for future Studies .....	106
<b>REFERENCES .....</b>	<b>107</b>
<b>CURRICULUM VITAE .....</b>	<b>111</b>

## ABBREVIATIONS

<b>afr</b>	: air-to-fuel mass flow rate ratio
<b>BB</b>	: Bypass burner
<b>BN</b>	: Bypass nozzle
<b>C</b>	: Compressor
<b>CC</b>	: Combustion chamber
<b>C-D</b>	: Convergent-divergent nozzle
<b>CEP</b>	: Coefficient of ecological performance
<b>CFD</b>	: Computational Fluid Dynamics
<b>CN</b>	: Core nozzle
<b>CPR</b>	: Compressor pressure ratio
<b>CPs</b>	: Combustion products
<b>ESA</b>	: European Space Agency
<b>F</b>	: Fan
<b>FHV</b>	: Fuel heating value
<b>H<sub>2</sub></b>	: Hydrogen
<b>H<sub>2</sub>O</b>	: Water vapor in combustion products
<b>HT</b>	: Hub turbine
<b>HPC</b>	: High-pressure compressor
<b>HPT</b>	: High-pressure turbine
<b>HTR</b>	: High-temperature helium regenerator
<b>HX</b>	: Heat exchanger
<b>HX1</b>	: Heat exchanger 1
<b>HX2</b>	: Heat exchanger 2
<b>HX3</b>	: Heat exchanger 3
<b>HX4H</b>	: High-temperature heat exchanger 4
<b>HX4L</b>	: Low-temperature heat exchanger 4
<b>HX5</b>	: Heat exchanger 5
<b>I</b>	: Intake
<b>kg</b>	: Kilogram
<b>kJ</b>	: Kilojoule
<b>kN</b>	: Kilonewton
<b>kPa</b>	: Kilopascal
<b>kW</b>	: Kilowatt
<b>LACE</b>	: Liquid Air Cycle Engine
<b>LAPCAT</b>	: Long Term Advanced Propulsion Concepts And Technologies
<b>LHV</b>	: Lower heating value
<b>LTR</b>	: Low-temperature helium regenerator
<b>LPC</b>	: Low-pressure compressor
<b>LPT</b>	: Low-pressure turbine
<b>MJ</b>	: Megajoule
<b>MW</b>	: Megawatt
<b>N</b>	: Nozzle

**$N_2$**  : Nitrogen  
 **$O_2$**  : Oxygen  
**PB** : Preburner  
**PR** : Pressure ratio  
**SABRE** : Synergetic Air Breathing Rocket Engine  
**T1** : Turbine 1  
**TCPR** : Total pressure ratio  
***TSFC*** : Thrust specific fuel consumption





## LIST OF SYMBOLS

$A$	: Area ( $\text{m}^2$ )
$c$	: Specific heat ( $\text{kJ kg}^{-1} \text{K}^{-1}$ ); Speed of sound
$C$	: Compressor
$CEP$	: Coefficient of ecological performance for propulsion engines
$d$	: Differential
$e$	: Differential-pressure-change-based correction factor
$f$	: Air-to-fuel mass flow rate ratio; Factor
$F$	: Thrust (kN)
$FHV$	: Fuel heating value ( $\text{kJ kmol}^{-1}$ ), ( $\text{kJ kg}^{-1}$ )
$g$	: Gravitational acceleration ( $\text{m s}^{-2}$ )
$h$	: Specific enthalpy ( $\text{kJ kg}^{-1}$ )
$\bar{h}$	: Specific enthalpy ( $\text{kJ kmol}^{-1}$ )
$H$	: Enthalpy (kJ)
$H_2$	: Hydrogen
$H_2O$	: Water vapor in combustion products
$H'$	: Specific enthalpy with respect to reference conditions (kJ/kg)
$k$	: Specific heat ratio; kinetic
$m$	: mass (kg)
$\dot{m}$	: Mass flow rate ( $\text{kg s}^{-1}$ )
$mf$	: Mass fraction
$M$	: Mach number
$N$	: Nozzle; Mole number
$N_2$	: Nitrogen
$\dot{n}$	: Molal flow rate ( $\text{kmol s}^{-1}$ )
$O_2$	: Oxygen
$P$	: Pressure (kPa)
$Q$	: Heat (kJ)
$\dot{Q}$	: Heat transfer rate (kW)
$r$	: Pressure ratio
$R$	: Ideal gas constant ( $\text{kJ kg}^{-1} \text{K}^{-1}$ )
$\bar{R}$	: Universal gas constant ( $\text{kJ kmol}^{-1} \text{K}^{-1}$ )
$s$	: Specific entropy ( $\text{kJ kg}^{-1} \text{K}^{-1}$ )
$\bar{s}$	: Specific entropy ( $\text{kJ kmol}^{-1} \text{K}^{-1}$ )
$S$	: Entropy ( $\text{kJ K}^{-1}$ )
$\dot{S}$	: Entropy generation ( $\text{kW K}^{-1}$ )
$t$	: Time (s)
$T$	: Temperature (K)
$u$	: Specific internal energy ( $\text{kJ kg}^{-1}$ )
$U$	: Internal energy (kJ)
$v$	: Velocity ( $\text{m s}^{-1}$ )
$V$	: Volume ( $\text{m}^3$ )

$\dot{W}$	: Power (kW)
$y$	: Mole fraction
$X$	: Specific exergy (kJ kg <sup>-1</sup> )
$\dot{X}$	: Total exergy flow rate of a stream (kW)
$z$	: Elevation (m)

### Greek Letters

$\phi$	: Nonflow exergy (kJ kg <sup>-1</sup> )
$\delta$	: Differential
$\Delta$	: Difference
$\eta$	: Efficiency
$\pi$	: Total pressure ratio at the intake
$\rho$	: Density (kg m <sup>-3</sup> )
$\tau$	: Static temperature ratio
$\theta$	: Index
$\psi$	: Stream exergy (kJ kg <sup>-1</sup> )

### Subscripts

$0$	: Stagnation condition; Reference conditions
$a$	: Fictional expansion point at intake
$aux$	: Auxiliary
$ave$	: Average
$b$	: Boundary
$BN$	: Bypass nozzle
$C$	: Compressor; Compression
$chem$	: Chemical
$cool$	: Cooling
$cr$	: Critical
$CV$	: Control volume
$dest$	: Destruction
$e$	: Exit
$exs$	: Exergetic sustainability
$ex$	: Exergy; Exergetic
$exd$	: Exergy destruction
$f$	: Fuel
$gen$	: Generation
$H_2$	: Hydrogen
$H_2O$	: Water vapor in combustion products
$He$	: Helium
$HX$	: Heat exchanger
$in$	: Incoming or entering
$int rev$	: Internally reversible
$KE$	: Kinetic efficiency
$max$	: Maximum
$N$	: Nozzle
$N_2$	: Nitrogen
$o$	: Overall
$out$	: Outgoing

<b><i>O</i><sub>2</sub></b>	: Oxygen
<b><i>p</i></b>	: Pressure; Product
<b><i>P</i></b>	: Propulsive
<b><i>r</i></b>	: Reactant
<b><i>s</i></b>	: Specific; Isentropic; Shock waves
<b><i>surr</i></b>	: Surroundings
<b><i>th</i></b>	: Thermal
<b><i>T</i></b>	: Turbine
<b><i>v</i></b>	: Volume

### **Superscripts**

<b><i>0</i></b>	: Reference conditions
<b><i>Chem</i></b>	: Chemical
<b><i>Kin</i></b>	: Kinetic
<b><i>Ph</i></b>	: Physical
<b><i>Ph,s</i></b>	: Static physical
<b>*</b>	: Throat in convergent-divergent nozzle



## LIST OF TABLES

	<u>Page</u>
<b>Table 3.1</b> : Mach range, installed specific impulse and installed thrust to weight ratio values for different liquid hydrogen/liquid oxygen and precooled engines (Webber et. al, 2007).....	27
<b>Table 3.2</b> : Various operating modes of the Scimitar engine (Fernandez-Villace and Paniagua, 2013a) .....	29
<b>Table 5.1</b> : Information gathered from open literature.....	96
<b>Table 5.2</b> : Properties of the air side .....	97
<b>Table 5.3</b> : Properties of hydrogen and helium .....	97
<b>Table 5.4</b> : Performance parameters.....	99



## LIST OF FIGURES

	<u>Page</u>
<b>Figure 2.1</b> : A convergent-divergent nozzle (C-D N) (Çengel and Boles, 2005). ...	12
<b>Figure 2.2</b> : An open-cycle gas turbine engine (Çengel and Boles, 2005).....	19
<b>Figure 3.1</b> : Mach number versus engine propulsive efficiency characteristics (Hünecke, 2003). .....	22
<b>Figure 3.2</b> : A two-spool turbofan engine (Cumptsy, 2009).....	22
<b>Figure 3.3</b> : <i>T-s</i> diagram of a two-spool turbofan engine (El-Sayed, 2008). .....	23
<b>Figure 3.4</b> : Schematic diagram of a ramjet engine (Hill and Peterson, 1992). .....	24
<b>Figure 3.5</b> : Supersonic diffuser (Çengel and Boles, 2005). .....	24
<b>Figure 3.6</b> : Subsonic diffuser (Çengel and Boles, 2005). .....	24
<b>Figure 3.7</b> : Real cycle of a ramjet (El-Sayed, 2008).....	25
<b>Figure 3.8</b> : Turborocket engine (El-Sayed, 2008). .....	25
<b>Figure 3.9</b> : Prototype of the precooler (Webber et. al, 2007). .....	28
<b>Figure 3.10</b> : Flow directions in precooler (Webber et. al, 2007).....	28
<b>Figure 3.11</b> : LAPCAT A2 (Marini et. al, 2013). .....	30
<b>Figure 3.12</b> : A 3D view of Scimitar engine (Fernandez-Villace and Paniagua, 2013a).....	30
<b>Figure 3.13</b> : Mach 0.9 and Mach 5.0 cruise modes of Scimitar engine (Fernandez-Villace and Paniagua, 2011). .....	31
<b>Figure 3.14</b> : Schematic diagram of the Scimitar engine at Mach 5.0 (Modified from Figure 4 in Jivraj et al. (2007) by (Uca et al, 2016)).....	33
<b>Figure 3.15</b> : <i>T-s</i> diagram of the Scimitar engine at Mach 5.0 (Uca et al, 2016).....	34
<b>Figure 3.16</b> : Thermal capacity ratios of fluids relative to hydrogen entering the cycle (Jivraj et al, 2007). .....	36
<b>Figure 3.17</b> : Helium heat exchanging process with matched thermal capacity.....	38
<b>Figure 4.1</b> : Enthalpy-entropy diagram of a compression process (Çengel and Boles, 2005). .....	40
<b>Figure 4.2</b> : <i>T-s</i> diagram of the process in the intake (Heiser et. al, 1994). .....	42
<b>Figure 4.3</b> : Compression process by small angles (Dixon, 2005). .....	48
<b>Figure 4.4</b> : Hydrogen <i>h-T</i> data at 18 bar (Url-1). .....	53
<b>Figure 4.5</b> : Critical point phase behavior of pure substances (Çengel and Boles, 2005). .....	54
<b>Figure 4.6</b> : A convergent-divergent nozzle (C-D N) (Çengel and Boles, 2005). ....	61
<b>Figure 4.7</b> : Expansion process by small pressure expansion steps (Dixon, 2005). .	66
<b>Figure 4.8</b> : Stream tube model for the global rate of energy balance of the Scimitar engine (Modified from Fernandez-Villace and Paniagua, 2013b).....	74
<b>Figure 4.9</b> : Propulsion system with nacelle and engine (Modified from Mattingly, 2006). .....	85





# **ENERGY AND EXERGY-BASED THERMODYNAMIC ANALYSIS OF THE SCIMITAR ENGINE AT MACH 5.0**

## **SUMMARY**

After the invention of the jet engines at the end of the Second World War, aeronautics sector, which was already seen as a major field in science and industry, entered a new era. With developing technology, new types of aircrafts that are capable of having longer ranges, carrying heavier payloads or being faster than any other aircraft were designed. Developments in compressible flow and aerodynamics made it possible to reach speeds up to speed of sound and even passing it. The race in aeronautics pushed humanity to go further. Aim of spaceflight was a new task and required new approaches.

Since there is no oxygen in the space, rockets needed to carry their own oxygen along with their fuel. This added extra weight on the vehicle. Extra weight caused more fuel to be burned which resulted in more expenditure. In the early 60's, a group of engineers from Marquardt Company proposed a new design and called it LACE (Liquid Air Cycle Engine). Theory behind LACE was to liquefy the incoming air with the liquid hydrogen fuel in a condenser, separate the liquid oxygen from the air and send it to combustion chamber (CC) where it is combusted with the hydrogen. This is proposed for decreasing the weight by extracting the oxygen from the atmosphere during the acceleration phase inside the atmosphere. The problem with the LACE was the amount of heat transferred in the condenser. It is transferred in such an amount that it is far more than needed to power the air compressor (C). Entropy generation during the heat transfer process is in such an amount that useful work extraction was a problematic task. However, SABRE (Synergetic Air Breathing Rocket Engine) resolves this problem by a new heat exchanger (HX) design that enables the cooling of air to a point just above condensation temperature to prevent unnecessary entropy generation.

Scimitar engine is derived from the SABRE engine. It is designed to propel LAPCAT A2 (Long Term Advanced Propulsion Concepts And Technologies) vehicle. The project is supervised by ESA (European Space Agency) and the main goal of the project is to reach antipodal distances around the world by 4-5 hours. Scimitar engine has the characteristics of three different propulsion engines namely: turbofan, ramjet and air-turborocket. In order to reach Mach 5.0 cruise speed, features of three different propulsion engines are combined. Between 0.0-2.5 Mach, turbofan mode is operational. Between 2.5 and 5.0 Mach, ramjet + air-turborocket mode is active and at Mach 5.0 cruise configuration air-turborocket mode, on which this thesis based, is active. This study aims on the thermodynamic analysis of the Scimitar engine at Mach 5.0.

Turbofan based cycle of the Scimitar engine operates as a conventional turbofan engine used in commercial aircrafts. Since Scimitar engine operates both at subsonic and supersonic flight speeds, it employs the use of a variable intake (I). After the

compression in the intake (I), air is separated into two parts, some part flowing towards the bypass duct while the other is flowing towards the engine core. Air is compressed in the C which is powered by the helium turbine. After leaving the C, air is burned with hydrogen fuel in preburner (PB). The flow in the bypass duct enters the fan (F), which is powered by the hub turbine (HT). HT is driven by the flow diverted from engine core to bypass duct. During the acceleration phase of the engine, bypass burner (BB) are active. After joining, flow expands in the bypass nozzle (BN). Core nozzle (CN) is not open in the turbofan mode.

Ramjet and air-turbo-rocket mode of the engine is active between 2.5-5.0 Mach. In the ramjet mode, both nozzles are operational. After the compression step in the I, if the flight speed is above Mach 3, precooling is active and air temperature is decreased to 635 K, which is the C inlet temperature decided by the designers. Compression process is followed by the combustion in PB and CC. Some of the high temperature gases leaving the PB are drawn to the HT to drive the F. Final process is the expansion process taking place at CN and BN.

The last flight mode is the air-turbo-rocket. In the air-turbo-rocket mode, bypass duct is closed. Also, since there is no acceleration in Mach 5.0, BBs are not active. Thrust is provided by the flow exiting the engine core. After the compression and precooling, the air enters the C. The cooling process may be considered as an intercooling step for compression processes. Flow exiting the C is burned in the PB and CC. In HX3, between PB and CC, combustion products (CPs) are cooled by helium to increase helium temperature to 1000 K which is an important parameter in the Scimitar engine. CPs expand in the CN and leave the engine at high speed, creating thrust.

Thermodynamic analysis plays a crucial role when investigating the performance of a thermal system or simply when determining the thermophysical properties of a fluid. Any thermal system that performs an open or closed thermodynamic cycle can be analysed by constructing correct model. Nowadays, there are many researchers making studies about the propulsion engines of different types on different flight conditions. In the literature, there are many studies about turbofan and turbojet engines. However, studies related with Scimitar engine are few and most of them are performed by CFD analysis or thermodynamics simulators. After realizing the need for a study regarding the processes taking place in detail for the Scimitar engine, this study commenced.

This study is based on the Mach 5.0 flight speed. Thermodynamic relations for the processes of the engine subcomponents are derived with the help of main textbooks and papers from the open literature. The exit of each subcomponent is coupled to the inlet of the following component. Since there are three different fluids moving through the engine, all three different sides are concerned as a main difference from turbofan and turbojet based studies. Air is considered as an ideal gas mixture composed of nonreacting species of  $O_2$  and  $N_2$ . The importance of chemical composition reveals itself in the convergent-divergent nozzle (C-D N) and combustion processes. Treating CPs as air results with a big difference (around 400 K) in the temperature of CPs at the exit of the CC. When combustion process is considered, using chemical balance is the correct approach to determine the exit temperature. Treating air and CPs as gas mixtures and using energy flow rates with respect to reference conditions enable us to include the fuel heating value (FHV)

directly. As chemical composition of the air changes, its molecular weight, gas constant and corresponding speed of sound also change.

Lastly, some performance parameters such as uninstalled thrust  $F_u$ , specific thrust  $F_S$ , thrust specific fuel consumption  $TSFC$ , propulsive efficiency  $\eta_p$ , thermal efficiency  $\eta_{th}$  and overall efficiency  $\eta_o$  are defined and calculated. Propulsive efficiency is found as  $\eta_p = 0.729$  which is 5% greater than the compared study. Also, thermal and overall efficiencies are 64.6% and 47.1% for this study and the results are 66.6 – 74.3% and 49.3 – 55.0% respectively for simulation study in comparison. The results in this study are not far away from the compared results which show that thermodynamic model is sufficiently applicable.





## SCIMITAR MOTORUNUN 5.0 MACH HIZDA ENERJİ VE EKSERJİ ESASLI TERMODİNAMİK ANALİZİ

### ÖZET

İkinci Dünya Savaşı'nın sonunda jet motorlarının icat edilmesiyle halihazırda önemli bir sektör olarak görülen havacılık sektörü yeni bir döneme girdi. Gelişen teknoloji ile daha uzun menzile sahip, daha fazla savaş yükü taşıyabilen ya da o zamana kadar üretilmiş diğer uçaklardan daha hızlı uçaklar geliştirildi. Sıkıştırılabilir akış ve aerodinamik alanlarındaki gelişmeler de ses hızına ulaşabilmeyi hatta ses hızını geçmeyi mümkün kıldı. Havacılık sektöründeki gelişmeler sayesinde insanlık ileriye gitmek için kendini zorladı. Uzay uçuşları yeni bir hedefti ve yeni yaklaşımlar gerektirmekte idi.

Uzayda oksijen olmamasından dolayı roketler yakıtlarıyla beraber yakıtı yakmak için gerekli olan kendi oksijenlerini de taşımak zorundadırlar. Bundan ötürü uzay araçlarının kütleleri atmosferde operasyon gerçekleştiren araçlara göre daha ağırdır. Bu ekstra kütle, daha fazla yakıt yakılması ile tepki kuvveti oluşturularak karşılandı ve bu da masraf artışına sebep oldu. 1960'ların ortasında, Marquardt Company'de çalışan bir grup mühendis yeni bir roket tasarımı önerdiler ve bu roketi LACE (Liquid Air Cycle Engine) ismini verdiler. Bu roketin çalışma prensibi motordan içeri giren havayı, bir yoğuşturucuda sıvı hidrojen yakıt ile soğutarak yoğuşturup, oksijeni sıvı havadan ayırıp yanma odasına göndererek, oksijenin burada hidrojen yakıt ile yanması esasına dayanmaktaydı. Burada amaçlanan, gerekli oksijeni atmosferde ivmelenme sırasında atmosferden elde etme yolu ile aracın kütlesini azaltmak idi. LACE ile ilgili problem yoğuşturucuda birim zamanda transfer edilen ısı miktarı ile ilgili idi. Isı, yoğuşturucuda birim zamanda o kadar yüksek miktarda transfer ediliyordu ki burada elde edilen güç potansiyeli kompresöre güç ileten türbini çalıştırmak için gerekenden çok fazlaydı. Isı transferi sırasında gerçekleşen entropi üretimi, gerekli faydalı güç sağlanması konusunda sorun çıkarıyordu. Fakat SABRE (Synergetic Air Breathing Rocket Engine) bu sorunu, havayı yoğuşma sıcaklığının hemen üzerine kadar soğutarak istenmeyen entropi üretimini kısıtlayan yeni bir ısı eşanjörünün tasarımı ile çözdü.

Scimitar motoru SABRE motorundan türetilmiş olup LAPCAT A2 (Long Term Advanced Propulsion Concepts And Technologies) aracını hareket ettirmesi istenmektedir. Proje ESA (European Space Agency-Avrupa Uzay Ajansı) tarafından yürütülmektedir ve projenin ana hedefi dünyanın çapı kadar uzak mesafelere 4 ile 5 saat süre zarfında uçmaktır. Scimitar motoru, 5.0 Mach hızına çıkabilmek için üç farklı jet motorunun özelliklerini barındırmaktadır: turbofan, ramjet ve hava turbo-roket. 0.0 ile 2.5 Mach aralığında turbofan modu aktiftir. 2.5 ile 5.0 Mach hız aralığında ise motor ramjet+hava-turbo-roket konfigürasyonunda çalışmaktadır. 5.0 Mach hızında ise bu tezin de konusu olan hava turbo-roket modunda çalışmaktadır. Bu çalışma, 5 Mach hızında çalışan Scimitar motorunun termodinamik analizi üzerine yoğunlaşmaktadır.

Scimitar motorunda, 0-2.5 Mach aralığında turbofan esaslı çevrim ticari uçuşlarda kullanılan geleneksel turbofan motorları gibi çalışmaktadır. Scimitar motoru hem sesaltı hem sesüstü hızlarda çalıştığı için değişken hava girişi kesit alanına sahip difüzör (Intake, I) kullanmaktadır. Difüzördeki sıkıştırma prosesinden sonra hava iki kola ayrılır, bir kısmı tali (bypass) kanaldan hareket ederken geri kalan kısmı motorun merkezinde hareket eder. Hava helyum türbini tarafından çalıştırılan kompresörde sıkıştırılır. Kompresörden ayrıldıktan sonra ön yakıcıda (Preburner, PB) bir miktar hidrojen yakıtı ile yakılır. Tali kanaldaki hava eş merkez türbini (Hub Turbine, HB) tarafından tahrik fana (F) girerek basıncını artırır. Bu eş merkez türbini ise motorun merkezinden bypass kanalına yönlendirilen yanma ürünü gazlar ile tahrik edilmektedir. Uçak hızlanma modunda ise tali yakıcılar (bypass burner, BB) devrededir. Akışlar tali kanalda birleştikten sonra tali kanal lülesinde (Bypass Nozzle, BN) genişlerler. Merkez lüle (Core Nozzle, CN) turbofan modunda açık değildir.

2.5 ile 5.0 Mach aralığında motorun ramjet ve hava-turboroket modu aktiftir. Ramjet modunda her iki lüle de aktiftir. Difüzördeki sıkıştırma prosesinden sonra, eğer uçuş Mach sayısı 3.0'ten büyükse, ön soğutma aktiftir ve girişte ısınan havanın sıcaklığı tasarımcılar tarafından belirlenen kompresör giriş sıcaklığı  $635\text{ K}$ 'e soğutulur. Sıkıştırma prosesini ön yakıcıdaki (PB) ve yanma odasındaki (Combustion Chamber, CC) yanma prosesini takip eder. Yanma odasından çıkan yüksek sıcaklıklı gazların bir kısmı fanı tahrik eden eşmerkez türbininin (HT) olduğu kanala doğru iletilir. Motordaki son proses hem merkez hem de tali lülelerde genişlemedir.

Son uçuş modu hava-turborokettir. Hava-turboroket modunda tali kanal kapalıdır. Aynı zamanda 5.0 Mach Scimitar motorunun en fazla hızı olduğu için daha fazla hızlanma söz konusu değildir. Tepki kuvveti sadece motor merkezinden hareket eden akışkandan sağlanır. Difüzördeki sıkıştırma ve soğutmadan sonra hava kompresöre girer. Buradaki soğutma prosesi ara soğutma gibi düşünülebilir. Kompresörden çıkan hava ön yakıcıda ve yanma odasında yanar. Bu iki yanma işlemi arasında HX3'te (Isı Eşanjörü-3) yanma ürünü gazlar helyum ile soğutulur. Burada esas amaç helyumun sıcaklığını  $1000\text{ K}$ 'e çıkarmaktır. Bu sıcaklık motor için önemli parametrelerden biridir. Yanma ürünü gazlar merkez lülede genişleyerek motoru yüksek hızda terkederler ve böylece tepki kuvveti elde edilmiş olur.

Termodinamik analiz, açık veya kapalı bir çevrim ile çalışan termal sistemlerin performansının değerlendirilmesinde veya basitçe bir akışkanın termodinamik özelliklerinin bulunmasında önemli rol oynamaktadır. Açık ya da kapalı herhangi bir çevrim esasına dayalı çalışan bir ısıl sistem doğru bir model uygulanarak analiz edilebilir. Günümüzde birçok araştırmacı farklı tipteki ve çalışma koşullarındaki tepki motorları ile ilgili çalışmalar yapmaktadır. Literatürde, turbofan ve turbojet motorları ile ilgili birçok çalışma bulunmaktadır. Fakat, Scimitar motoru ile ilgili çalışma sayısı az olmakla beraber, bunların çoğunluğu Hesaplamalı Akışkanlar Dinamiği (HAD) ya da termodinamik simülatör kullanımıyla yapılmıştır. Motor içerisinde gerçekleşen proseslerin gösterildiği bir çalışmanın eksikliğinin gözlemlenmesi sonrası bu çalışma başlatılmıştır.

Bu çalışma 5.0 Mach uçuş hızı göz önünde bulundurularak yapılmıştır. Motor bileşenleri ile ilgili prosesler, konular ile ilgili temel ders kitapları ve makaleler göz önünde bulundurularak termodinamik denklemler türetilmiştir. Bir bileşenin çıkışı bir diğer bileşenin girişine kuple edilmiştir. Motorda üç farklı akışkan bulunmasından ötürü akışkanların üçü de hesaplarda yer almıştır. Bu sebeple diğer

motorlardan ve bunlar ile ilgili yapılmış çalışmalardan farklı olma özelliği taşımaktadır. Hava birbiri ile tepkimeye girmeyen  $O_2$  ve  $N_2$  den oluşan bir ideal gaz karışımı olarak ele alınmıştır. Havanın kimyasal kompozisyonunun göz önünde bulundurulması kendisini yakınsak-ıraksak (Convergent-Divergent, C-D) lülede ve yanma proseslerinde göstermektedir. Yanma ürünü gazları hava olarak değerlendirmek, akışın yanma odasından çıkış sıcaklığının  $400\text{ K}$  gibi büyük bir farkla tayin edilmesine sebebiyet vermiştir. Yanma proseslerini göz önünde bulundurmak ve kimyasal denklığı kullanmak akışkanın çıkış sıcaklığını tayin etmede daha doğru bir yaklaşımdır. Havayı bir karışım olarak ele almak ve referans koşullarına göre enerji akış değerlerini hesaplamak doğrudan yakıt ısıl değerinin hesaplamaya dahil edilmesini mümkün kılmıştır. Ayrıca lüledeki genişleme prosesi ele alındığında, havanın kimyasal kompozisyonu ile beraber, havanın moleküler ağırlığı, gaz sabiti ve karşılık gelen ses hızı değişiklik göstermektedir.

Son olarak, bu çalışmada montaj öncesi tepki kuvveti  $F_u$ , özgül tepki kuvveti  $F_s$ , birim tepki kuvveti için yakıt tüketimi  $TSFC$ , itme verimi  $\eta_p$ , ısıl verim  $\eta_{th}$  ve toplam verim  $\eta_o$  gibi performans parametreleri tanımlanıp hesaplanmıştır. İtme verimi  $\eta_p = 0.729$  olarak hesaplanmıştır ve karşılaştırma yapılan simülasyon çalışmasında belirtilen değerden %5 fazla çıkmıştır. Fakat ısıl ve toplam verim sırası ile bu çalışmada %64.6 ve %47.1 olarak hesaplanmıştır. Karşılaştırma yapılan çalışmada ise bu sonuçlar %66.6 – %74.3 ve %49.3 – %55.0 aralığında verilmiştir. Bu çalışmanın sonuçları karşılaştırma yapılan simülasyon çalışmasının çok uzağında değildir. Dolayısıyla, bu çalışmada ortaya konan termodinamik model uygulanabilir görülmektedir.





## **1. INTRODUCTION**

Scimitar engine is a hypersonic rocket engine that is designed to operate at Mach 5.0. This thesis concentrates on the thermodynamic analysis of the Scimitar engine providing the derivations of the thermodynamic relations for each engine subcomponent and the rate of global energy balance. The information gathered from the literature survey is used to understand the purpose of building the Scimitar engine, engine flight modes with respect to Mach numbers and technical data. After careful examination of the literature, a thermodynamic model is created.

### **1.1 Purpose of Thesis**

The purpose of the thesis is to develop a thermodynamic analysis model in order to provide the processes and detailed derivations of the thermodynamic relations for each process of the Scimitar engine in an obvious manner. Some performance parameters are also defined, calculated and presented for evaluating the performance of the Scimitar engine at the cruise speed of Mach 5.0.

### **1.2 Literature Review**

A literature review has been made to gather the information about thermodynamic analysis of aircraft engines and rocket engines especially on the design parameters and working principle of the Scimitar Engine.

Çengel and Boles (2005), which is a widely used textbook for thermodynamics courses, provides many fundamental concepts such as the zeroth, first and second laws of thermodynamics, thermodynamic cycles and an introductory level of compressible flow and gas turbine engines. Many numerical examples of gas turbine engines and compressible flow such as flow through a convergent-divergent nozzle (C-D N) can be found in the book.

Important information about the history and development of aircraft engines, types, working principles, aerothermodynamics, cycle analysis, performance parameters

and turbomachinery can be found in (Hill and Peterson, 1992; Heiser et al, 1994; Cohen et al, 1996; Hünecke, 2003; Anderson, 2003; Mattingly et al, 2002; Mattingly, 2006; El-Sayed, 2008; and Cumpsty, 2009). These books may be considered as core textbooks when studying gas turbine and rocket engines. There are many numerical examples of aerothermodynamics aspects of jet engines and operation of turbomachinery in the gas turbine engines in these books.

A study, which can be considered as a core paper when studying the Scimitar engine, has been performed by (Jivraj et al, 2008). Purpose of design for such an engine, working fluids and fuel, which are different than the conventional gas turbine engines, theoretical calculation for a precooled Scimitar engine at Mach 5, design constrains for some turbomachinery in the engine such as compressor (C) inlet temperature and helium turbine (T1) inlet temperature, and simulation results of stator-less contra-rotating helium T1 are given in this study. As a preliminary design investigation step, designers concentrated on the thermodynamic relations for the possibility of air compression process considering theoretical cooling of the air in the C with the fuel of liquid hydrogen *having energy and entropy conserved* during the compression process assuming a *perfect process*. Since flight and liquid hydrogen storage conditions are known, compressor pressure ratio (CPR) of the air compression process at the inlet is left as a design choice.

Next,  $\bar{V}_{eff}$  (effective exhaust velocity defined as the thrust per unit mass flow rate of fuel) is found as a parameter of air-to-fuel mass flow rate ratio (afr) with the help of conservation of energy and conservation momentum equations. Variations of Equivalence Ratio (which is the ratio of “*the afr in designers’ selection*” to “*the theoretical afr*”) versus Mach number and  $\bar{V}_{eff}$  versus Mach number have been drawn which helped designers to decide on some important design parameters such as the thermal capacity ratio in the heat exchange process. Thermal capacity ratio which is the  $\dot{m}c_p$  ratios of the fluids entering the heat exchangers (HXs), is the main logic behind heat exchange processes. After these steps, thermal capacity ratios in the complex thermodynamic cycles have been explained, also the maximum value of air temperature at the C inlet is given as 635 K and the temperature of helium at the helium T1 inlet is given as 1000 K. Lastly, the simulation results including air-to-fuel ratio mass flow rate ratios, mass flow rate of air at the inlet of engine, thrust generated are given together with the simulation results of contra-rotating helium T1.

As a result, designers state that most challenging R&D work would be on the reduction of  $NO_x$  formation at the high-temperature combustion required in Mach 5.0 cruise since other components and the thermodynamic cycle are very well achievable (Jivraj et al, 2008).

A simulation study at Mach 5.0 configuration of the Scimitar engine is made by using the simulator “EcosimPro” (Fernandez-Villace and Paniagua, 2011). In the study, turbofan, ramjet and air-turbo-rocket cycle modes are explained by active engine components at that flight mode as well as the flight speed of the engine. From intake (I) to C-D N all the engine subcomponents including helium regenerator HXs and turbomachinery are brought from EcosimPro library to the simulation worksheet where related physical equations are modified by user with respect to Scimitar engine’s needs. The positions of engine subcomponents with respect to other subcomponents, numerical calculation methods regarding the subcomponent and their geometry, turbomachinery scaling and corrections are explained before tabulating the results and showing the engine simulation model. At Mach 5.0 which corresponds to air-turbo-rocket mode of the engine, inlet and exit sides of the subcomponents are given a station number and pressure, temperature and mass flow rates of the fluid passing the stations are specified. The exergy efficiency and specific impulse of the engine is given as a function of  $afr$ . Also the reason why the helium T1 operates near design point for different throttling levels is explained. The amount fuel required by the preburner (PB) is dictated by the constant helium T1 inlet temperature which is 1000 K. Since the helium T1 inlet temperature is kept constant, turbine performance is always kept at an optimum level.

Another simulation study of the Scimitar engine is also performed by using the simulator “EcosimPro” again (Fernandez-Villace and Paniagua, 2013a). The study includes 3 different working modes of the Scimitar engine at different speeds and elevations. The same procedure of explaining the active engine subcomponents with respect to flight speed, complex helium cycle, mathematical expressions regarding the I, HXs and turbomachinery are followed as in (Fernandez-Villace and Paniagua, 2011). The main differences from the previous study are that this study includes engine control rules and the operation of the engine core components is between Mach 2.5 and Mach 5. Although it is stated that during the operation between Mach 2.5 and Mach 5, engine bypass channel is open which enables the operation of hub

turbine (HT), fan (F), bypass burner (BB) and bypass nozzle (BN), the simulation shows the results of the engine core only. Bypass part of the engine is not simulated. Engine control is achieved by inserting valves into some important positions inside the engine such as behind the I to enable bypassing the precooler when total (stagnation) temperature of the air is less than C inlet temperature, at the exit of the high-temperature helium regenerator (HTR), just before the inlets of the PB and combustion chamber (CC) and finally between the helium turbines that power the helium regenerator Cs. Engine control is performed by some valve opening command which is dependent of the state of flow. For example, bypass valve behind the I closes only when the total temperature at the I exit rises above  $635\text{ K}$  so that flow does not bypass the precooler. Opening conditions of the valves include measurement device's sensitivity. The control logic is constructed in such a way that it would only depend on one parameter: fuel consumption. With respect to total fuel consumption, engine control is shown in figures in Fernandez-Villace and Paniagua (2013a) to easily visualize the process. Fuel flow vs. Mach number vs. Altitude diagram is separated into zones. These zones indicate engine's operation mode by showing Mach number and altitude. Also, as the operation mode, altitude and the flight speed of the engine changes, valve openings in the engine are shown in the study. Lastly, the mass flow rates, static and total pressures and temperatures of the air, helium and hydrogen are given at simulation results at different flight conditions along with turbomachinery PR, adiabatic efficiency corrected speed with respect to fuel consumption and flight condition.

A first law and second law analysis of a hypersonic engine designed for Mach 5.0 cruise is made by (Fernandez-Villace and Paniagua, 2013b). An air breathing hypersonic engine model is created as a stream tube or a control volume by applying conservation and momentum equations for the engine. The control volume model is constructed by considering the air entering the control volume with a certain speed, exhaust gases leaving the system, heat rejected to the atmosphere during a non-adiabatic combustion process, auxiliary power input the control volume (propulsion engine) and finally the fuel entering the system. Starting the analysis by applying the first law of thermodynamics for a steady-flow open system and substituting the kinetic energies of the flows, formation enthalpies of the species entering the engine and sensible enthalpies, the equations are modified. In the analysis, lower heating

value (LHV) of the fuel is considered since the temperature of the water inside the product gases is always greater than  $373.15\text{ K}$ . In the combustion process, the study (mistakenly) considered that the reference temperature is the flame temperature at which the combustion takes place, as a result it greatly changes the LHV of hydrogen. Hence, thermal efficiency of the engine is found between  $66.6 - 74.3\%$  based on the reference temperature (i.e., flame temperature) changes when a first law thermal efficiency definition of *the conversion ratio of thermal power and the auxiliary power to the kinetic power* is used. Propulsive efficiency defined as *the conversion ratio of kinetic power to the propulsive power* is found as  $67.5\%$ . Overall efficiency defined as *the conversion ratio of the thermal power and the auxiliary power to the propulsive power* is the multiplication of thermal and propulsive efficiencies. Overall efficiency result is in the range of  $49.3 - 55\%$ . In order to eliminate the fuel LHV dependency of efficiency terms, definition of efficiency is changed to an expression which includes direct change of enthalpy terms instead of LHV of the fuel which is expressed as dependent on combustion temperature in the study. The results are  $66.5\%$  and  $98.5\%$  for overall and thermal efficiencies, respectively. The high thermal efficiency is due to the consideration of only loss as heat rejection in non-adiabatic combustion. So, by introducing the second law terms starting with Carnot efficiency to the system and exergy balance for the control volume, thermal and overall effectiveness which is *multiplication of propulsive efficiency and thermal effectiveness* of the engine is defined and calculated as  $60.9\%$  and  $41.1\%$ . Exergy analysis includes exergy destruction terms for each component of the engine. After the thermodynamic analysis, mission analysis of the engine is made by using a body diagram for the engine including drag, weight, lift and uninstalled thrust parameters. Exergy analysis results show that the biggest exergy destruction happens in combustion processes in PB and CC with  $7\%$ . Exergy loss in the helium cycle when compared to the rest of the thermodynamic cycle of the engine is very little by  $4\%$ ; while its  $1\%$  in regenerator where HXs have matched thermal capacity ratios,  $2\%$  in helium hydrogen HXs and  $1\%$  in the C – helium T1 spool. Internal irreversibility of the engine does not change much when decreasing flight speed from Mach 5.0 to Mach 2.5. Also, thermal effectiveness which is *the ratio of power produced to the maximum power available* of the engine decreases by only  $5\%$  from  $61\%$  to  $56\%$  when flight speed is again changed from Mach 5.0 to

Mach 2.5 which shows it is a robust design over a wide range (Fernandez-Villace and Paniagua, 2013b).

A CFD (Computational Fluid Dynamics) and experimental study has been performed by Marini et al. (2013) on Scimitar engine nozzles. The aim of the study is to verify the theoretical design, to reduce the base pressure effects, to determine the thrust generated by different N types for the engine, and to investigate the combustion process where  $NO_x$  forms and some portion of the fuel remains unburned. On an x-y plane, dimensions of V0 and V1 nozzles are given in the study. It is seen that V1 nozzle (V1 N) is shorter in length and also smaller in diameter. Also, simulation options such as density based equation which corresponds to compressible flow, Reynolds averaged Navier-Stokes equations for cell centered finite volume calculation methods are given. As it is done for chemical reactions, reduced and detailed Jachimowski air-hydrogen approaches are used. Jachimowski approaches are air-hydrogen reaction mechanisms that are investigated and compared with experimental data in terms of ignition delay versus temperature, pressure and burning velocities versus hydrogen mole fractions for combustion processes in scramjets (Jachimowski, 1988). Pressure and temperature of the CPs leaving the CC are known. Before starting the simulation, gas behavior such as perfect gas and thermally perfect gas, flow characteristic of laminar and inviscid flow and lastly laminar or turbulent options are specified and both options are used in the simulation. The results showed that there is a big difference between the assumption of thermally perfect gas and ideal gas, and that V1 N can operate without a shock occurring inside the N. Although V1 N is smaller in both diameter and length, it has the same characteristics of flow Mach number inside the N. As it is found for chemical reactions, reduced and detailed Jachimowski methods do not give very different results for fluid pressure, temperature, Mach number and  $NO_x$  formation. However, detailed Jachimowski method gives an over expected unburned  $H_2$  mass flow rate. At Mach 0.9, 2.5 and 4, BN and core nozzle (CN) are both simulated since at those Mach numbers the engine will use both Ns. Simulation results shows that the wake is created by the flow coming from BN while passing over the CN. This wake is highly dependent on the Mach number of the flow coming from BN. An experimental study has been made in the supersonic wind tunnel to see the real world performance. Results showed that CFD results and real results of under expanded N behavior,

turbulence modelling, two and three flow interactions are parallel. The study showed that V1 N configuration is usable for Scimitar engine, therefore, with the V1 design, N exit area is reduced from  $7.05 \text{ m}^2$  to  $5.38 \text{ m}^2$ , and that there is no shock occurring inside the N. Although gross thrust at V1 N configuration reduces 20% at take-off conditions when compared to the V0 nozzle (V0 N) configuration, V1 N offers pressure thrust when underexpanded at all Mach numbers except subsonic speeds.

An exergy analysis of J85-GE-21 turbojet engine is performed by (Ehyaie et al, 2013). In this study, all the engine subcomponents are shown in a diagram as well as the mass flows and bypassing mass flows. From diffuser inlet to the N exit all the engine components are coupled and the thermodynamic relations are written. In the exergy analysis part, exergy types are defined. One by one, exergy analysis of each subcomponent is performed. The analysis is made in two different flight conditions. At sea level and with  $200 \text{ m/s}$  flight speed and at  $11000 \text{ m}$  elevation and  $200 \text{ m/s}$  flight speed. For each condition the results of each component are tabulated. The results show that in exergy analysis most efficient parts are C with 96.7 %, N with 93.7 % and turbine 92.3 % at sea level. At  $11000 \text{ m}$ , the first the two most efficient parts are C and N and the third most efficient subcomponent is diffuser. The least efficient engine subcomponent is the afterburner followed by CC. Consequently, the highest entropy generation rate is at afterburner and then at CC. Lastly, air speed plays an important role in exergy efficiency in the engine performance. It is seen that reducing the air speed decreases the exergy efficiency.

An exergy analysis of a small turbojet engine for an unmanned aircraft is made by (Turan, 2012). In this study, CPR is varied between 2 and 7 and turbine inlet temperature is varied between  $1200 \text{ K}$  and  $1400 \text{ K}$ . The results show that exergy efficiency of C increases with increasing PR, turbine inlet temperature does not affect the exergy efficiency of C, and combustor efficiency increases as turbine inlet temperature increases. The highest value of exergy efficiency is found as 59.72 % at  $1500 \text{ K}$  with CPR equal to 7. Exergy efficiency of the axial flow turbine increases as inlet temperature increases between  $1200 \text{ K}$  and  $1400 \text{ K}$  and CPR increases between 2 and 4. However, when inlet temperature is  $1500 \text{ K}$ , increasing CPR decreases the exergy efficiency of the turbine which means that there is room for improvement at high turbine inlet temperatures. Decreasing flight speed decreases

efficiency. Finally, highest flight speed, compression ratio and turbine inlet temperature result with highest efficiency.

There are also some core textbooks about the exergy analysis of thermal systems and processes such as (Szargut et. al, 1988 and Kotas, 1995). There are some studies showing the importance of exergy analysis of gas turbine engines while designing and evaluating the performance of the engines (Etele and Rosen, 2001; Rosen and Etele, 2004; Dincer and Rosen, 2007; Turgut et. al, 2007; Turgut et. al, 2009; Turan et. al, 2014)

In addition, optimization studies of thermal systems by finite-time thermodynamics have been reviewed by Durmayaz et al. (2004), a thermodynamic optimization of a turbofan engine has been performed by (Najjar and Al-Sharif, 2006).

An ecological optimization of a turbofan engine with the help of a parameter defined as Coefficient of Ecological Performance (CEP) have been performed by (Tanbay et al, 2015; Colakoglu et al, 2014; Colakoglu et al, 2016; Colakoglu, 2015).

Upon all the reviewed information and background knowledge in the literature, this graduate thesis study has been performed.



## 2. THERMODYNAMICS BACKGROUND

### 2.1 Purpose

In this chapter, some important terms, definitions, concepts and laws of thermodynamics utilized frequently in the thesis are reviewed by the aid of literature (Çengel and Boles, 2005; Wark, 1983; Anderson, 2003).

### 2.2 Stagnation Properties

When a flowing fluid is investigated, the term enthalpy, which is a combination of internal energy and flow work, is considered. If kinetic and potential energies are neglected, *enthalpy* is equal to the total energy of the flowing fluid entering into or leaving from the control volume. During the analysis of high-speed flows as encountered in jet and rocket engines, kinetic energy cannot be neglected.

After reaching 0.3 times of the speed of sound, kinetic energy term in the energy balance equation creates a difference that cannot be neglected. In that case, enthalpy and kinetic energy are combined into a single term called *stagnation enthalpy* or *total enthalpy*. Stagnation enthalpy can be considered as the total enthalpy of the fluid when it is brought to rest adiabatically (Çengel and Boles, 2005). It can be written in  $J/kg$  as

$$h_0 = h + \frac{v^2}{2} \quad (2.1)$$

Hence, in the absence of potential energy, stagnation enthalpy represents the total energy of the moving fluid. If we put this knowledge to work for a steady-flow device such as a diffuser or Nozzle (N), we can use equation (2.1) for the determination of the other properties (such as temperature, pressure and density) of the flowing fluid.

Writing *the first law of thermodynamics* for a process of an adiabatic, steady-flow system (control volume) that involves no work and heat interaction (Çengel and Boles, 2005) as

$$\dot{Q} - \dot{W} = \sum_{out} \dot{m} \left( h + \frac{v^2}{2} + gz \right) - \sum_{in} \dot{m} \left( h + \frac{v^2}{2} + gz \right) \quad (2.2)$$

in addition, neglecting potential energies, equation (2.2) becomes

$$h_{in} + \frac{v_{in}^2}{2} = h_{out} + \frac{v_{out}^2}{2} \quad (2.3)$$

Equation (2.3) can be expressed in a more general form by changing the subscripts *in* and *out* to 1 and 2 in order to denote entering and leaving enthalpies to and from the control volume respectively and 0 denoting stagnation states (and stagnation properties such as enthalpy, temperature or pressure) as

$$h_{01} = h_{02} \quad (2.4)$$

As long as there is no heat transfer from or to, and work done on or by the control volume, stagnation enthalpies will be the same. If the flowing fluid is brought to rest adiabatically in the absence of heat and work interactions, then equation (2.4) becomes

$$h_1 + \frac{v_1^2}{2} = h_{01} = h_{02} \quad (2.5)$$

If the flowing fluid is an *ideal gas*, then the relationship between enthalpy change and temperature change in differential form becomes

$$dh = c_p(T) dT \quad (2.6)$$

since internal energy and enthalpy of ideal gases are only functions of temperature. In equation (2.6),  $c_p(T)$  denotes *specific heat at constant pressure*, which depends on the gas temperature only for an ideal gas. If we further assume that gas is a *calorically perfect gas* (Mattingly, 2006) in which  $c_p$  is not a function of temperature (i.e.,  $c_p$  is constant), then equation (2.6) becomes

$$\Delta h = c_p \Delta T \quad (2.7)$$

With the help of equation (2.7) and calorically perfect gas assumption, we can rearrange equation (2.5) as

$$c_p T_1 + \frac{v_1^2}{2} = c_p T_{02} \quad (2.8)$$

Dividing all terms by  $c_p$ , we obtain the stagnation temperature at the end of the adiabatic process as

$$T_1 + \frac{v_1^2}{2c_p} = T_{02} \quad (2.9)$$

Since the fluid is considered as an ideal gas and if the process is both adiabatic and reversible, then we can use the *isentropic relation for constant specific heats* to find pressure as

$$\frac{P_0}{P} = \left( \frac{T_0}{T} \right)^{k/(k-1)} \quad (2.10)$$

while  $k$  denotes the specific heat ratio ( $k = \frac{c_p}{c_v}$ ).

### 2.3 Speed of Sound and Mach Number

When dealing with high-speed flows, *speed of sound* and *Mach number* are mostly used in the analyses. As the name suggests, speed of sound is the sound speed in a medium. Speed of sound is a function of two parameters: type of the medium and temperature.

Speed of sound is denoted by the letter  $c$ , and at a specified temperature it is determined as

$$c = \sqrt{kRT} \quad (2.11)$$

In equation (2.11),  $k$  is the ratio of specific heats,  $R$  is the gas constant and  $T$  is the absolute temperature in  $K$ .

Another important concept is the Mach number  $Ma$ , named after the Austrian physicist Ernst Mach (1838-1896) (Çengel and Boles, 2005). Mach number is the ratio of the speed of the fluid (or the system) to the speed of sound.

$$Ma = \frac{V}{c} \quad (2.12)$$

When  $Ma = 1$ , flow speed is equal to the speed of sound.

## 2.4 Convergent-Divergent Nozzle

Main goal of an aircraft propulsion engine is to create a momentum and pressure difference between the exit and inlet conditions of the working fluid. To achieve this, C-D Ns are used in jet engines.

C-D Ns invented by Swedish engineer Carl G. P. De Laval in 1893 to drive the blades of his steam turbine are mainly used in steam and gas turbines, rockets and aircrafts for different purposes (Anderson, 2003).

A C-D N is illustrated in Figure 2.1. (Çengel and Boles, 2005).

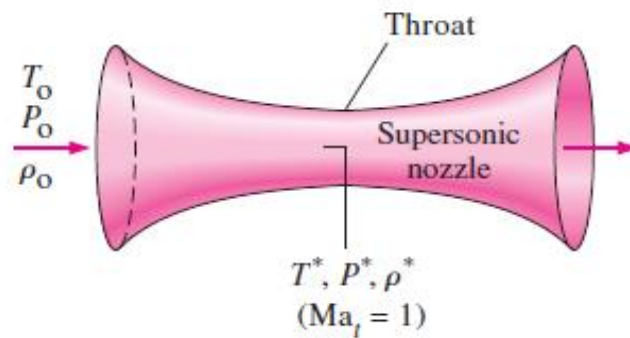


**Figure 2.1** : A convergent-divergent nozzle (C-D N) (Çengel and Boles, 2005).

The N is designed to reach speed of sound at the smallest cross section along the N, which is called the *throat*. When the back pressure to total pressure ratio (TPR) reaches a certain value, flow speed becomes  $Mach = 1$  at the throat. This also called “*choking*”. After the flow is choked and as it moves along the divergent part, it will expand and leave the N at supersonic ( $Mach > 1$ ) speeds. In addition, lowering back pressure when the flow is choked will have no effect on the mass flow. If the flow is not choked at the throat, flow will decelerate in the divergent part (Çengel and Boles, 2005).

## 2.5 Entropy

The first law of thermodynamics deals with the conservation of energy. But it does not explain the direction of the processes occurring in the nature and the theory behind it. A process that does not violate the first law of thermodynamics may be violating the second law of thermodynamics. Hence, upon all these considerations, the second law of thermodynamics presents a new definition called *entropy*. One may simply describe entropy as molecular disorder. Another important concept in understanding the entropy is the *Clasius Inequality* given by

$$\oint \frac{dQ}{T} \leq 0 \quad (2.13)$$

Equation (2.13) states that cyclic integral of  $\delta Q/T$  is always less than or equal to zero. Cyclic integral as the name suggests is performed on the cycle. Knowing that cyclic integral of a quantity is zero, Clasius realized that he defined a new property and called it entropy (Çengel and Boles, 2005).

If a cycle is internally reversible than the result for the cyclic integral is 0, if an irreversible cycle is considered than the result of the cyclic integral is less than 0. For an internally reversible process, the definition of entropy originates from its change as

$$dS = \left( \frac{\delta Q}{T} \right)_{int,rev} \quad (2.14)$$

If one integrates equation (2.14) between states 1 and 2, it becomes

$$\Delta S = S_2 - S_1 = \int_1^2 \left( \frac{\delta Q}{T} \right)_{int,rev} \quad (2.15)$$

In reality, the specific heats at constant pressure and at constant volume ( $c_p$  and  $c_v$ ) of ideal gases change with changing temperature with the exception of monatomic gases. On the other hand, assuming constant specific heats at the average temperature of the initial and final states for ideal gases may be an acceptable approximation at the expense of some loss in accuracy when temperature difference does not exceed a few hundred degrees. Hence, under the constant-specific heats approximation, the entropy-change relations for ideal gases can be obtained as

$$s_2 - s_1 = c_{v,avg} \ln \frac{T_2}{T_1} + R \ln \frac{v_2}{v_1} \quad (2.16)$$

$$s_2 - s_1 = c_{p,avg} \ln \frac{T_2}{T_1} - R \ln \frac{P_2}{P_1} \quad (2.17)$$

However, if temperature difference is greater than a few hundred degrees, then constant-specific heats approximation should not be preferred to use and variation of specific heats with temperature should be accounted for the entropy change calculations (Çengel and Boles, 2005).

For a control volume with steady flow, entropy balance in the rate form can be written as

$$\dot{S}_{gen} = \Delta \dot{S}_{CV} + \Delta \dot{S}_{surr} = 0 + \Delta \dot{S}_{surr} \quad (2.18)$$

$$\dot{S}_{gen} = \sum \dot{m}_e \dot{s}_e - \sum \dot{m}_i \dot{s}_i - \sum \frac{\dot{Q}}{T} \quad (2.19)$$

since  $\Delta \dot{S}_{CV} = 0$  for a steady flow process.

## 2.6 Exergy

Before explaining what exergy is, one must clearly define and understand what dead state is. When a system has no pressure difference, temperature difference as well as chemical composition difference, kinetic and potential energy difference with its surroundings, it is said to be at dead state. Exergy or availability is the amount of useful work potential of a system or the maximum useful work that could be obtained from a system as it undergoes a reversible process from the specified initial state to the state of its environment, that is, the dead state (Çengel and Boles, 2005).

In the absence of any chemical and nuclear reaction components, exergy of a closed system in  $J/kg$  is

$$\phi = (u - u_0) + P_0(v - v_0) - T_0(s - s_0) + \frac{v^2}{2} + gz \quad (2.20)$$

Exergy of a stream in  $J/kg$  is

$$\psi = (h - h_0) - T_0(s - s_0) + \frac{v^2}{2} + gz \quad (2.21)$$

where  $(u - u_0) + P_0(v - v_0) - T_0(s - s_0)$  terms in equation (2.20) and  $(h - h_0) - T_0(s - s_0)$  terms in equation (2.21) are the thermophysical components of the exergy,  $v^2/2$  is the kinetic exergy component and  $gz$  is the potential exergy component.

As explained previously, in real life applications there is no reversible process which results with no entropy generation hence no exergy destruction during the process. In reality, exergy destruction and entropy generation are proportional as

$$X_{destroyed} = T_0 S_{gen} \quad (2.21)$$

Exergy balance for an open system can be written as

$$X_{in} - X_{out} - X_{destroyed} = \Delta X_{system} \quad (2.22)$$

In equation (2.22),  $X_{in}$  and  $X_{out}$  terms include exergy transfer by heat, work and mass. Equation (2.22) can also be written in the rate form for steady-flow processes as

$$\dot{X}_{in} - \dot{X}_{out} - \dot{X}_{destroyed} = \frac{dX_{system}}{dt} \quad (2.23)$$

## 2.7 Gas Mixtures

Airbreathing aircraft engines use atmospheric air for thrust generation. However, air is a mixture of gases, and air composition before and after combustion processes in gas turbines or rocket engines is not the same, i.e., it will change. In order to determine the properties of gas mixtures, composition of the mixture and properties of each component should be known.

This can be achieved in two ways: either by determining the mole fraction of each component which is called *molar analysis* or by determining the mass fraction of each component which is called *gravimetric analysis* (Çengel and Boles, 2005).

Total mass and total number of moles of a gas mixture can be found in *kg* and *kmol* as

$$m_m = \sum_{i=1}^k m_i \quad (2.24)$$

$$N_m = \sum_{i=1}^k N_i \quad (2.25)$$

Total mass of a gas mixture is the sum of mass for each component individually from 1 to  $k$  species. Similarly, total number of moles of a gas mixture is the sum of mole numbers for each component.

Ratio of *the mass of each component to the total mass of the mixture* is called *mass fraction*. Ratio of *the mole number of each component to the total number of moles of the mixture* is called *mole fraction*. They are very important tools in determining the properties of gas mixtures. Mass fraction and mole fraction for the  $i^{\text{th}}$  component of a gas mixture can be calculated respectively as

$$mf_i = \frac{m_i}{m_m} \quad (2.26)$$

$$y_i = \frac{N_i}{N_m} \quad (2.27)$$

where subscript  $i$  denotes the species and  $m$  denotes the gas mixture. By the aid of equations (2.26) and (2.27), one can show that the sum of the mass fraction or mole fraction of the species in a mixture is equal to 1:

$$\sum_{i=1}^k mf_i = 1 \quad (2.28)$$

$$\sum_{i=1}^k y_i = 1 \quad (2.29)$$

The *mass* of a substance is the multiplication of its *molar mass* and *number of moles*. Then, one can compute average molar mass in  $kg\ kmol^{-1}$  and gas constant in  $kJ\ kg^{-1}K^{-1}$  of a mixture respectively as



$$M_m = \frac{m_m}{N_m} = \frac{\sum m_i}{N_m} = \frac{\sum N_i M_i}{N_m} = \sum_{i=1}^k y_i M_i \quad (2.30)$$

$$R_m = \frac{R_u}{M_m} \quad (2.31)$$

$M_m$  and  $R_m$  are the *average molar mass* and the *gas constant* of a mixture, respectively, while  $R_u$  is the universal gas constant.

When calculating the extensive properties of a nonreacting ideal gas mixture, one simply add contributions of each component of the mixture (Çengel and Boles, 2005). Thus, total enthalpy, internal energy and entropy of a mixture can be calculated by

$$H_m = \sum_{i=1}^k m_i h_i \quad (2.32)$$

$$U_m = \sum_{i=1}^k m_i u_i \quad (2.33)$$

$$S_m = \sum_{i=1}^k m_i s_i \quad (2.34)$$

Enthalpy, internal energy and entropy per unit mass in  $kJ/kg$  and  $kJkg^{-1}K^{-1}$  can also be calculated, respectively, dividing equations (2.32) - (2.34) by mass of the mixture as

$$h_m = \sum_{i=1}^k m f_i h_i \quad (2.32)$$

$$u_m = \sum_{i=1}^k m f_i u_i \quad (2.33)$$

$$s_m = \sum_{i=1}^k m f_i s_i \quad (2.34)$$

Instead of mass fraction  $mf_i$ , mole fraction  $y_i$  can be used if enthalpy, internal energy and entropy values per  $kmol$  are present, then similar expressions can be written.

When calculating the change in internal energy and enthalpy ( $\Delta u$  and  $\Delta h$  values) of a mixture during a process, only  $u$  and  $h$  values at the initial and final temperatures are taken into account. Under ideal gas assumption, one assumes that properties of gases are not influenced by that of the other gases and temperature is the same as the mixture temperature. This principle is known as *Gibbs-Dalton law*. Another useful principle is the *Dalton's law of additive pressures* which states that partial pressure of a component in a mixture is proportional with its mole fraction.

While calculating  $\Delta s$  of an ideal gas mixture, both Gibbs-Dalton Law and Dalton's law of additive pressures are very useful since entropy calculation includes pressure terms as well (Çengel and Boles, 2005). Hence, entropy change in  $kJ kmol^{-1}K^{-1}$  can be calculated by

$$\Delta \bar{s}_i = \bar{s}_{i,2}^o - \bar{s}_{i,1}^o - R_u \ln \frac{P_{i,2}}{P_{i,1}} \cong \bar{c}_{p,i} \ln \frac{T_{i,2}}{T_{i,1}} - R_u \ln \frac{P_{i,2}}{P_{i,1}} \quad (2.35)$$

In this study, air is considered as a mixture of  $O_2$  and  $N_2$  with mole fractions of 0.210084 and 0.789916, respectively. After the combustion processes in PB and CC, *air* is not treated as the same mixture and composition anymore. It is treated as *CPs with the product of water vapor* in the mixture. All the internal energy, enthalpy, entropy,  $c_p$ ,  $c_v$  and  $k$  values of the air and CP gas mixtures are calculated by considering the equations and laws explained in this section.

## 2.8 Brayton, Gas Turbine Engine and Jet Engine Cycles

Brayton cycle is an ideal closed cycle for gas turbine engines resembling the cycles used in both industrial gas turbines for power generation and in gas turbines for aircraft propulsion. Brayton cycle operates with air as the working fluid, heat transfer from a source to the air through a HX is used instead of the combustion process and heat rejection through a HX from the air to a sink is assumed instead of the removal of the CPs under air standard assumptions.

When a real gas turbine engine is considered, the engine uses an open cycle in which fresh air is taken from atmosphere, combustion takes place in the CC and CPs are rejected after expansion as it is seen in Figure 2.2.

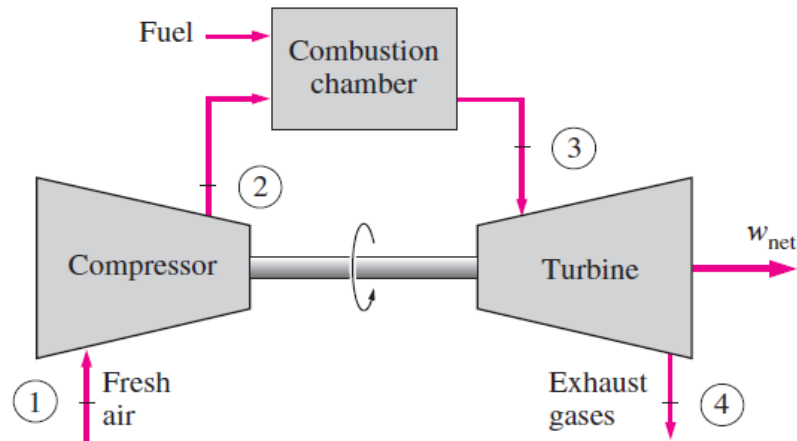


**Figure 2.2 :** An open-cycle gas turbine engine (Çengel and Boles, 2005).

The processes of an open-cycle gas turbine engine shown in Figure 2.2 are

- Fresh air taken from atmosphere enters the C
- Air is compressed to a high pressure and temperature in the C
- Compressed air burns with fuel in the CC
- CPs expands to a lower pressure while its temperature decreases in the turbine. During the expansion process, turbine produces work output.
- CPs are rejected to ambient.

The main differences between an industrial gas turbine open cycle used for power generation and a jet engine open cycle used for aircraft engines are as follows:

- Industrial gas turbines are mainly used to produce electricity. Jet engines are used to produce propulsive power and some auxiliary power.
- Turbine is connected to a C via a coaxial shaft to provide it enough power, hence, the net work output of a jet propulsion cycle is zero.
- Industrial gas turbines expand CPs to atmospheric pressure in order to produce as much power as possible while aircraft engines expand CPs to a pressure just to provide enough power for C because after the expansion process in turbine, gases expand further in the N for acceleration (Çengel and Boles, 2005).



### **3. TURBOFAN, RAMJET, TURBOROCKET AND SCIMITAR ENGINES**

#### **3.1 Purpose**

First, an introductory level of information about turbofan, ramjet and turborocket engines is presented in this chapter since Scimitar engine employs the usage of the three different engine modes during its operation from take-off to landing.

Then, Scimitar engine with its design features and operating principles is presented in detail. Although turbofan and ramjet modes of Scimitar engine are not investigated in the thesis, it is appropriate to present brief information about processes regarding these flight modes as well as turbofan engines and ramjets in this chapter.

#### **3.2 Turbofans**

Currently, turbofan engines are the most popular and widely used jet engine type for commercial aircrafts. Their goal of invention was to fill the gap of turbojet and turboprop engines when flight conditions of around Mach 0.8 speed at around 11 *km* elevation is considered. This flight speed is too high for turboprop and low for turbojets when high propulsive efficiency is considered. Mach number versus engine propulsive efficiency characteristics are shown in Figure 3.1 (Hünecke, 2003).

As a different feature from turbojet engines, turbofan engines reject CPs at a lower speed but with a higher mass flow rate since turbofan engines deal with higher mass flow rates. This feature resulted in less jet noise which is an important parameter in jet engine design (Cohen et al, 1996).

As stated in Section 2.7, gas turbines used in aircraft propulsion differ from those used in industrial applications by means of the aim of usage and the expansion ratio in the turbine section. In addition, aircraft engine has a diffuser in the I section and an exhaust N in the exit section of the engine. Components and flow directions of a two spool turbofan engine are shown in Figure 3.2.

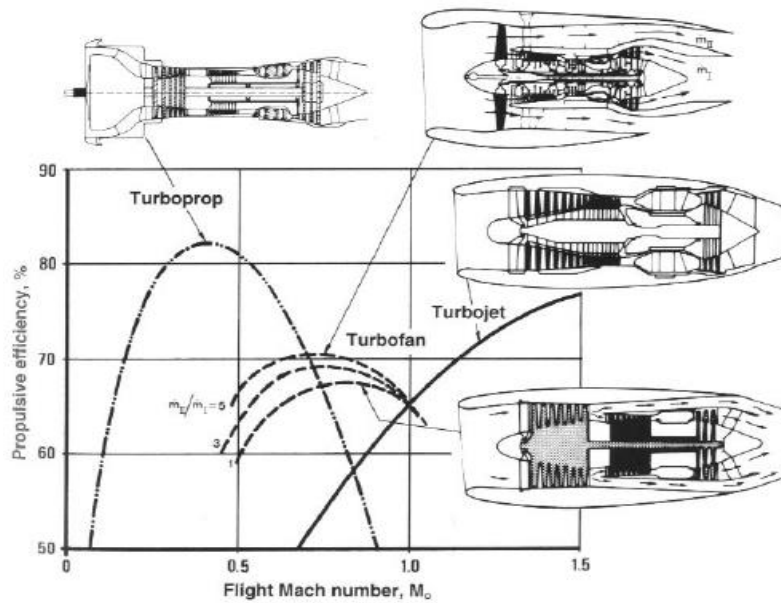


**Figure 3.1 :** Mach number versus engine propulsive efficiency characteristics (Hünecke, 2003).

As it is seen in Figure 3.2, air entering the engine separates in two ways after the F, some of the air flows through bypass duct while remaining air flows through the main core of the engine. Turbofan engines may also be modified to have an afterburner system to provide further thrust.

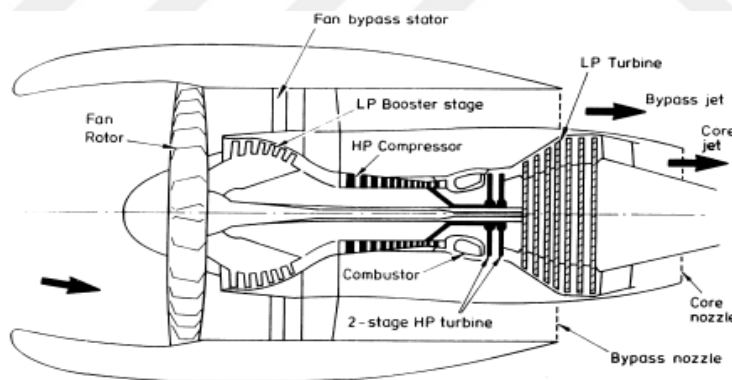


**Figure 3.2 :** A two-spool turbfan engine (Cumptsy, 2009).

Processes of an open cycle irreversible two-spool turbfan engine are shown on a  $T-s$  diagram in Figure 3.3. The station numbering and processes (El-Sayed, 2008). shown in Figure 3.3 are as follows:

- “ $a$ ” denotes atmospheric (ambient) conditions.
- “02” denotes stagnation conditions at the diffuser exit after the air pressure and temperature are increased.

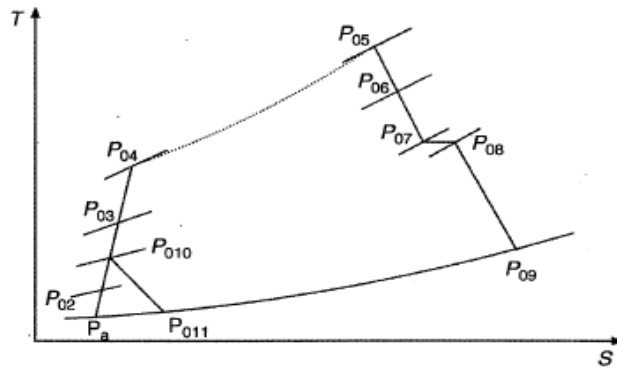


**Figure 3.3 :**  $T$ - $s$  diagram of a two-spool turbofan engine (El-Sayed, 2008).

- “010” denotes the compressed air leaving the F and moving through bypass duct.
- “011” denotes the air after expanding in the BN.
- “03” denotes the air exiting the low-pressure compressor (LPC).
- “04” denotes the air leaving the high-pressure compressor (HPC).
- “05” denotes the CPs leaving the CC.
- “06” denotes the CPs leaving the high-pressure turbine (HPT).
- “07” denotes the CPs leaving the low-pressure turbine (LPT).
- “08” denotes the stagnation condition at the end of jet pipe and its pressure is slightly decreased due to skin friction.
- “09” denotes the CPs leaving the CN.

### 3.3 Ramjets

Ramjets are the simplest air-breathing propulsion engines since they have no moving or rotating parts. Pressure increase in turbofans and turbojets is achieved through active compression by rotating turbomachinery. However, in ramjets, pressure of air is increased by the “ram” effect as it moves through the diffuser. Therefore, ramjets cannot move from standstill. Schematic diagram of a ramjet engine to provide information about its components and compression steps is shown in Figure 3.4. After slowing down in the diffuser, air enters the CC where combustion takes place. Last part of the engine is the C-D N where hot gases expand and accelerate. In order to complete combustion properly, Mach number is around Mach 0.2 – 0.3 at the

inlet of the CC. This shows that ramjets can operate at subsonic speeds but their pressure build up will be low in this case. Hence, using ramjets in supersonic regime ( $Mach > 1$ ) will result in greater expansion in the C-D N, which will create more thrust (Hill and Peterson, 1992).

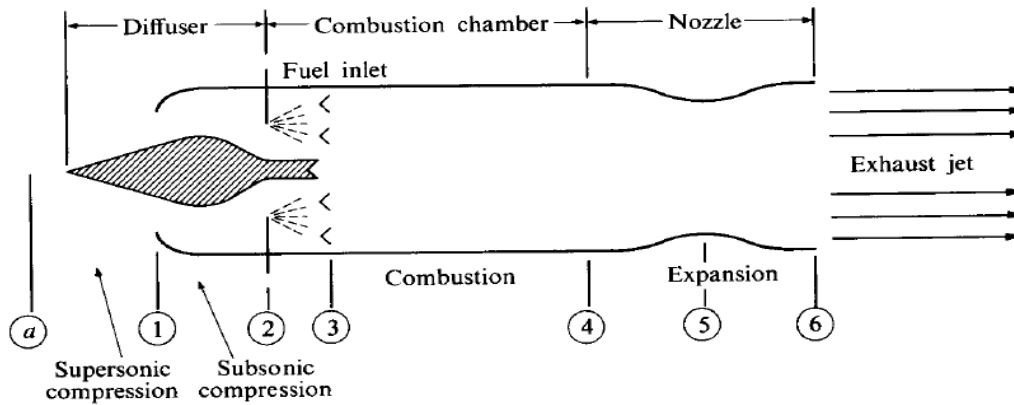


**Figure 3.4 :** Schematic diagram of a ramjet engine (Hill and Peterson, 1992).

A supersonic diffuser and a subsonic diffuser is illustrated in Figures 3.5 and 3.6, respectively.

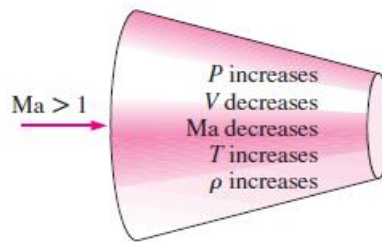


**Figure 3.5 :** Supersonic diffuser (Çengel and Boles, 2005).

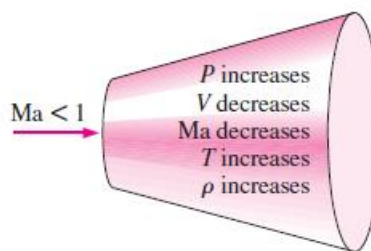


**Figure 3.6 :** Subsonic diffuser (Çengel and Boles, 2005).

In Figures 3.5 and 3.6, one can see that supersonic flow is first decelerated in a diffuser with decreasing cross section and its static pressure and temperature increases. Due to the normal shock in the supersonic difuser, total pressure decreases. After the normal shock, flow is entirely subsonic and flow is decelerated further by



an enlarging cross section diffuser. Variation of flow Mach number and cross section equations are derived in the following sections.

The processes of a ramjet engine are shown on a  $T-s$  diagram in Figure 3.7.

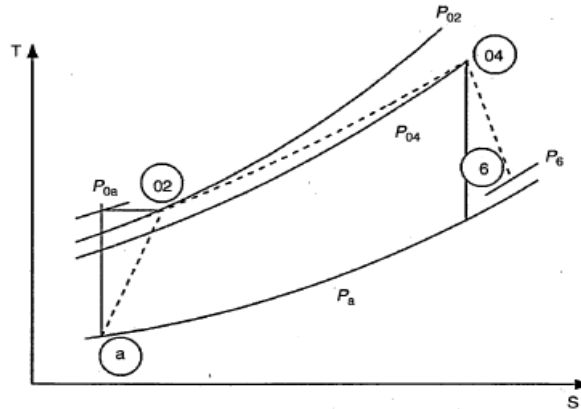


**Figure 3.7 :** Real cycle of a ramjet (El-Sayed, 2008).

Due to the irreversibilities of normal shock and friction, there exist pressure drops in the ramjet cycle shown in Figure 3.7 (El-Sayed, 2008).

### 3.4 Turbo-rockets

One of the major differences between turbo-rockets and the other jet engines (i.e., turbojets, turbofans and ramjets) is that turbo-rockets carry their own oxygen for combustion. A turbo-rocket engine is illustrated in Figure 3.8 (El-Sayed, 2008).

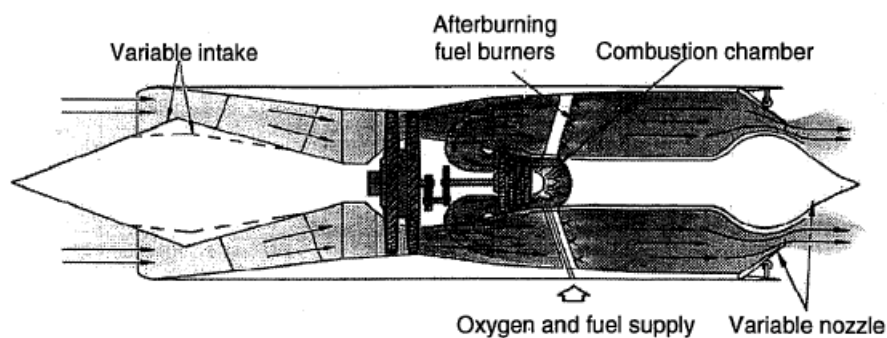


**Figure 3.8 :** Turbo-rocket engine (El-Sayed, 2008).

There exists an LPC that is driven by a multistage turbine. The turbine is driven by the thermal power obtained from the combustion of kerosene fuel and liquid oxygen in a CC. Gas temperature is expected to be around  $3500^{\circ}\text{C}$ ; hence, in order to reduce the temperature in the CC, additional fuel is injected into CC for cooling purpose before the gas enters to turbine. This gas mixture can be considered as fuel rich and it

is diluted with air coming from the C, and additional fuel is burned in a conventional afterburning system. When compared with the turbojets and ramjets, fuel consumption of turbo-rockets are higher than that of the others (El-Sayed, 2008).

### **3.5 Scimitar Engine; Design Features and Operating Principles**

Scimitar engine has been derived from the British company Reaction Engines Limited (REL) Sinergetic Air-Breathing Rocket Engine (SABRE). SABRE engine was designed by REL to propel the SKYLON single-stage-to-orbit (SSTO) reusable spaceplane. Scimitar engine has also been designed by REL to propel the aircraft namely A2 Long-Term Advanced Propulsion Concepts and Technologies (A2 LAPCAT) to fly a range of approximately 20,000 km (such as a range from Sydney to Bruxelles) at an altitude of 25.4 km in 4-5 hours at speeds up to Mach 5. It will have an acceptable level of efficiency at Mach 0.9 and longer life than that of SABRE. It will be quiet at take-off by eliminating sonic booms. Another innovative feature of the Scimitar engine is that its core (main) C and turbine do not use the same fluid; C will use air and turbine will use helium while they operate at their own optimum conditions regardless from cruise speed and operating modes (Jivraj et al., 2007; Uca et al, 2016).

In the past, some air breathing propulsion engines were considered for an SSTO rocket development. The turbojet engine, which is widely used at low Mach numbers, becomes limited in terms of performance when flight speed reaches to Mach 2. Due to the high stagnation temperatures, mass flow is decreased at an achievable CPR. However, a turbo-ramjet configuration would allow further acceleration by spilling the air into the bypass duct and combusting the fuel hydrogen with the oxygen in the air in the BBs. However, ramjets have no moving or rotating parts and in order to accelerate the engine it should have an I with variable cross-sectional area, which would increase the complexity and weight. Thrust to weight (T/W) ratio is low for turbo-ramjet configuration and this makes the engine impractical to use.

Liquid Air Cycle Engine (LACE) was also considered in 1960's for SSTO operation. This engine is also an airbreathing concept but with a cooling process before compression. Liquefaction (liquefaction) process in LACE is achieved by liquid hydrogen. It was intended to gather the oxygen inside the air before compression and

use the oxygen in the combustion process. However, the pinch point, which is the point in a HX where temperature difference is the minimum between hot and cold streams, dictates the amount of liquid hydrogen for cooling process. The liquid hydrogen must absorb the latent heat of condensation of air to liquefy it. However, in order to achieve it, hydrogen must have enough thermal capacity. Moreover, the maximum temperature of liquid hydrogen is limited with the air saturation temperature. A comparison (for Mach range, installed specific impulse and installed thrust to weight ratio value) of airbreathing engines and rockets versus precooled engines is given in Table 3.1.

**Table 3.1 :** Mach range, installed specific impulse and installed thrust to weight ratio values for different liquid hydrogen/liquid oxygen and precooled engines (Webber et. al, 2007).

Engine	Mach range	Installed I <sub>sp</sub> (s)	Installed T/W (N/kg)
<b>LH/LOX</b>			
Rocket (vac)	0 – 27	450 – 475	60 – 80
Ramjet (LH)	1 – 6	1500 – 3000	1 – 3.5
Scramjet	4 – 15	1000 – 3000	0.5 – 2
Turbojet	0 – 2.5	2000 – 6000	1 – 4
<b>Precooled Engine:</b>			
- LACE	0 – 6	600 – 1000	6 – 14
- SABRE	0 – 5.5	1500 – 3200	6 – 14

As it can be seen from Table 3.1, LACE has a good T/W ratio but a low specific impulse; on the other hand, SABRE not only has a good T/W ratio but also has a good specific impulse value. Limiting factors regarding the LACE design are eliminated in the SABRE by a new precooler design. During the precooling process of LACE, heat is transferred in such an amount that work capacity achieved by the heating is far more than it is needed to drive the C, hence the precooling process is a huge source of irreversibility. SABRE eliminates this problem by reducing the required mass flow rate of fuel by cooling the air just above its vaporization line and still providing enough work capacity for driving the AC.

### 3.5.1 Precooler of the scimitar engine

With the invention of the new precooling mentioned in the previous subsection and abandoning the liquefaction of air idea, SABRE and Scimitar engines are made possible (Webber et. al, 2007).

A prototype of the precooling and the flow directions of air leaving I and of the coolant helium in the precooling are illustrated in Figures 3.9 and 3.10, respectively.

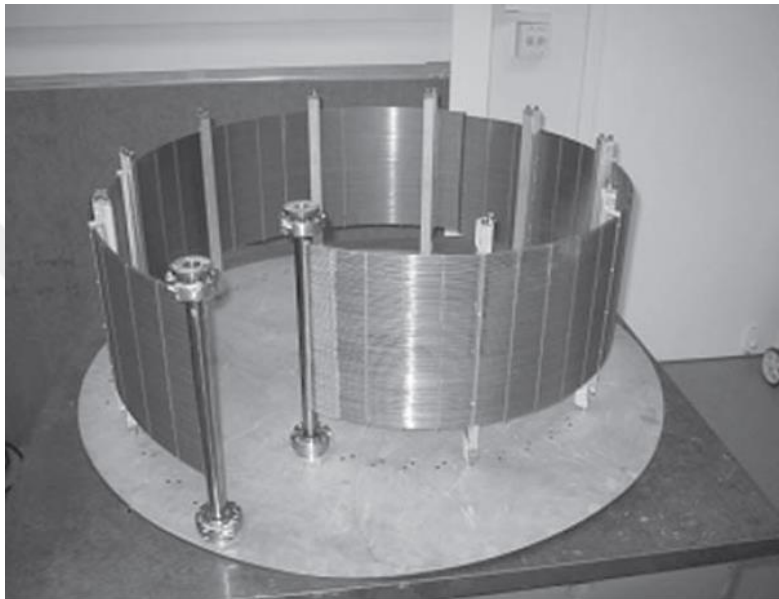


**Figure 3.9 :** Prototype of the precooling (Webber et. al, 2007).

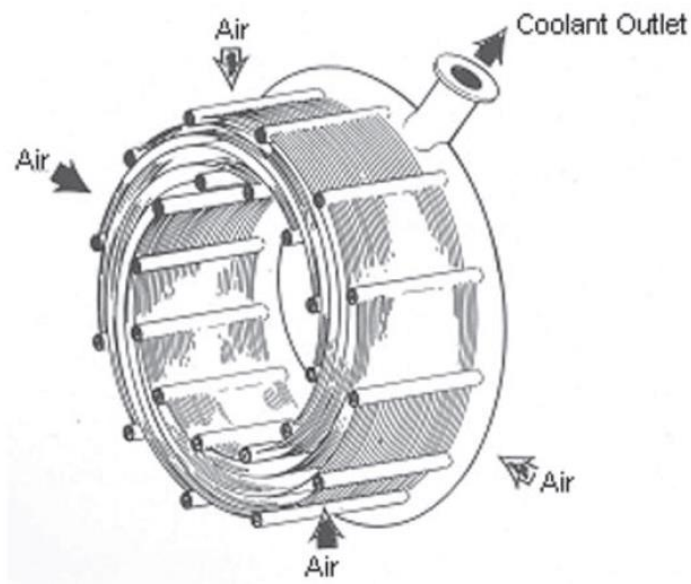


**Figure 3.10 :** Flow directions in precooling (Webber et. al, 2007).

### 3.5.2 Operating principles of the scimitar engine

Scimitar engine has the features of three different propulsion engines explained in Sections 3.2-3.4. In order to reach a speed of Mach 5, features of these three propulsion engines should be combined together.

The operating modes and the BB and BN status during acceleration and cruise phases at different speeds of the Scimitar engine are summarized in Table 3.2 (Fernandez-Villace and Paniagua, 2013a).

**Table 3.2 :** Various operating modes of the Scimitar engine (Fernandez-Villace and Paniagua, 2013a).

Mach Range	Regime	Mode	Bypass Burner	Bypass Nozzle
0-0.9	Acceleration	Turbofan	On	Open
0.9	Cruise	Turbofan	Off	Fully Open
0.9-2.5	Acceleration	Turbofan	On	Open
2.5-5.0	Acceleration	ATR+Ramjet	On	Open
5.0	Cruise	ATR	Off	Closed

As it is seen in Table 3.2, Scimitar engine operates in turbofan mode until the speed of Mach 2.5, in turbofan + air-turbo rocket (ATR) modes between Mach 2.5-5.0 and in ATR mode at Mach 5.0. Hence, only ATR mode is used while BB and BN are not active during the cruise of the Scimitar engine at the highest speed of Mach 5.0.

While cruising at Mach 5.0 stagnation temperature of the air is very high to be handled by the C. One of the most innovative features of this engine is having a lightweight HX that employs with the use of high-pressure (HP) helium, which powers the statorless contra-rotating helium T1. From a thermodynamic point of view, coupling of C and helium T1 is very clever idea since  $c_p$  value of helium is almost 4.5 times greater than that of air, which means that helium has 4.5 times lower temperature drop.

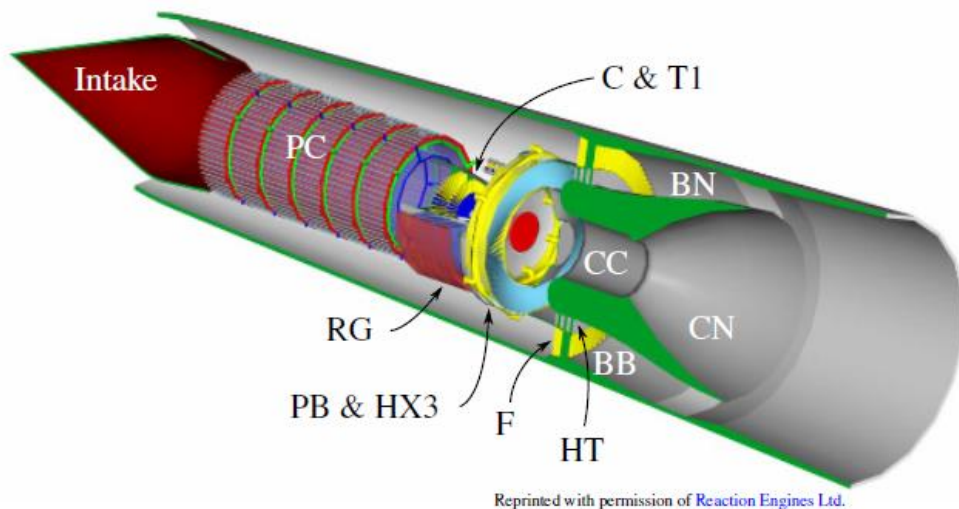
As it is for the ratio of specific heats,  $k$  value of helium is almost 20 percent greater than that of air, and it would result in lower pressure drop in helium T1. The same fluid, as their name suggests, does not couple C and helium T1. This is an important advantage when compared to turbofan and turbojet engines. Because, the CPR, the amount of fuel and the thermal energy added to the air during the combustion affect the exit temperature of CC in turbofan and turbojet engines. The temperature of CPs at the exit of CC is also equal to the turbine inlet temperature, which is an important

value for both material safety of turbine and power production for C (Jivraj et. al, 2007).

The LAPCAT A2 aircraft that will use the Scimitar engine and a 3D view of the Scimitar engine are illustrated in Figures 3.11 and 3.12, respectively (Marini et. al, 2013; Fernandez-Villace and Paniagua, 2013a).



**Figure 3.11 :** LAPCAT A2 (Marini et. al, 2013).



Reprinted with permission of Reaction Engines Ltd.

**Figure 3.12 :** A 3D view of Scimitar engine (Fernandez-Villace and Paniagua, 2013a).

As very well stated by Fernandez-Villace and Paniagua (2013a), helium follows a closed Brayton cycle between pre-cooler and hydrogen-helium HXs. When operating

above Mach 3, precooler is active and incoming air is cooled by precooler in which the coolant is helium. In order to complete the cycle, helium needs to reject heat to a sink which is hydrogen fuel in Scimitar engine.

Mach 0.9 and Mach 5.0 cruise modes of Scimitar engine are shown in Figure 3.13.

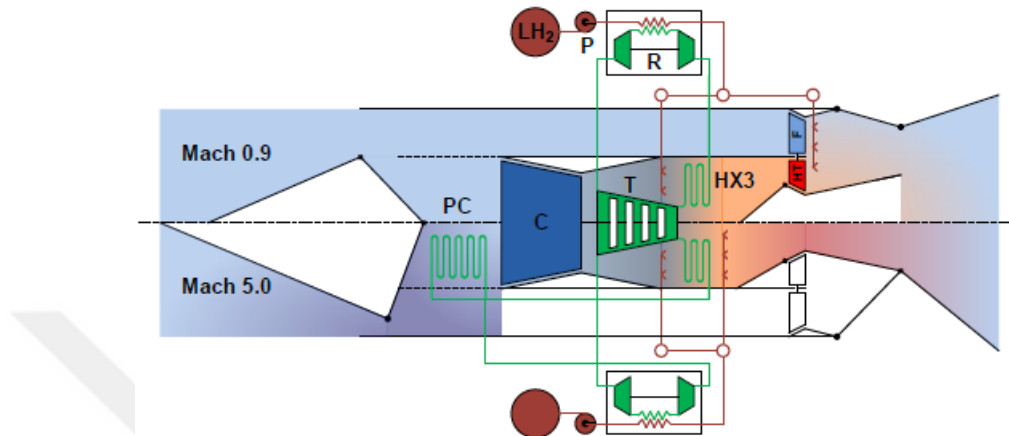


**Figure 3.13 :** Mach 0.9 and Mach 5.0 cruise modes of Scimitar engine (Fernandez-Villace and Paniagua, 2011).

Turbofan mode of the Scimitar engine is active between Mach 0 and 2.5. After the I, air is diverted into two separate ways. Some part of the air moving through the core of the engine while remaining air flows through the bypass channel. In the turbofan mode, precooler (PC) is not active since total temperature of the air is not higher than the helium temperature leaving the helium regenerators. Therefore, air directly enters the C and leaves the C with a higher temperature and pressure and moves to PB where it is combusted with hydrogen. Main duty of PB is to increase the temperature of the CPs, which exchange heat with helium in heat exchanger 3 (HX3). Helium leaving the HX3 enters the helium T1 at a fixed temperature of 1000 K independent of flight Mach number to keep helium T1 performance at optimum level. After the PB, all the core flow is diverted to bypass channel where they expand in the HT. HT powers the F which compresses bypass air. In the bypass channel, CPs from the core of the engine and air from the bypass channel are mixed and burned in BBs. CN is not used in turbofan mode. Lastly, expansion process takes in the BN.

Between Mach 2.5 and Mach 5, Scimitar engine acts as an air-turbo rocket with a ramjet burner in the bypass channel. In this configuration, both Ns are operational. Core flow is not completely drawn to bypass channel. Some part of the flow enters

the CC and expands in the CN. Meanwhile, mixed flow and hydrogen fuel is combusted in the BBs and expands in the BN.

At Mach 5.0, Scimitar engine operates as an air-turbo rocket only, which is the subject of this thesis. While air-turbo rocket mode is active, bypass channel is completely closed. Only core of the engine is active. After the I, air pressure and temperature is increased. C inlet temperature is limited to 635 K by the designers, consequently air needs to be cooled and the transferred energy is used to power C through helium T1 by the helium. After the C stage, a small amount of hydrogen fuel is burned in the PB to further increase the temperature of the air leaving the C. In HX3, the helium cools CPs as it reaches 1000 K and enters helium T1. After being cooled in HX3, oxygen rich CPs enter CC to be combusted with the remaining hydrogen. Resultant high temperature gas enters the CN for expansion process (Fernandez-Villace and Paniagua, 2011; Jivraj et al, 2008).

### **3.5.3 Scimitar engine in atr mode at mach 5.0**

Schematic diagram of the Scimitar engine at Mach 5.0 is illustrated in Figure 3.14 (Modified from Figure 4 in Jivraj et al. (2007) by (Uca et al, 2016)).

Air enters the engine at Mach 5.0 speed. After being compressed, air flows towards the precooler since Valve 1 is closed. Closing Valve 1 disables flow towards the bypass channel. Therefore, in the fan-hub turbine spool, BB and BN are not active. Valve 2, which enables bypassing precooler in lower Mach number flights is closed. In lower Mach numbers, air leaving the I is not very hot and no precooling is needed. Also, if temperature of air leaving the I is higher than the C inlet temperature  $T_{05}$ , which should not exceed 635 K, but lower than the HTR exit temperature which is  $T_{66}$ , air enters the low temperature segment of the precooler which is the HX2 (Fernandez-Villace and Paniagua, 2013a).

In this case air is only cooled by the stream with temperature  $T_{88}$  coming from the LTR. If air temperature is lower than 635 K no precooling is needed. If total temperature of the air leaving I,  $T_{02} = T_{03}$ , is greater than the  $T_{66}$ , which is the case in Mach 5.0, Valve 2 is closed and air is forced to flow through precooler. After leaving precooler air enters C where its temperature and pressure is increased. After compressor, it enters the PB where it is combusted by a small amount of hydrogen to increase its temperature. Between CC and PB air is



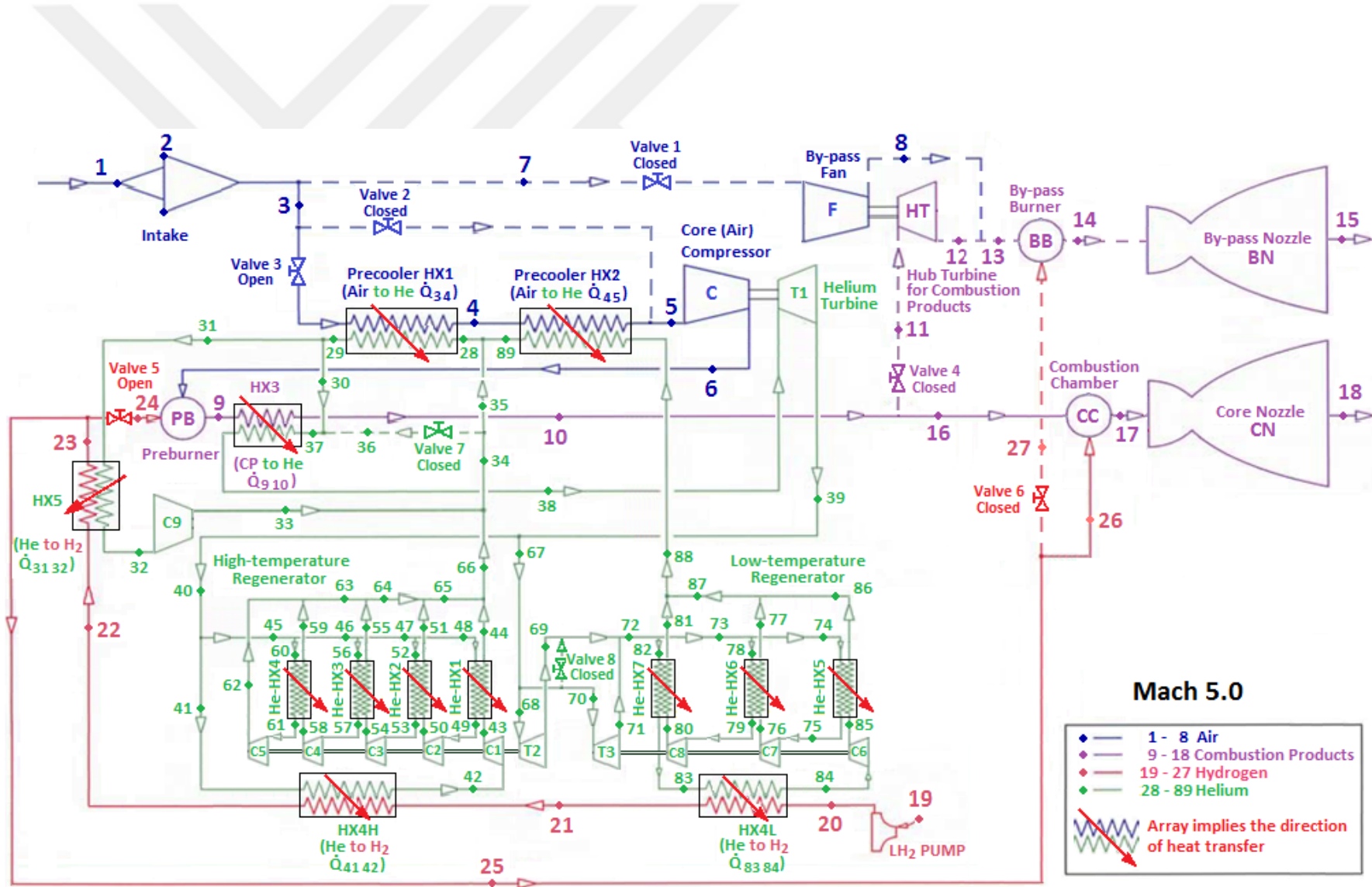


Figure 3.14 : Schematic diagram of the Scimitar engine at Mach 5.0 (Modified from Figure 4 in Jivraj et al. (2007) by (Uca et al, 2016)).

cooled in HX3. After a cooling about 40 K, CPs enter CC where they are combusted by the remaining hydrogen fuel and their temperature is increased significantly. Final step for CPs is the expansion where they are rejected in C-D N at very high speeds.

**3.5.4 T-s diagram and processes in atr mode of the propellant fluid of the scimitar engine at mach 5.0**

Processes, fuel mass flow rates and heat transfer rates are illustrated on a T-s diagram of the propellant fluid of the Scimitar engine at Mach 5.0 drawn during the thesis in Figure 3.15 (Uca et al, 2016).

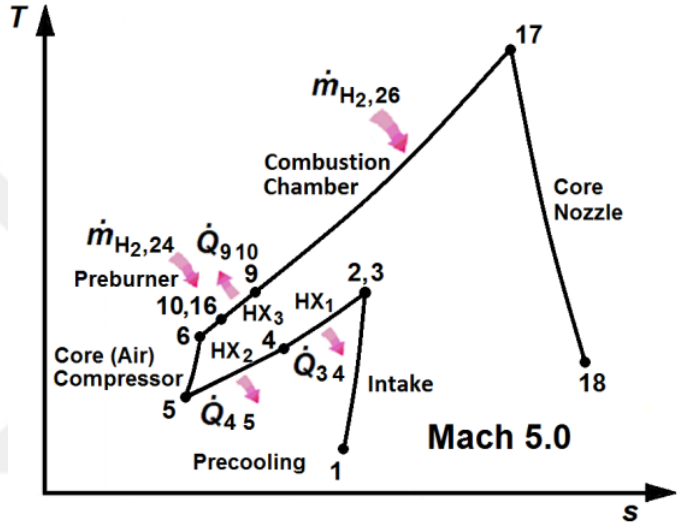


Figure 3.15 : T-s diagram of the Scimitar engine at Mach 5.0 (Uca et al, 2016).

As it can be seen in Figure 3.15, Scimitar engine at Mach 5.0 operates on an open irreversible air-breathing air-turbo rocket (ATR) cycle with a precooling step between points 2, 3 and 5 in heat exchangers 1 and 2 (HX1 and HX2).

Although the T-s diagram is a representative drawing, it still clearly shows the temperature, pressure and entropy changes of the propellant fluid in the cycle. Hence, the T-s diagram represents the cycle consisting of the processes of the propellant fluid, which is air up to point 6, and CPs from point 6 to point 18.

By the aid of, Figure 3.15, processes in ATR mode of the Scimitar engine at Mach 5.0 at an altitude of 25.4 km can be listed as follows:

- 1-2: Air entering at ambient conditions with a speed of Mach 5.0 is compressed and slowed down through I. Since valve 1 (V1) is closed, states 2 and 3 have the same properties.

- 3-4: Air is cooled by high-pressure (HP) He through HX1 in the first part of the precooler (PC) after leaving I.
- 4-5: Air is further cooled by HP He through HX2 in the second part of PC.
- 5-6: Air is compressed to a higher pressure and temperature by C.
- 6-9: A small part of the H<sub>2</sub> fuel is burnt with O<sub>2</sub> in the air in PB.
- 9-10: CPs leaving PB transfers heat to He to increase its temperature to 1000 K. Valve 4 (V4) is closed, therefore the properties of positions 10 and 16 are the same.
- 16-17: Remaining H<sub>2</sub> fuel is burnt with O<sub>2</sub> in the entering CPs in CC to increase the temperature of CPs to around 2700 K.
- 17-18: CPs leaving CC are accelerated by the C-D CN.

### 3.5.5 Helium cycle of the scimitar engine

In Scimitar engine, helium is used as an intermediate medium that operates between hot air and cryogenic hydrogen. Helium transfers heat from hot air and with it produces work for C and helium C-turbine spool in high- and low-temperature helium regenerators (HTR-LTR). Helium cools the air in two different segments of the precooler. These segments are namely HX1 and HX2. HX1 and HX2 use different mass flow rates, which is the key concept in heat transfer processes in helium cycle.

Helium is a monatomic ideal gas and  $c_p$ ,  $c_v$  and  $k$  value of ideal gases are functions of temperature. However,  $c_p$ ,  $c_v$  and  $k$  values of monatomic gases change very little with respect to temperature so they can be considered as constants throughout the cycle. Knowing that thermal capacity is very important in HXs, a selection of a monatomic gas will make things a lot easier. By only changing the mass flow rate, one can change thermal capacity ratio across a HX. Knowing thermal capacity ratios will directly give the inventor an idea about temperature drops and rises in hot and cold streams.

Figure 3.16 shows the thermal capacity ratios relative to hydrogen in the Scimitar engine.

Although in real life applications  $c_p$  values of air and especially hydrogen change with temperature, red numerals on the green line that indicate helium cycle is very

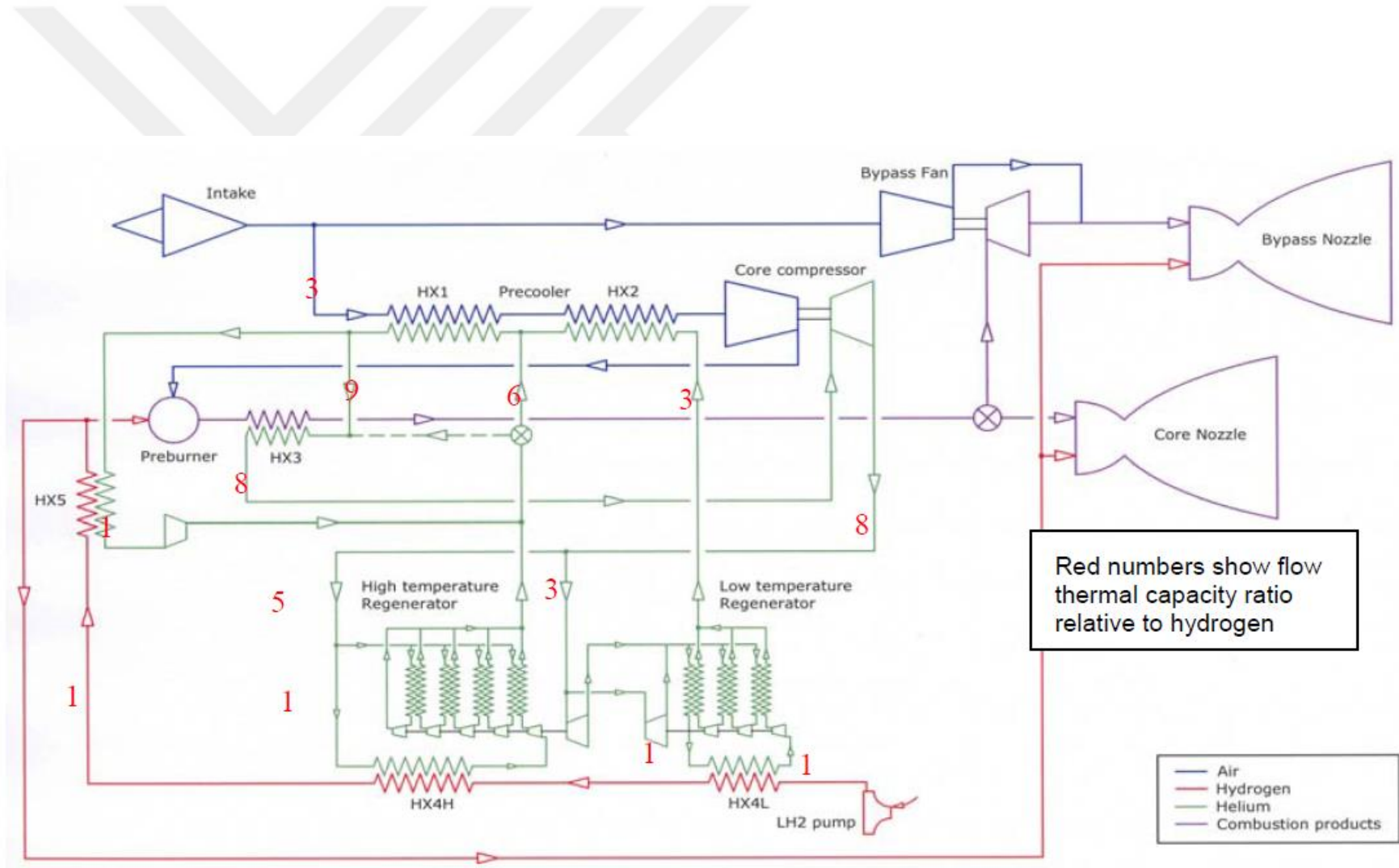


**Figure 3.16 :** Thermal capacity ratios of fluids relative to hydrogen entering the cycle (Jivraj et al, 2007).

useful for understanding the mass flows of helium since its  $c_p$  value is considered constant. Scimitar engine uses hydrogen as fuel and hydrogen is kept at very low temperatures (at 20 K) in liquid state due to storage volume considerations. In Low-temperature heat exchanger 4 (HX4L), hydrogen changes phase and before and after the heat transfer there is a considerable change in  $c_p$  of hydrogen. In precooler heat exchangers, thermal capacity ratios of air and helium is changed by changing helium mass flow rates. Thermal capacity ratios may not be exactly as stated in Figure 3.16 but they are close. For example, in the HX1 temperature drop ratio is almost 1/3. In the HX2, thermal capacity ratio of the helium is 3 and in the HX1 it is 9, which means helium stream coming from the LTR and entering the HX2 is mixed with the stream whose mass flow rate is 2 times of it. The stream leaving the HX1 separates into two arms where 1/9 of the mass flow enters the heat exchanger 5 (HX5) to reject heat to hydrogen stream. Other part of the stream enters the HX3 to cool the air slightly while increasing its temperature to 1000 K. This helium stream enters the helium T1. Therefore, by examining Figure 3.16 we can say that at Mach 5.0, a helium stream that has 1/8 of the mass flow entering helium T1 recirculates between stations 31 – 32 – 33 – 34 – 35 – 31. This helium stream joins the stream coming from the HTR and cools the air, then separates from the stream and enters the HX5 and rejects heat to hydrogen eventually causing hydrogen fuel to get hotter.

Helium rejects heat to hydrogen not only in HX5 but also in two more different HXs. Helium stream with a mass flow 1/8 of the mass flow entering helium turbine ( $0.125\dot{m}_{He}$  and mass flow rate of the helium entering the turbine is  $\dot{m}_{He}$ ), rejects heat to hydrogen fuel at storage conditions causing it to evaporate. After the heat transfer process in HX4L, helium stream enters the C where its pressure and temperature are increased. In helium regenerator HXs helium streams are cooled by other helium streams having equal mass flow rates therefore having matched thermal capacities. Matched thermal capacities mean temperature drop on the hot side is equal to the temperature rise in the cold side. For example; hot stream from station 74 gets colder in HX and enters the C at station 75. After the compression process at station 76 where it has higher pressure and temperature enters the next HX and cools the hotter stream flowing between station 78 – 79. Same procedure is followed in the HTR. After the expansion process in main helium turbine, helium

streams are separated from each other, one having  $0.625\dot{m}_{He}$  mass flow rate and the other one having  $0.375\dot{m}_{He}$  mass flow rate.

The stream with high mass flow enters the HTR while the stream with low mass flow rate enters helium turbines T2 and T3 that power the Cs in high and LTRs respectively. After the expansion in the turbines, the helium streams mix and continue into the LTR.

Helium heat exchanging process with matched thermal capacity is illustrated in Figure 3.17.

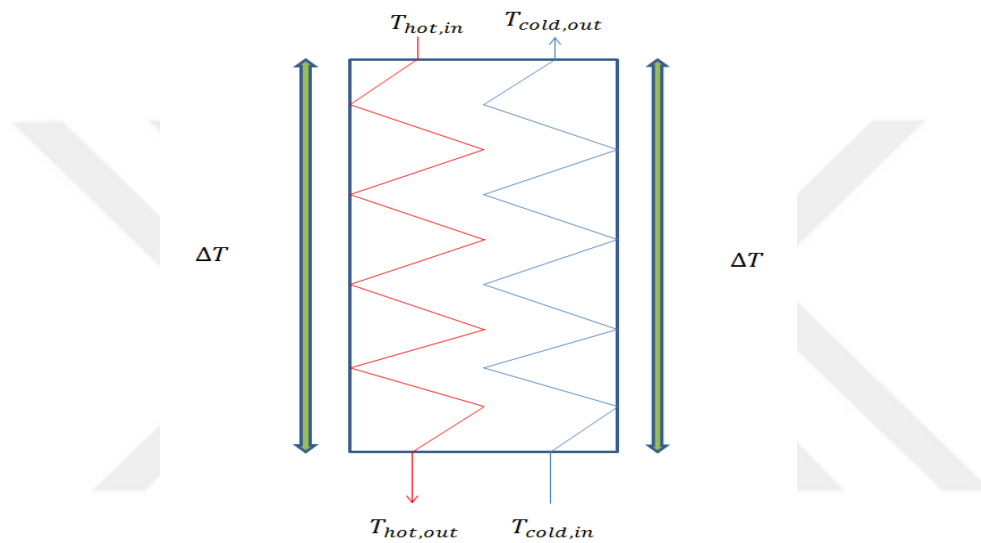


**Figure 3.17 :** Helium heat exchanging process with matched thermal capacity.

Since helium streams have matched (same) thermal capacity ratios, the temperature drop on the hot side will be equal to the temperature rise in the cold side.

## 4. THEORETICAL MODEL OF THE SCIMITAR ENGINE

Assumptions for the Scimitar engine model utilized during calculations, derivations of the thermodynamic relations for the Scimitar engine subcomponents, the rate of global energy balance and performance parameters for the Scimitar engine are presented in this chapter.

### 4.1 Assumptions for the Scimitar Engine Model

Assumptions for the Scimitar engine model in this study are as follows:

- An open irreversible cycle for a precooled ATR engine is considered.
- Cruise speed is Mach 5.0.
- Air is an ideal gas mixture of  $O_2$  and  $N_2$ . While determining the thermophysical properties of air and CPs, thermophysical properties of each species are considered separately. CPs includes water vapor in the mixture.
- During the compression in I and C, average  $c_p$  and  $k$  values of the processes are used by considering constant specific heats at an average temperature.
- He is an ideal gas with constant specific heats;  $c_{p,He} = 5.1926 \text{ kJ/kgK}$  and  $k_{He} = 1.667$ .
- $H_2$  has varying specific heats.
- $v_{20}$  and  $A_{20}$  related to  $H_2$  fuel are neglected.
- For each component, pressure drop is 5% in HX1, HX2, HX3 and it is 10%.in PB and CC for the propellant air and CPs side.
- Compressor pressure ratio (CPR) defined as  $r_c = P_{06}/P_{05}$  is 4.1.
- All processes involving steady-flow components (such as I, HXs, Cs, Ts, PB, CC and C-D N) are steady-flow processes, potential energy-exergy changes in, and heat losses from all of these components are negligible in the Scimitar Engine at Mach 5.0.

- Polytropic efficiencies of turbomachinery are used.
- Power consumed in C9 is neglected.
- In the combustion processes, adiabatic flame temperature approach is used.

## 4.2 Thermodynamic Relations Derived for the Scimitar Engine Subcomponents

In this section, derivation of the thermodynamic relations of the propellant fluid for each subcomponents from I to C-D N including combustion process relations and those of the helium cycle of the Scimitar engine utilized in the analysis are presented in detail.

### 4.2.1 Intake

Scimitar engine is designed to cruise at Mach 5.0 which means the air entering the engine is very fast. In order to slow down the incoming air, supersonic cruisers, ramjets and scramjets use supersonic variable intakes that create a shockwave to slow the incoming air and causing a drop in stagnation pressure.

Scimitar engine uses a supersonicI that employs the use of ceramics. Therefore, it can be modeled as adiabatic (Fernandez-Villace, 2013a).

Enthalpy-entropy diagram of a compression process is shown in Figure 4.1.

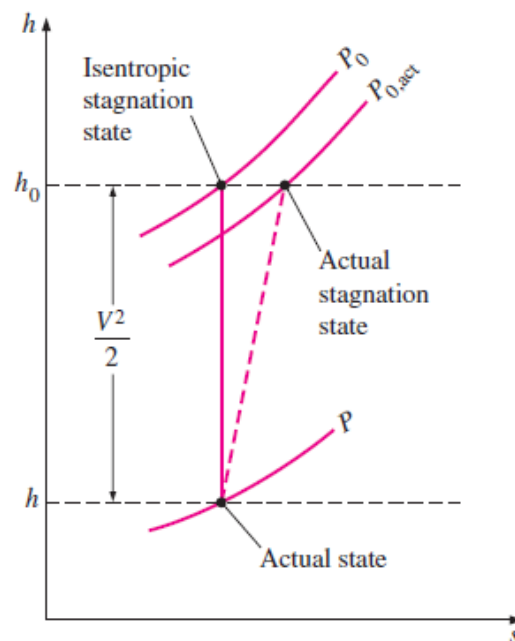


**Figure 4.1** : Enthalpy-entropy diagram of a compression process (Çengel and Boles, 2005).



Steady flow energy balance equation for a control volume is given in equation (2.2). As stated in section 4.1, considering the Scimitar engine I as adiabatic, also knowing that there is no work done on or by the I control volume (therefore, there will be no heat and work interaction), also assuming there is no change of elevation and no mass addition and also replacing subscripts 1 and 2 with *in* and *out* to denote inlet and exit conditions of I in equation (2.2) becomes

$$h_1 + \frac{v_1^2}{2} = h_2 + \frac{v_2^2}{2} \quad (4.1)$$

If the flow were brought to rest, there would only be stagnation (total) enthalpy at the exit  $h_{02}$  as it is given in equation (2.5). In order to find stagnation temperature, constant  $c_p$  terms at an average temperature can be applied. Also, dividing both sides by  $c_p$ , equation (4.1) yields

$$T_1 + \frac{v_1^2}{2c_p} = T_2 + \frac{v_2^2}{2c_p} \quad (4.2)$$

Also, since the process is adiabatic, total (stagnation) temperatures at the inlet  $T_{01}$  and exit  $T_{02}$  will be equal to equation (4.2) as it is given in equation (2.9). Dividing both sides of equation (4.2) by  $T_1$  yields

$$\frac{T_{02}}{T_1} = 1 + \frac{v_1^2}{2c_p T_1} \quad (4.3)$$

Using fundamental relations for the gas constant as the difference between specific heats and the ratio of specific heats,

$$R = c_p - c_v \quad (4.4)$$

$$k = \frac{c_p}{c_v} \quad (4.5)$$

and rearranging,  $c_p$  becomes

$$c_p = \frac{kR}{k-1} \quad (4.6)$$

In addition, flow velocity in terms of Mach number, Çengel and Boles (2005), is

$$v_1 = M_1 \sqrt{kRT_1} \quad (4.7)$$

Finally, substituting equations (4.6) and (4.7) into equation (4.3) yields the total temperature at the I exit and inlet as

$$T_{02} = T_{01} = T_1 \left[ 1 + \frac{k-1}{2} M_1^2 \right] \quad (4.8)$$

Equation (4.8) is the relationship between flight Mach number and total temperature at the I exit. If this process is assumed as reversible, then isentropic relations can be used since the process becomes reversible and adiabatic which means isentropic.

Writing the isentropic relation among total pressure  $P_{01}$ , static pressure  $P_1$ , total temperature  $T_{01}$  and static temperature  $T_1$  as it is presented in equation (2.10) yields the total pressure  $P_{01}$ . In supersonic intakes, there is a great total pressure loss due to friction and normal shock.

*Kinetic efficiency* is the ratio of kinetic energy at the I exit “a” if the flow were expanded to atmospheric conditions isentropically, to the freestream kinetic energy at the I inlet “1”. It is an important efficiency term used in supersonic inlets since it is directly related to kinetic energy. Capturing the freestream kinetic energy is very important in ramjets and scramjets because the thrust is created by the incoming kinetic energy. During the derivations, a fictional point “a” is defined to indicate the state of the isentropically expanded flow from the actual state 02. Figure 4.2 shows the real compression process between “0” to “3” and the fictional isentropic expansion process from “3” to “x” in the I.

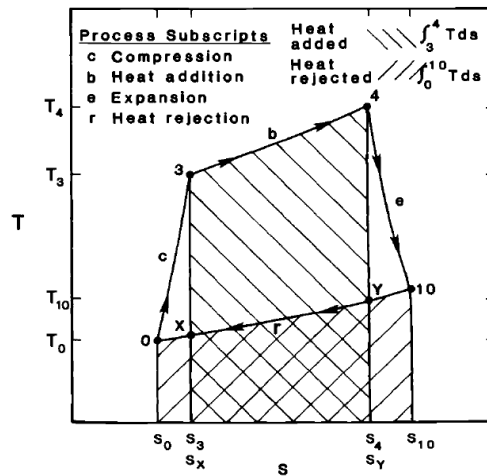


**Figure 4.2 :**  $T$ - $s$  diagram of the process in the intake (Heiser et. al, 1994).

The notations used in Figure 4.2 and in this thesis are different but the calculation procedure is the same. Air at free stream conditions at “0” enters the I. Its temperature and pressure are increased to “3”. The state “x” denotes the fictional state what expanded isentropically to the free stream pressure. It can be confirmed by examining that “x” and “0” are at the same pressure line. Notations used in this thesis are “1”, “a” and “02” instead of using “0”, “x”, “3” used in Figure 4.2, respectively.

Now, for the processes of 0-3 and 3-x (from initial state 0 to final state x) given in Figure 4.2 which corresponds to processes 1-2 and 2-a (from initial state 1 to final state a) with the utilized notations in the thesis, *kinetic efficiency* (denoted by  $\eta_{KE}$ ) is defined by (Heiser et. al, 1994) as

$$\eta_{KE} = \frac{v_a^2}{v_1^2} \quad (4.9)$$

Equation (4.2) can be rearranged gathering  $c_p$  terms together, dividing both sides by  $v_1^2$ , to yield  $v_a^2/v_1^2$ , then it is combined with equation (4.9) and rearranging yields

$$\eta_{KE} = 1 - \frac{2c_p(T_a - T_1)}{v_1^2} \quad (4.10)$$

Substituting equations (4.13) and (4.14) into equation (4.20) and simplifying yields

$$\eta_{KE} = 1 - \frac{2}{(k-1)M_1^2} \left( \frac{T_a}{T_1} - 1 \right) \quad (4.11)$$

Now, let us define a new parameter called TPR (the ratio of total pressures at I exit to I inlet) and denoting it by the symbol  $\pi_c$  (as it is used in textbooks such as by Heiser et al, (1994) and Mattingly (2006)) as

$$\pi_c = \frac{P_{02}}{P_{01}} \quad (4.12)$$

$\pi_c$  can also be written as

$$\pi_c = \frac{P_2}{P_1} \cdot \frac{\frac{P_{02}}{P_2}}{\frac{P_{01}}{P_1}} \quad (4.13)$$

The second term on the right hand side of equation (4.13) can be written by using the relations between static and stagnation temperatures of inlet and exit. Then,  $\pi_C$  becomes

$$\pi_C = \frac{P_2}{P_1} \cdot \frac{\left(\frac{T_{02}}{T_2}\right)^{k/(k-1)}}{\left(\frac{T_{01}}{T_1}\right)^{k/(k-1)}} \quad (4.14)$$

Substituting the explicit forms of total to static temperature ratios results with

$$\pi_C = \frac{P_2}{P_1} \cdot \frac{\left(1 + \frac{k-1}{2} M_2^2\right)^{k/(k-1)}}{\left(1 + \frac{k-1}{2} M_1^2\right)^{k/(k-1)}} \quad (4.15)$$

Now, *static temperature ratio*  $\tau$  is introduced. Equation (4.15) shows the TPR as a function of static pressures and Mach numbers on both sides of the I. However, value of  $M_2$  is not concerned at the moment since there is a need for a TPR expression that includes  $\eta_{KE}$ .  $\tau$  is equal to

$$\tau = \frac{T_2}{T_1} \quad (4.16)$$

Equation (4.16) can be written in terms of the total to static temperature ratios as

$$\tau = \frac{\frac{T_{01}}{T_1}}{\frac{T_{02}}{T_2}} = \frac{1 + \frac{k-1}{2} M_1^2}{1 + \frac{k-1}{2} M_2^2} \quad (4.17)$$

$T_{01}$  and  $T_{02}$  are equal to each other, hence they cancel in equation (4.17). Substituting equation (4.17) into (4.15) yields

$$\pi_C = \frac{P_2}{P_1} \cdot \left(\frac{1}{\tau}\right)^{k/(k-1)} \quad (4.18)$$

The compressed flow is expanded to free stream conditions isentropically. Therefore, entropy difference must be the same (Heiser et. al, 1994).

$$s_2 - s_1 = s_a - s_1 \quad (4.19)$$

which clearly shows that  $s_2 = s_a$  for the isentropic process 2-a. The states a and 1 are at the same pressure. Hence, equation (4.19) becomes

$$s_2 - s_1 = s_a - s_1 = c_p \ln\left(\frac{T_a}{T_1}\right) - R \ln(1) \quad (4.20)$$

For the entropy change between states 1 and 2

$$s_2 - s_1 = c_p \ln\left(\frac{T_2}{T_1}\right) - R \ln\left(\frac{P_2}{P_1}\right) \quad (4.21)$$

It is known from equation (4.19) that entropy changes are the same. Hence, results of equations (4.20) and (4.21) are the same, which yields

$$c_p \ln\left(\frac{T_a}{T_1}\right) = c_p \ln\left(\frac{T_2}{T_1}\right) - R \ln\left(\frac{P_2}{P_1}\right) \quad (4.22)$$

Gathering temperature related terms together results with

$$\ln\left(\frac{T_a T_1}{T_1 T_2}\right)^{c_p} = \ln\left(\frac{P_2}{P_1}\right)^{-R} \quad (4.23)$$

$$\left(\frac{T_a}{T_2}\right)^{c_p} = \left(\frac{P_2}{P_1}\right)^{-R} \quad (4.24)$$

Then, static PR can be found as

$$\frac{P_2}{P_1} = \left(\frac{T_2}{T_a}\right)^{\frac{c_p}{R}} \quad (4.25)$$

Arranging equation (4.25) in a way to include  $\tau$  yields

$$\frac{P_2}{P_1} = \left(\tau \frac{T_1}{T_a}\right)^{\frac{c_p}{R}} \quad (4.26)$$

Substituting equation (4.6) for the power of the right hand side term in equation (4.26) yields

$$\frac{P_2}{P_1} = \left( \tau \frac{T_1}{T_a} \right)^{\frac{k}{k-1}} \quad (4.27)$$

Substituting equation (4.27) into (4.18) yields

$$\pi_C = \left( \tau \frac{T_1}{T_a} \right)^{\frac{k}{k-1}} \cdot \left( \frac{1}{\tau} \right)^{\frac{k}{k-1}} \quad (4.28)$$

$$\pi_C = \left( \frac{T_1}{T_a} \right)^{\frac{k}{k-1}} \quad (4.29)$$

which can be rearranged to obtain

$$\frac{T_a}{T_1} = \left( \frac{1}{\pi_C} \right)^{\frac{k-1}{k}} \quad (4.30)$$

Substituting equation (4.30) into (4.11) yields

$$\eta_{KE} = 1 - \frac{2}{(k-1)M_1^2} \cdot \left[ \left( \frac{1}{\pi_C} \right)^{\frac{k-1}{k}} - 1 \right] \quad (4.31)$$

Writing TPR term  $\pi_C$  in the left hand side results with

$$\left( \frac{1}{\pi_C} \right)^{\frac{k-1}{k}} - 1 = \frac{(1 - \eta_{KE})(k-1)M_1^2}{2} \quad (4.32)$$

$$\pi_C = \left[ 1 + \frac{(1 - \eta_{KE})(k-1)M_1^2}{2} \right]^{\frac{-k}{k-1}} \quad (4.33)$$

TPR across the I is found. This arrangement is very useful when calculating the total pressure at the I exit with respect to  $M_1$  and  $\eta_{KE}$ . Heiser et al (1994) and Fernandez-Villace and Paniagua (2013a) directly use this approach for finding the total pressure at the exit.

Mattingly (2006), proposes another approach for the same expression  $\pi_C$ . The TPR, which is  $P_{02}/P_{01}$  in this study, is referred as *pressure recovery factor*. It is written as

$$r_D = \frac{P_{02}}{P_{01}} \quad (4.34)$$

$r_D$  can be written as

$$r_D = r_{D,f} r_{D,s} \quad (4.35)$$

where,  $r_{D,f}$  is the friction related and  $r_{D,s}$  is the shockwave loss related term. They both represent the pressure loss occurring during the process through the I.  $r_{D,f}$  can be taken as a value close to 1, however shock related term can not be taken since it is given as a partial function of flight Mach number. When flight speed is subsonic which means Mach number is less than 1, consequently there is no shockwave occurring inside the I. However, when flight speed is greater than Mach 1, the functions given as

$$r_{D,s} = \begin{cases} 1 - 0.075(M_0 - 1)^{1.35} & 1 < M_0 < 5 \\ \frac{800}{M_0^4 + 935} & 5 < M_0 \end{cases} \quad (4.36)$$

can be used (Mattingly, 2006; Colakoglu, 2015). Equation (4.36), which is the military specification MIL-E-5008B, is a generalized expression of the ram recovery for supersonic and hypersonic vehicles (Mattingly, 2006).

When Scimitar engine flight conditions are used in equations (4.33) and (4.34), there is great difference with the simulation results of the Fernandez-Villace and Paniagua (2013a) which is considered as an important study while studying Scimitar engine. Therefore, instead of using equation (4.36) including MIL-E-5008B, equation (4.33) is used for TPR calculations in this thesis as it is used in (Fernandez-Villace and Paniagua, 2013a).

Next step is calculating the total energy flow rates with respect to the reference conditions, which are the atmospheric conditions of air at the inlet of I,  $P_1 = 2.4 \text{ kPa}$  and  $T_1 = 222 \text{ K}$  at the flight conditions of 25.4 km altitude.

In this study, air total energy flow rates regarding the engine subcomponents are considered. Air is treated as an ideal gas mixture consisting of  $O_2$  and  $N_2$ .

$$\dot{E}_{01} = \dot{m}_1 \left( c_p T_1 + \frac{v_1^2}{2} - h_1 \right) \quad (4.37)$$

There are no heat and work interactions through the I. Therefore, the total energy flow rates entering and exiting the I will be equal.

$$\dot{E}_{02} = \dot{m}_1 \left( c_p T_2 + \frac{v_2^2}{2} - h_1 \right) \quad (4.38)$$

#### 4.2.2 Air compressor

Thermodynamic relations regarding the C are derived in this subsection. Figure 4.3 shows the *h-s* digram of a compression process.

In this study, C is considered as adiabatic but irreversible. In real life applications PR of turbomachinery changes. A C may be considered as a turbomachine performing large numbers of small compression steps. When CPR changes, total efficiency of the C changes. This may be misleading when Cs with two different CPRs are compared in terms of isentropic efficiency (Dixon, 2005).

Although the process in C is not polytropic such as a compression with heat transfer, polytropic efficiency is used as a correction factor for the isentropic relations for an adiabatic but irreversible process. Therefore, it is used as *differential pressure change based irreversibility correction factor for an isentropic relation* (Çolakoğlu, 2015).

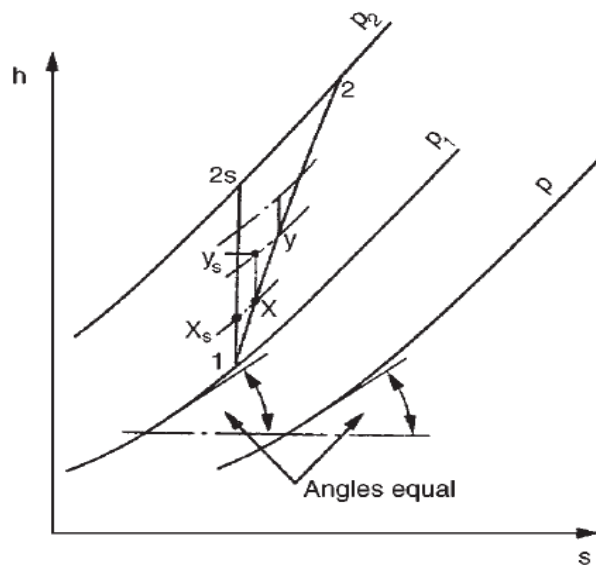


**Figure 4.3 :** Compression process by small angles (Dixon, 2005).



Here, polytropic efficiency of C is denoted by  $e_c$

$$e_c = \frac{\text{enthalpy change in isentropic process}}{\text{enthalpy change in actual process}} = \frac{dh_{0s}}{dh_0} \quad (4.39)$$

Assuming the process is adiabatic and written for stagnation conditions

$$T_0 ds = 0 \quad (4.40)$$

and

$$dh_{0s} - v_0 dP_0 = 0 \quad (4.41)$$

$$dh_{0s} = v_0 dP_0 \quad (4.42)$$

Recalling efficiency term

$$e_c = \frac{dh_{0s}}{dh_0} = \frac{v_0 dP_0}{c_p dT_0} \quad (4.43)$$

For an ideal gas

$$v_0 = \frac{RT_0}{P_0} \quad (4.44)$$

Substituting equation (4.44) into equation (4.43)

$$e_c = \frac{R}{c_p} \frac{T_0}{P_0} \frac{dP_0}{dT_0} \quad (4.45)$$

Substituting equation (4.6) into the first term on the right hand side of equation (4.45) yields

$$\frac{dT_0}{T_0} = \left( \frac{k-1}{k e_c} \right) \frac{dP_0}{P_0} \quad (4.46)$$

Integrating equation (4.46) between the states 1-2 presented in Figure 4.3 for the stagnation conditions yields

$$\ln \frac{T_{02}}{T_{01}} = \left( \frac{k-1}{k e_c} \right) \ln \frac{P_{02}}{P_{01}} \quad (4.47)$$

Remembering the definition of compressor pressure ratio  $r_c = P_{02}/P_{01}$  and rearranging equation (4.47) gives the exit temperature of the C as

$$T_{02} = T_{01} \left( r_c^{\frac{k-1}{k e_c}} \right) \quad (4.48)$$

a function of CPR and polytropic efficiency  $e_c$ . Now, substituting the real station numbers (shown in Figure 3.14 for the Scimitar Engine) in equation (4.48) results with

$$T_{06} = T_{05} \left( r_c^{\frac{k-1}{k e_c}} \right) \quad (4.49)$$

Also, the total pressure at the C exit is

$$P_{06} = P_{05} r_c \quad (4.50)$$

Equation (4.49) is also used for the helium regenerator Cs.

Power requirement of the C is given by

$$\dot{W}_C = \dot{m}_1 c_p (T_{05} - T_{06}) \quad (4.51)$$

Equation (4.51) will give a negative result, which has a meaning that C is consuming power.

The last step is the determination of the energy flow rates at C inlet and exit, which are calculated by

$$\dot{E}_{05} = \dot{m}_1 (c_p T_{05} - h_1) \quad (4.52)$$

$$\dot{E}_{06} = \dot{m}_1 (c_p T_{06} - h_1) \quad (4.53)$$

### 4.2.3 Precooler

Scimitar engine precooler consists of two segments namely HX1 and HX2. High temperature air entering the engine flows radially inside for cooling. Air is first cooled in the HX1 which has more coolant mass flow rate than the HX2 because air temperature entering the HX2 relatively low (Fernandez-Villace and Paniagua, 2013a).

Air leaving the I has the same energy flow with the air entering the HX1.

$$\dot{E}_{02} = \dot{E}_{03} \quad (4.54)$$

Jivraj et al (2007) states that as a design parameter C inlet should not exceed 635 K. Therefore, heat removed from the air is the difference between energy flow rates of I exit and C inlet. Heat transferred in the precooler is denoted by  $\dot{Q}_{precooler}$

$$\dot{Q}_{precooler} = \dot{E}_{03} - \dot{E}_{05} \quad (4.55)$$

Simulation results of Fernandez-Villace and Paniagua (2013a) show that heat transferred in the HX1 is almost 2 times that of in the HX2. Calling heat transferred in the HX1 as  $\dot{Q}_{HX1}$  and heat transferred in the HX2 as  $\dot{Q}_{HX2}$ , their relations with  $\dot{Q}_{precooler}$  is

$$\dot{Q}_{precooler} = \dot{Q}_{HX1} + \dot{Q}_{HX2} \quad (4.56)$$

$$\dot{Q}_{HX1} = \frac{2}{3} \dot{Q}_{HX1} \quad (4.57)$$

$$\dot{Q}_{HX2} = \frac{1}{3} \dot{Q}_{HX2} \quad (4.58)$$

From the heat transfer rates, helium temperatures can be determined. Helium mass flow entering the HX2 is 0.375 times that of entering the helium turbine. Mass flow rate of the helium entering the helium turbine is denoted as  $\dot{m}_{He}$ . Therefore, heat transfer equation becomes

$$\dot{Q}_{HX2} = 0.375 \dot{m}_{He} c_{p,He} (T_{89} - T_{88}) \quad (4.59)$$

Energy flow and enthalpy at station 4 is

$$\dot{E}_{04} = \dot{E}_{05} + \dot{Q}_{HX2} \quad (4.60)$$

$$h_{04} = \frac{\dot{E}_{04}}{\dot{m}_{in}} + h_1 \quad (4.61)$$

After leaving the HX1, helium stream at station 89 mixes with the stream coming from the HTR. Attention must paid when following the helium streams because the

helium stream leaving the helium turbine divides in two parts one having 0.625 times of the  $\dot{m}_{He}$  and entering HTR, the other stream having 0.375 times of the  $\dot{m}_{He}$  entering the LTR. However, there is a helium stream making a loop between 31-32-33-34-35. So, the stream exiting the HX2 mixes with the flow coming from station 35 which has a mass flow 0.750 times of  $\dot{m}_{He}$ . The rate of energy balance for the steady-flow mixing process can be evaluated by using equation (2.2).

Since during the mixing there is no heat and work interaction, neglecting kinetic and potential energies of the helium flow, equation (2.2) becomes

$$0.375\dot{m}_{He}c_{p,He}T_{89} + 0.750\dot{m}_{He}c_{p,He}T_{35} = 1.125\dot{m}_{He}c_{p,He}T_{28} \quad (4.62)$$

where enthalpy terms are written as specific heat times temperature since specific heat of helium is assumed constant throughout the cycle.

Rearrangement reduces equation (4.62) to

$$T_{28} = \frac{T_{89} + 2T_{35}}{3} \quad (4.63)$$

After determining  $T_{28}$ , HX1 exit temperature on the helium side,  $T_{29}$ , can be found

$$\dot{Q}_{HX1} = 1.125\dot{m}_{He}c_{p,He}(T_{29} - T_{28}) \quad (4.64)$$

In the precooler, air pressure drops in HXs are assumed to be 5%.

$$P_{02} = P_{03} \quad (4.65)$$

$$P_{04} = P_{03}(0.95) \quad (4.66)$$

$$P_{05} = P_{04}(0.95) \quad (4.67)$$

#### 4.2.4 Hydrogen line

In the previous sections, air properties are determined before the combustion in PB. Before calculating the combustion, hydrogen fuel temperature and pressure at the PB inlet should be known. These pressure and temperature values are the same at the CC inlet since there is no other process between PB and CC for hydrogen.

In Scimitar engine hydrogen is stored at 18 bar and 20 K (Jivraj et. al, 2007; Fernandez-Villace and Paniagua, 2013a-2013b). At these conditions, hydrogen is in liquid state (Url-1; Jivraj et. al, 2007). In low-temperature heat exchanger 4 (HX4L), hydrogen cools the helium stream. It is expected for hydrogen to change phase and evaporate. Figure 4.4 shows the enthalpy-temperature data of hydrogen with 0.5 K increments.

Isobaric Data for P = 18.000 bar

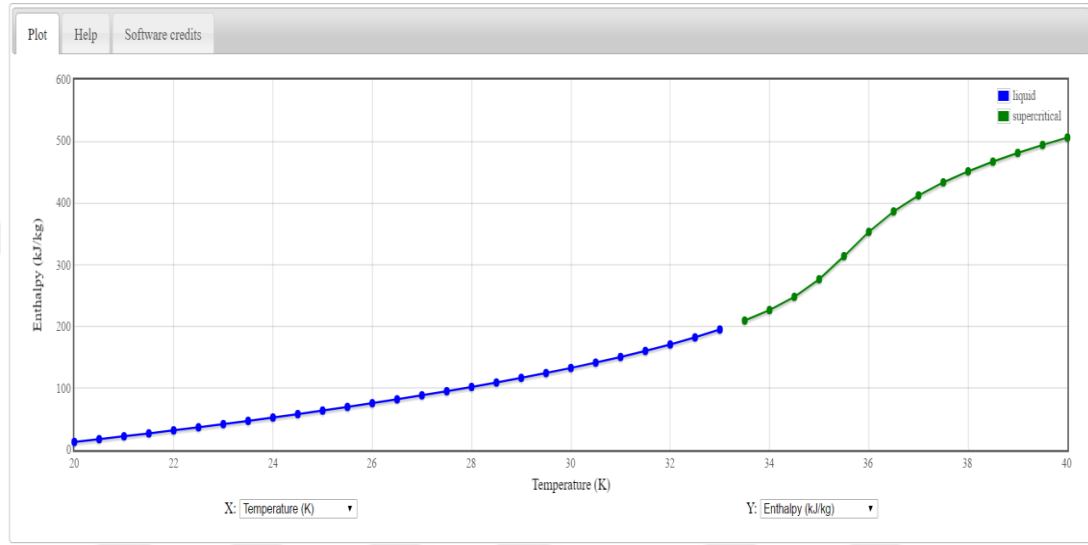


**Figure 4.4 :** Hydrogen  $h$ - $T$  data at 18 bar (Url-1).

At 18 bar, between 20 K and 33 K hydrogen is in liquid phase. However, after 33.5 K, as indicated by the green line in Figure 4.4, hydrogen is at supercritical conditions.

Critical point is defined as the point at which “saturated vapor and saturated liquid lines are identical” (Çengel and Boles, 2005, p. 119). Figure 4.5 shows that there is no apparent phase change line when  $P > P_{cr}$ . Therefore, in hydrogen case, we cannot use  $h_{fg}$  value for the evaporation process. Yet, heat transfer rate from the helium side can be calculated, since heat released is equal to the heat taken in a HX. Heat transferred in the HX4L is denoted by  $\dot{Q}_{HX4L}$ . Enthalpy value of the hydrogen is calculated as

$$\dot{Q}_{HX4L} = 0.125\dot{m}_{He}c_{p,He}(T_{83} - T_{84}) \quad (4.68)$$

$$\dot{Q}_{HX4L} = \dot{m}_{H_2}(h_{21} - h_{20}) \quad (4.69)$$

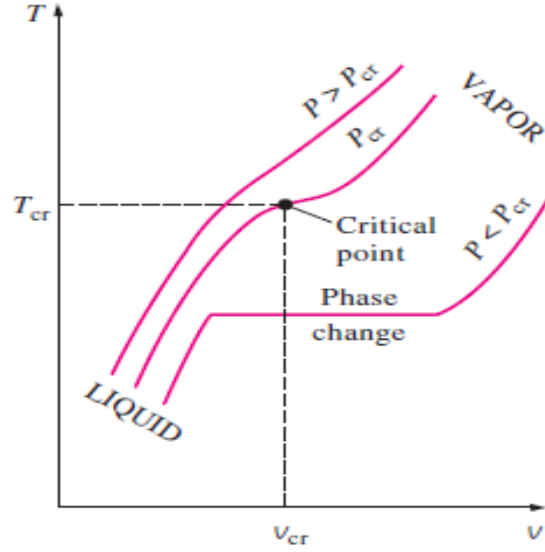


**Figure 4.5 :** Critical point phase behavior of pure substances (Çengel and Boles, 2005).

Hydrogen enthalpy at the exit of HX4L is

$$h_{21} = \frac{\dot{Q}_{HX4L}}{\dot{m}_{H_2}} + h_{20} \quad (4.70)$$

Corresponding temperatures at corresponding pressures are found from NIST. Hydrogen pressures are taken from (Fernandez-Villace, 2013a).

After the HX4L, hydrogen enters the high-temperature heat exchanger 4 (HX4H) where it cools a stream of helium flowing between stations 41-42. Same procedure is followed here.

$$\dot{Q}_{HX4H} = 0.125\dot{m}_{He}c_{p,He}(T_{41} - T_{42}) \quad (4.71)$$

Hydrogen enthalpy at the exit of HX4H is

$$h_{22} = \frac{\dot{Q}_{HX4H}}{\dot{m}_{H_2}} + h_{21} \quad (4.72)$$

Hydrogen enters HX5 for the final cooling before the combustion.

$$\dot{Q}_{HX5} = 0.125\dot{m}_{He}c_{p,He}(T_{31} - T_{32}) \quad (4.73)$$

$$h_{23} = \frac{\dot{Q}_{HX5}}{\dot{m}_{H_2}} + h_{22} \quad (4.74)$$

In HX5, heat transfer is greatly affected by the  $T_{34}$  or  $T_{35}$ .  $T_{31}$  is equal to  $T_{29}$  which is the HX1 exit temperature. If  $T_{34}$  is known then  $T_{32}$  which is the HX5 exit temperature on the helium side can be calculated as

$$0.125\dot{m}_{He}c_{p,He}T_{32} + 0.625\dot{m}_{He}c_{p,He}T_{66} = 0.750\dot{m}_{He}c_{p,He}T_{34} \quad (4.75)$$

$$T_{32} = \frac{6T_{34} - 5T_{66}}{6} \quad (4.76)$$

Note that circulator (C9) is neglected. Properties of station 33 and 32 are the same. In addition, since Valve 7 is closed since HX1 is active at Mach 5 cruise, properties of station 34 and 35 are the same.

#### 4.2.5 Preburner

Small amount of hydrogen is completely combusted in the PB to increase the temperature of the air exiting the C. This heat addition is used in HX3 to increase the temperature of the helium flow leaving HX1 (Jivraj et al, 2007).

The combustion process is modeled with adiabatic flame temperature approach assuming there is no heat loss to the surroundings (Çengel and Boles, 2005).

Hydrogen fuel entering the preburner at station 24 with a mass flow rate of  $\dot{m}_{H_2} = \dot{m}_{24} = 0.14 \text{ kg/s}$  and air at station 06 with a mass flow rate of  $\dot{m}_{air} = \dot{m}_1 = \dot{m}_{06} = 172.6 \text{ kg/s}$ , which includes some excess air, perform a combustion process in the preburner.

In the combustion calculations, air is treated as an ideal gas mixture composed of  $O_2$  and  $N_2$ . In the thesis, it is assumed that  $N_{air} = 4.76 \text{ kmol}$  of air is composed of  $N_{O_2} = 1 \text{ kmol}$  of  $O_2$  and  $N_{N_2} = 3.76 \text{ kmol}$  of  $N_2$ .

*Mole fractions of the  $O_2$  and  $N_2$  in the gas mixture air can be calculated as*

$$y_{O_2,06} = \frac{N_{O_2,06}}{N_{air,06}} = 0.210084 \quad (4.77)$$

$$y_{N_2,06} = \frac{N_{N_2,06}}{N_{air,06}} = 0.789916 \quad (4.78)$$

Molecular masses of  $O_2$ ,  $N_2$  in the gas mixture air and that of the stable element  $H_2$  are  $M_{O_2} = 31.9988 \text{ kg kmol}^{-1}$ ,  $M_{N_2} = 28.0134 \text{ kg kmol}^{-1}$  and  $M_{H_2} = 2.016 \text{ kg kmol}^{-1}$ , respectively (Url-3; Url-4; Url-5). Then, molecular mass of air as a gas mixture is calculated as

$$M_{air} = M_{air,06} = y_{O_2,06}M_{O_2} + y_{N_2,06}M_{N_2} = 28.85067 \text{ kg kmol}^{-1} \quad (4.79)$$

Dividing the mass flow rate of the reactants of the stable element  $H_2$  and of the gas mixture air with their molar mass, gives their molal flow rates as

$$\dot{n}_{H_2,24} = \frac{\dot{m}_{H_2,24}}{M_{H_2}} = 0.069444 \text{ kmol s}^{-1} \quad (4.80)$$

$$\dot{n}_{air,06} = \frac{\dot{m}_{air,06}}{M_{air,06}} = 5.98253027 \text{ kmol s}^{-1} \quad (4.81)$$

Also, molal flow rates of the reactants of  $O_2$  and  $N_2$  in the gas mixture air become

$$\dot{n}_{O_2,06} = y_{O_2,06}\dot{n}_{air,06} = 1.256834 \text{ kmol s}^{-1} \quad (4.82)$$

$$\dot{n}_{N_2,06} = y_{N_2,06}\dot{n}_{air,06} = 4.725569622 \text{ kmol s}^{-1} \quad (4.83)$$

Moreover, molal flow rate of the  $H_2O$  is equal to the molal flow rate of the hydrogen fuel because of the same amount of hydrogen content in both species. Then, the molal flow rates of  $H_2O$ ,  $O_2$  and  $N_2$  in the gas mixture of combustion products become

$$(\dot{n}_{H_2O,09})_p = (\dot{n}_{H_2,24})_r = 0.069444 \text{ kmol s}^{-1} \quad (4.84)$$

$$(\dot{n}_{O_2,09})_p = (\dot{n}_{O_2,06})_r - (\dot{n}_{H_2O,09})_p = 1.221121 \text{ kmol s}^{-1} \quad (4.85)$$

$$(\dot{n}_{N_2,09})_p = (\dot{n}_{N_2,06})_r = 4.725569622 \text{ kmol s}^{-1} \quad (4.86)$$

As a result, the molal flow rate of mass balance, in  $\text{kmol s}^{-1}$ , in the combustion reaction becomes



$$\begin{aligned}
&0.069444H_2 + 1.2568341O_2 + 4.725569622N_2 \\
&\rightarrow 0.069444H_2O + 1.2221121O_2 + 4.725569622N_2
\end{aligned} \tag{4.87}$$

Total rate of energy of the reactants, in  $kW$ , is

$$\begin{aligned}
\dot{E}_r = &\dot{n}_{H_2,24}(\bar{h}_{f,H_2}^0 + \bar{h}_{H_2,24} - \bar{h}_{H_2}^0) + \dot{n}_{O_2,06}(\bar{h}_{f,O_2}^0 + \bar{h}_{O_2,06} - \bar{h}_{O_2}^0) \\
&+ \dot{n}_{N_2,06}(\bar{h}_{f,N_2}^0 + \bar{h}_{N_2,06} - \bar{h}_{N_2}^0)
\end{aligned} \tag{4.88}$$

Total rate of energy of the products, in  $kW$ , is

$$\begin{aligned}
\dot{E}_p = &\dot{n}_{H_2O,09}(\bar{h}_{f,H_2O}^0 + \bar{h}_{H_2O,09} - \bar{h}_{H_2O}^0) \\
&+ \dot{n}_{O_2,09}(\bar{h}_{f,O_2}^0 + \bar{h}_{O_2,09} - \bar{h}_{O_2}^0) \\
&+ \dot{n}_{N_2,09}(\bar{h}_{f,N_2}^0 + \bar{h}_{N_2,09} - \bar{h}_{N_2}^0)
\end{aligned} \tag{4.89}$$

In this study, the reactant air is evaluated by considering it as a gas mixture of  $O_2$  and  $N_2$ . Hence, the ideal gas property tables for  $O_2$  and  $N_2$  by Çengel and Boles (2005) are used while calculating the gas mixture property ( $h_{air}$ ,  $u_{air}$ ,  $c_{p,air}$ ,  $c_{v,air}$ ,  $k_{air}$ ) values of air. As a calculation example for these gas mixture properties, air enthalpy in  $kJ\ kg^{-1}$  can be calculated as

$$h_{air} = h_{air,06} = h_{06} = \frac{y_{O_2,06}\bar{h}_{O_2,06} + y_{N_2,06}\bar{h}_{N_2,06}}{M_{air,06}} \tag{4.90}$$

Considering the reference conditions as  $T^0 = T_1 = 222\ K$  and  $P^0 = P_1 = 2.4\ kPa$ , total energy flow rate of the air at the C exit with respect to the reference conditions, which is equal to the total rate of energy of the air (in the reactant part of the equation (4.87)) entering the PB with respect to reference conditions, can be calculated as

$$\dot{E}_{06} = \dot{E}_{air} = \dot{n}_{air,06} \left( y_{O_2,06}(\bar{h}_{O_2,06} - \bar{h}_{O_2}^0) + y_{N_2,06}(\bar{h}_{N_2,06} - \bar{h}_{N_2}^0) \right) \tag{4.91}$$

By equating total rate of energy for the reactants and that for the products ( $\dot{E}_r = \dot{E}_p$ ) and rearranging, and considering the formation enthalpies of the stable elements being zero (i.e.,  $\bar{h}_{f,H_2}^0 = \bar{h}_{f,O_2}^0 = \bar{h}_{f,N_2}^0 = 0$ ), equations (4.88) and (4.89) yields

$$\begin{aligned}
& \underbrace{[-\dot{n}_{H_2O,09} \bar{h}_{f,H_2O}^0]}_{\dot{n}_{H_2,24} FHV}]_p \\
& + \left[ \dot{n}_{H_2,24} (\bar{h}_{H_2,24} - \bar{h}_{H_2}^0) + \underbrace{\dot{n}_{O_2,06} (\bar{h}_{O_2,06} - \bar{h}_{O_2}^0) + \dot{n}_{N_2,06} (\bar{h}_{N_2,06} - \bar{h}_{N_2}^0)}_{\dot{E}_{06}} \right]_r \\
& = \left[ \underbrace{\dot{n}_{H_2O,09} (\bar{h}_{H_2O,09} - \bar{h}_{H_2O}^0) + \dot{n}_{O_2,09} (\bar{h}_{O_2,09} - \bar{h}_{O_2}^0) + \dot{n}_{N_2,09} (\bar{h}_{N_2,09} - \bar{h}_{N_2}^0)}_{\dot{E}_{09}} \right]_p
\end{aligned} \tag{4.92}$$

where  $\bar{h}_{f,H_2O}^0$  is the formation enthalpy of the product  $H_2O$  and its absolute value yields the fuel heating value (FHV) of the fuel  $H_2$ . Since energy flow rates of the air before the combustion and energy flow rate of the CPs after the combustion include both chemical composition and reference conditions terms, also considering  $\dot{n}_{H_2O} = \dot{n}_{H_2}$ , equation (4.92) can be rewritten, in kW, in a simpler form

$$\dot{n}_{H_2,24} FHV + \dot{n}_{H_2,24} (\bar{h}_{H_2,24} - \bar{h}_{H_2}^0) + \dot{E}_{06} = \dot{E}_{09} \tag{4.93}$$

from which  $h_{09}$  is calculated as

$$h_{09} = \frac{\dot{E}_{09}}{\dot{m}_{air,06} + \dot{m}_{H_2,24}} + h_1 \tag{4.94}$$

Pressure drop during the combustion process is taken as 10%.

$$P_{09} = P_{06}(0.90) \tag{4.95}$$

#### 4.2.6 Heat exchanger 3

CPs leaving the PB enter HX3 where they reject heat to the helium stream coming from HX1.  $T_{38}$  which is exit temperature of the helium side is selected as 1000 K as a design parameter (Jivraj et. al, 2007). Heat transferred in the HX3 is obtained as

$$\dot{Q}_{HX3} = \dot{m}_{He} c_{p,He} (T_{38} - T_{37}) \tag{4.96}$$

$\dot{E}_{09}$  was calculated in PB section. Hot CP side loses heat to the helium stream.  $h_{010}$  is calculated from the energy flow rate ( $\dot{E}_{010}$ ) of the CPs leaving the HX3 as

$$\dot{E}_{010} = \dot{E}_{09} - \dot{Q}_{HX3} \tag{4.97}$$

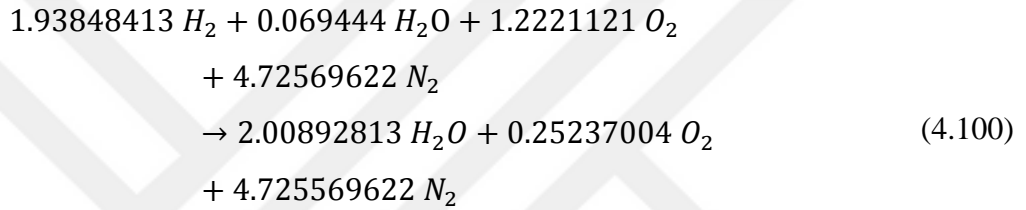
$$h_{010} = \frac{\dot{E}_{010}}{\dot{m}_{in} + \dot{m}_{24}} + h_1 \quad (4.98)$$

Pressure drop in HX3 is taken as 5%. Total pressure at HX3 for the air side is

$$P_{010} = P_{09}(0.95) \quad (4.99)$$

#### 4.2.7 Combustion chamber

Remaining amount of hydrogen fuel is completely combusted in CC to increase the temperature of the CPs. The molal flow rate of mass balance, in  $kmol s^{-1}$ , in the combustion reaction in CC is obtained (as explained for the PB) as



$H_2$  mass flow rate entering the CC is denoted by

$$\dot{m}_{26} = \dot{m}_{H_2,20} - \dot{m}_{24} \quad (4.101)$$

Molal flow rate of the hydrogen ( $\dot{n}_{H_2,26}$ ) is obtained by the aid of an equation similar to equation (4.80). Energy balance for the reactants is

$$\begin{aligned} \dot{E}_r = &\dot{n}_{26}(\bar{h}_{f,H_2}^0 + \bar{h}_{H_2,26} - \bar{h}_{H_2}^0) \\ &+ \dot{n}_{H_2O,016}(\bar{h}_{f,H_2O}^0 + \bar{h}_{H_2O,016} - \bar{h}_{H_2O}^0) \\ &+ \dot{n}_{O_2,016}(\bar{h}_{f,O_2}^0 + \bar{h}_{O_2,016} - \bar{h}_{O_2}^0) \\ &+ \dot{n}_{N_2,016}(\bar{h}_{f,N_2}^0 + \bar{h}_{N_2,016} - \bar{h}_{N_2}^0) \end{aligned} \quad (4.102)$$

Formation enthalpies of the elements are zero and the absolute value of the formation enthalpy of the water vapor at the reactant side was used as FHV in the PB. Also, there is no process between stations 10-16, hence their properties are the same.

$$\dot{E}_{010} = \dot{E}_{016} \quad (4.103)$$

Molal flow rate of the new water vapor formed in the products is denoted by  $(\dot{n}_{H_2O} + \dot{n}_{26})$  since molal flow rate of the water vapor formed is equal to the molal flow rate of the hydrogen entering the CC. There is already an amount of water vapor in the flow entering the CC. Therefore, total molal flow rate of the water vapor is the sum of the water vapor produced in these two combustion processes.

Energy balance for the products is where subscript  $p$  indicates the molal flow rates of the stable elements  $O_2$  and  $N_2$  in the products

$$\begin{aligned}\dot{E}_p &= \underbrace{(\dot{n}_{H_2,26} + \dot{n}_{H_2O,016})}_{\dot{n}_{H_2O,017}} (\bar{h}_{f,H_2O}^0 + \bar{h}_{H_2O,017} - \bar{h}_{H_2O}^0) \\ &\quad + \dot{n}_{O_2,017} (\bar{h}_{f,O_2}^0 + \bar{h}_{O_2,017} - \bar{h}_{O_2}^0) \\ &\quad + \dot{n}_{N_2,017} (\bar{h}_{f,N_2}^0 + \bar{h}_{N_2,017} - \bar{h}_{N_2}^0)\end{aligned}\quad (4.104)$$

Considering the total rate of energy of the reactants is equal to the total rate of energy of the products and substituting  $\bar{h}_{f,O_2}^0 = \bar{h}_{f,N_2}^0 = 0$  for the stable elements we obtain

$$\begin{aligned}&[\dot{n}_{H_2,26} (\bar{h}_{H_2,26} - \bar{h}_{H_2}^0) + \dot{n}_{H_2O,016} (\bar{h}_{f,H_2O}^0 + \bar{h}_{H_2O,016} - \bar{h}_{H_2O}^0) \\ &\quad + \dot{n}_{O_2,016} (\bar{h}_{O_2,016} - \bar{h}_{O_2}^0) + \dot{n}_{N_2,016} (\bar{h}_{N_2,016} - \bar{h}_{N_2}^0)]_r \\ &= [(\dot{n}_{H_2,26} + \dot{n}_{H_2O,016}) (\bar{h}_{f,H_2O}^0 + \bar{h}_{H_2O,017} - \bar{h}_{H_2O}^0) \\ &\quad + \dot{n}_{O_2,017} (\bar{h}_{O_2,017} - \bar{h}_{O_2}^0) + \dot{n}_{N_2,017} (\bar{h}_{N_2,017} - \bar{h}_{N_2}^0)]_p\end{aligned}\quad (4.105)$$

Rearranging yields

$$\begin{aligned}&\dot{n}_{H_2,26} (\bar{h}_{H_2,26} - \bar{h}_{H_2}^0) - \overbrace{(\dot{n}_{H_2,26} + \dot{n}_{H_2O,016}) \bar{h}_{f,H_2O}^0}^{-\dot{n}_{26} \bar{h}_{f,H_2O}^0 = \dot{n}_{26} FHV} + \dot{n}_{H_2O,016} \bar{h}_{f,H_2O}^0 \\ &\quad + \dot{n}_{H_2O,016} (\bar{h}_{H_2O,016} - \bar{h}_{H_2O}^0) \\ &\quad + \dot{n}_{O_2,016} (\bar{h}_{O_2,016} - \bar{h}_{O_2}^0) + \dot{n}_{N_2,016} (\bar{h}_{N_2,016} - \bar{h}_{N_2}^0) \\ &= (\dot{n}_{H_2,26} + \dot{n}_{H_2O,016}) (\bar{h}_{H_2O,017} - \bar{h}_{H_2O}^0) \\ &\quad + \dot{n}_{O_2,017} (\bar{h}_{O_2,017} - \bar{h}_{O_2}^0) \\ &\quad + \dot{n}_{N_2,017} (\bar{h}_{N_2,017} - \bar{h}_{N_2}^0)\end{aligned}\quad (4.106)$$

Right hand side of equation (4.106) is in the form of energy flow rate, in kW.

Rearranging yields

$$\begin{aligned} & \dot{n}_{H_2,26}(\bar{h}_{H_2,26} - \bar{h}_{H_2}^0) - \overbrace{(\dot{n}_{H_2,26} + \dot{n}_{H_2O})\bar{h}_{f,H_2O}^0 + \dot{n}_{H_2O}\bar{h}_{f,H_2O}^0}^{\dot{n}_{26}FHV} \\ & + \underbrace{\dot{n}_{H_2O,016}(\bar{h}_{H_2O,016} - \bar{h}_{H_2O}^0) + \dot{n}_{O_2,016}(\bar{h}_{O_2,016} - \bar{h}_{O_2}^0) + \dot{n}_{N_2,016}(\bar{h}_{N_2,016} - \bar{h}_{N_2}^0)}_{\dot{E}_{016}} \quad (4.107) \\ & = \dot{E}_{017} \end{aligned}$$

Bringing  $\bar{h}_{f,H_2O}^0$  terms together and using FHV term for them and considering the third, fourth and fifth terms altogether are equal to  $\dot{E}_{016}$ , equation (4.107) can be rearranged to yield

$$\dot{E}_{017} = \dot{n}_{H_2,26}(\bar{h}_{H_2,26} - \bar{h}_{H_2}^0) + \dot{n}_{H_2,26} FHV + \dot{E}_{016} \quad (4.108)$$

Pressure drop in CC is taken as 10%.

$$P_{017} = P_{016}(0.90) \quad (4.109)$$

#### 4.2.8 Convergent-divergent nozzle

In order to reach hypersonic speeds, a C-D N should be used. C-D N converts the total energy at its inlet to kinetic energy at its exit with the help of area change and pressure difference. A C-D N is illustrated in Figure 4.6.

In this study, flow through the N is considered as adiabatic steady flow. Entrance conditions of the nozzle  $T_{017}$  and  $P_{017}$  can be calculated by the methods in the previous chapters. Exit area of the N,  $A_{exit}$ , is obtained from (Marini et. al, 2013). In order to find the exit static pressure, static temperature and velocity, an area related Mach number function for an isentropic flow should be obtained (Anderson, 2003; Çengel and Boles, 2005).

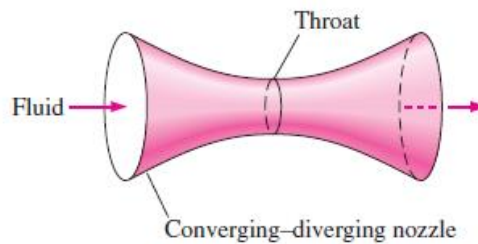


**Figure 4.6 :** A convergent-divergent nozzle (C-D N) (Çengel and Boles, 2005).

For steady flows, mass flow rate is constant and it is equal to

$$\dot{m} = \rho AV = \text{constant} \quad (4.110)$$

If equation (4.110) is differentiated

$$d\rho AV + dA\rho V + dV\rho A = 0 \quad (4.111)$$

Dividing equation (4.111) by  $\dot{m}$  given in equation (4.110) yields

$$\frac{d\rho}{\rho} + \frac{dA}{A} + \frac{dV}{V} = 0 \quad (4.112)$$

Recall equation (4.1) which is derived from the first law of thermodynamics for a steady-flow process of an open system with no heat and work interaction. Equation (4.1) states that  $h + \frac{v^2}{2} = \text{constant}$ . Differentiating equation (4.1) yields

$$dh + VdV = 0 \quad (4.113)$$

To continue,  $Tds$  relations for an isentropic process must be used as

$$Tds = dh - vdP \quad (4.114)$$

For an isentropic process,  $ds = 0$ , hence

$$dh = vdP \quad (4.115)$$

$$dh = \frac{1}{\rho} dP \quad (4.116)$$

Equation (4.113) becomes

$$\frac{dP}{\rho} + VdV = 0 \quad (4.117)$$

Substituting equation (4.117) into equation (4.112) yields

$$\frac{dA}{A} = \frac{dP}{\rho} \left( \frac{1}{V^2} - \frac{d\rho}{dP} \right) \quad (4.118)$$

As long as soundwaves are of concern, by definition they are considered as weak wave. There is no heat transfer to or from the flow crossing the soundwave and since wave effect that is changing the properties of the flow is weak, it is assumed that irreversibilities in flow is very small. Hence, flow can be assumed as adiabatic and irreversible. For isentropic flow, substituting  $\left(\frac{\partial \rho}{\partial P}\right)_s = 1/c^2$  in equation (4.118), it can be concluded (Anderson, 2003; Çengel and Boles, 2005) that

$$\frac{dA}{A} = \frac{dP}{\rho} \left( \frac{1}{V^2} - \frac{1}{c^2} \right) \quad (4.119)$$

$$\frac{dA}{A} = \frac{dP}{\rho} \left( \frac{1}{M^2 c^2} - \frac{M^2}{M^2 c^2} \right) \quad (4.120)$$

$$\frac{dA}{A} = \frac{dP}{\rho V^2} (1 - M^2) \quad (4.121)$$

which shows the relationships between area change and pressure. At subsonic speeds  $(1 - M^2)$  value is positive and equation (4.121) is examined  $dA$  and  $dP$  should have the same sign. This shows the validity of the behavior of convergent nozzles at subsonic flow since as area decreases, pressure decreases. When  $M > 1$ ,  $(1 - M^2)$  value is negative and it means pressure and area change terms should have negative signs. In divergent part, as area increases pressure decreases for supersonic flow (Çengel and Boles, 2005).

Recalling equation (4.118) and leaving only  $dP$  term on the left hand side

$$dP = -\rho V dV \quad (4.122)$$

Substituting it into equation (4.121)

$$\frac{dA}{A} = -\frac{dV}{V} (1 - M^2) \quad (4.123)$$

The relation between area and velocity can be seen in equation (4.123). For subsonic flow  $dA/dV$  has negative sign meaning as the area increases the flow decelerates. For supersonic flow  $dA/dV$  has positive sign meaning as the area increases flow accelerates.

Another important concept in C-D nozzles is the choking. As back pressure  $P_b$  at the N exit is being lowered, back pressure to N entrance pressure or chamber pressure ( $P_b/P_0$ ) ratio reaches a certain value. When this ratio is reached, mass flow rate through the N reaches a maximum value. Further reduction of  $P_b$  has no effect on mass flow rate. This is called choking. Furthermore, when the flow is choked Mach number at the throat is 1.

Knowing that mass flow through the N is constant and flowing gas is ideal gas.

$$P = \rho RT \quad (4.124)$$

Substituting equation (4.124), (2.11) and (2.12) to (4.110) yields

$$\dot{m} = \frac{P}{RT} A M \sqrt{kRT} \quad (4.125)$$

Substituting equations (4.8) and (2.10) in equation (4.125) results with the mass flow rate through the C-D N as

$$\dot{m} = \frac{P_0 A M \sqrt{\frac{k}{RT_0}}}{\left(1 + \frac{k-1}{2} M^2\right)^{(k+1)/2(k-1)}} \quad (4.126)$$

Knowing the CC exit (C-D N inlet) conditions and the mass flow rate through the C-D N, by setting  $M = 1$  for the throat, throat area ( $A^*$ ) can be determined. When  $M = 1$ , mass flow rate has its the maximum value. Hence, equation (4.126) can be rearranged for the throat to give

$$\dot{m}_{max} = \frac{P_0 A^* \sqrt{\frac{k}{RT_0}}}{\left(\frac{k+1}{2}\right)^{(k+1)/2(k-1)}} \quad (4.127)$$

Rewriting equations (4.126) and (4.127) for  $A$  and  $A^*$  as

$$A = \frac{\dot{m} \left(1 + \frac{k-1}{2} M^2\right)^{(k+1)/2(k-1)}}{P_0 M \sqrt{\frac{k}{RT_0}}} \quad (4.128)$$



$$A^* = \frac{\dot{m}_{max}}{P_0 \sqrt{\frac{k}{RT_0}} \left(\frac{2}{k+1}\right)^{(k+1)/2(k-1)}} \quad (4.129)$$

and setting  $\dot{m}_{max} = \dot{m}$ , then,  $A/A^*$  can be written as

$$A/A^* = \frac{1}{M} \left( \frac{2}{k+1} \left( 1 + \frac{k-1}{2} M^2 \right) \right)^{(k+1)/2(k-1)} \quad (4.130)$$

From equation (4.130), Mach number at any cross-sectional area  $A$  through C-D N can be found. If  $A = A_{exit}$ , Mach number at the exit conditions can be determined.

C-D N inlet and exit conditions are denoted by 017 and 18, respectively. Using these subscripts in equations (4.8) and (2.10) for the Scimitar engine yields

$$T_{18s} = T_{017} \left( 1 + \frac{k-1}{2} M_{18}^2 \right) \quad (4.131)$$

$$P_{18s} = P_{017} \left( 1 + \frac{k-1}{2} M_{18}^2 \right)^{k/(k-1)} \quad (4.132)$$

Assuming  $P_{18s} = P_{18}$ , velocity of CPs after an isentropic expansion  $v_{18s}$  in C-D N and isentropic efficiency  $\eta_N$  of the C-D N are obtained by

$$v_{18s} = M_{18} \sqrt{kRT_{18s}} \quad (4.133)$$

$$\eta_N = \frac{h_{017} - h_{18}}{h_{017} - h_{18s}} = \frac{v_{18}^2}{v_{18s}^2} \quad (4.134)$$

#### 4.2.9 Helium turbine

The approach of using a correction factor for an isentropic relation with differential pressure based irreversibility is considered in the expansion process as well (Çolakoğlu, 2015). Expansion process by small pressure expansion steps is presented in Figure 4.7.

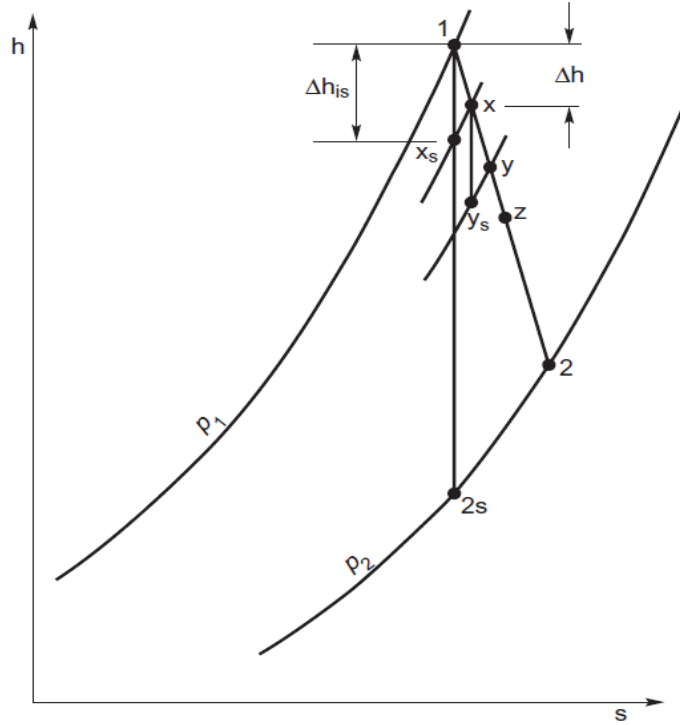


**Figure 4.7 :** Expansion process by small pressure expansion steps (Dixon, 2005).

By definition, polytropic efficiency of an expansion process

$$e_{T1} = \frac{\text{enthalpy change in actual process}}{\text{enthalpy change in isentropic process}} = \frac{dh}{dh_s} \quad (4.135)$$

Assuming the process is adiabatic and applying equations (4.40)-(4.42), the efficiency term becomes

$$e_{T1} = \frac{dh}{dh_s} = \frac{c_{p,He}T}{v dP} \quad (4.136)$$

Helium is an ideal gas, hence we can write

$$v = \frac{RT}{P} \quad (4.137)$$

Substituting equation (4.137) to (4.136), we obtain

$$e_{T1} = \frac{dh}{dh_s} = \frac{c_{p,He}}{R} \frac{P}{T} \frac{dT}{dP} \quad (4.138)$$

Substituting equation (4.6) into equation (4.138) gives

$$\frac{dP}{P} = \frac{k_{He}}{k_{He} - 1} \frac{1}{e_{T1}} \frac{dT}{T} \quad (4.139)$$

Integrating equation (4.139) from state 38 to state 39 for the real station numbers in Figure 3.14 for the Scimitar Engine results with

$$\ln\left(\frac{P_{39}}{P_{38}}\right) = \frac{k_{He}}{k_{He} - 1} \frac{1}{e_{T1}} \ln\left(\frac{T_{39}}{T_{38}}\right) \quad (4.140)$$

Calling  $r_{T1} = \frac{P_{39}}{P_{38}}$  and rearranging equation (4.140) yields

$$T_{39} = T_{38} (r_{T1})^{\frac{(k_{He}-1)e_{T1}}{k_{He}}} \quad (4.141)$$

Finally, power generated in the helium turbine is

$$\dot{W}_{T1} = \dot{m}_{He} c_{p,He} (T_{38} - T_{39}) \quad (4.142)$$

#### 4.2.10 Low-temperature regenerator

After the expansion process in the helium turbine, helium stream with mass flow rate of  $0.375\dot{m}_{He}$  enters the regenerator. In LTR, there are 3 compressors namely: compressor 6 (C6), compressor 7 (C7), compressor 8 (C8). These Cs are powered by helium turbine 3 (T3). Other five Cs are powered by the helium turbine 2 (T2). Power need in the HTR is higher than the lower since it uses 5 Cs. This is the reason of having mass flow entering T2 is 2 times that of T3 (Jivraj et al, 2007; Fernandez-Villace and Paniagua, 2011; Fernandez-Villace and Paniagua, 2013a; Fernandez-Villace and Paniagua, 2013b).

C and turbine exit temperature equations are derived in sections 4.2.2 and 4.2.9 respectively.

Expansion process in T2 is calculated as

$$\frac{P_{69}}{P_{68}} = r_{T2} \quad (4.143)$$

$$T_{69} = T_{68}(r_{T2})^{\frac{(k_{He}-1)e_{T2}}{k_{He}}} \quad (4.144)$$

Power generated by T2 is

$$\dot{W}_{T2} = 0.250\dot{m}_{He}c_{p,He}(T_{68} - T_{69}) \quad (4.145)$$

For the T3 expansion process is

$$\frac{P_{71}}{P_{70}} = r_{T3} \quad (4.146)$$

$$T_{71} = T_{70}(r_{T3})^{\frac{(k_{He}-1)e_{T3}}{k_{He}}} \quad (4.147)$$

Power generated by T3 is

$$\dot{W}_{T3} = 0.125\dot{m}_{He}c_{p,He}(T_{70} - T_{71}) \quad (4.148)$$

When the fuel flow is increased in different flight modes and conditions, precooler cooling capacity changes and with that C-T1 spool power need changes. When power need decreases, mass flow of the helium entering the T1 is reduced. This results in less power provide for LTR. In order to compensate this loss, Valve 8 is opened to reduce the power need of the LTR. At Mach 5 it is closed (Fernandevillace and Paniagua, 2013a).

After the expansion in the T2 and T3 a mixing process takes place at station 72. The rate of energy balance for the mixing is written and simplified as

$$0.125\dot{m}_{He}c_{p,He}T_{71} + 0.250\dot{m}_{He}c_{p,He}T_{69} = 0.375\dot{m}_{He}c_{p,He}T_{72} \quad (4.149)$$

$$T_{72} = \frac{T_{71} + 2T_{69}}{3} \quad (4.150)$$

After the mixing, helium stream separates in 3 each having  $0.125\dot{m}_{He}$  mass flow rate, at stations 82 and 78 and remaining follows the same line entering He-HX5.

For the compression process in C6,

$$\frac{P_{85}}{P_{84}} = r_{C6} \quad (4.151)$$

$$T_{85} = T_{84}(r_{C6})^{\frac{(k_{He}-1)}{k_{He}e_6}} \quad (4.152)$$

Power consumed in C6 is

$$\dot{W}_{C6} = 0.125\dot{m}_{He}c_{p,He}(T_{84} - T_{85}) \quad (4.153)$$

CPR of C6, C7 and C8 are the same. They can be calculated alternatively by

$$r_{C6} = \frac{1}{r_{T1}r_{T2}} \quad (4.154)$$

Helium stream entering the LTR expands two times. First expansion happens in T1, second one happens in T2 and T3 simultaneously. C6, C7 and C8 increase their pressure to T1 entrance value. PRs of T2 and T3 are also the same.

Heat transfer in HXs are calculated by knowing the C inlet temperatures from (Fernandez-Villace and Paniagua, 2013a).

Since helium streams have matched thermal capacity ratios, temperature drop on hot side will be equal to the temperature rise in the cold side as explained in section 3.5.5.

For the He-HX5, the rate of energy balance reduces to

$$T_{86} = T_{85} + (T_{74} - T_{75}) \quad (4.155)$$

For the compression process in C7,

$$r_{C7} = \frac{1}{r_{T1}r_{T2}} = \frac{P_{76}}{P_{75}} \quad (4.156)$$

$$T_{76} = T_{75}(r_{C7})^{\frac{(k_{He}-1)}{k_{He}e_{C7}}} \quad (4.157)$$

Power consumed in C7 is

$$\dot{W}_{C7} = 0.125\dot{m}_{He}c_{p,He}(T_{75} - T_{76}) \quad (4.158)$$

For the He-HX6, the rate of energy balance yields

$$T_{77} = T_{76} + (T_{78} - T_{79}) \quad (4.159)$$

For the compression process in C8,

$$r_{C8} = \frac{1}{r_{T1}r_{T2}} = \frac{P_{80}}{P_{79}} \quad (4.160)$$

$$T_{80} = T_{79}(r_{C8})^{\frac{(k_{He}-1)}{k_{He}e_{C8}}} \quad (4.161)$$

Power consumed in C8 is

$$\dot{W}_{C8} = 0.125\dot{m}_{He}c_{p,He}(T_{79} - T_{80}) \quad (4.162)$$

Last heat exchanger in LTR is He-HX7. The rate of energy balance reduces to

$$T_{81} = T_{80} + (T_{82} - T_{83}) \quad (4.163)$$

HX exit streams mix and exit the regenerator for cooling purposes in precooler. First mixing takes place at the junction of stations 77 and 86 to give the rate of energy balance as

$$0.125\dot{m}_{He}c_{p,He}T_{86} + 0.125\dot{m}_{He}c_{p,He}T_{77} = 0.250\dot{m}_{He}c_{p,He}T_{87} \quad (4.164)$$

$$T_{87} = \frac{T_{86} + T_{77}}{2} \quad (4.165)$$

The second mixing process takes place at the junction of stations 87 and 81, which yields the rate of energy balance as

$$0.250\dot{m}_{He}c_{p,He}T_{87} + 0.125\dot{m}_{He}c_{p,He}T_{81} = 0.375\dot{m}_{He}c_{p,He}T_{88} \quad (4.166)$$

$$T_{88} = \frac{T_{81} + 2T_{87}}{3} \quad (4.167)$$

#### 4.2.11 High-temperature regenerator

Same calculation procedure as done in LTR is followed here. Helium stream with a mass flow rate of  $0.625\dot{m}_{He}$  enters the HTR.

Helium stream following stations 67-40-41-42, enters HX4H before entering C1. CPR of C1, C2, C3, C4, C5 and their efficiencies are the same (Fernandez-Villace and Paniagua, 2013a). CPR of the Cs can be found by

$$r_{C1} = \frac{1}{r_{T1}} \quad (4.168)$$

After the expansion in T1, helium does not enter any expansion device as it does in LTR. Between stations 40 and 41, helium stream with mass flow rate of  $0.500\dot{m}_{He}$  flow towards the Cs and HXs.

For the compression process in C1,

$$r_{C1} = \frac{1}{r_{T1}} = \frac{P_{43}}{P_{42}} \quad (4.169)$$

$$T_{43} = T_{42}(r_{C1})^{\frac{(k_{He}-1)}{k_{He}e_{C1}}} \quad (4.170)$$

Power consumed in C1 is

$$\dot{W}_{C1} = 0.125\dot{m}_{He}c_{p,He}(T_{42} - T_{43}) \quad (4.171)$$

The rate of energy balance in He-HX1 reduces to

$$T_{44} = T_{43} + (T_{48} - T_{49}) \quad (4.172)$$

For the compression process in C2,

$$r_{C2} = \frac{1}{r_{T1}} = \frac{P_{50}}{P_{49}} \quad (4.173)$$

$$T_{50} = T_{49}(r_{C2})^{\frac{(k_{He}-1)}{k_{He}e_{C2}}} \quad (4.174)$$

Power consumed in C2 is

$$\dot{W}_{C2} = 0.125\dot{m}_{He}c_{p,He}(T_{49} - T_{50}) \quad (4.175)$$

The rate of energy balance in He-HX2 reduces to

$$T_{51} = T_{50} + (T_{52} - T_{53}) \quad (4.176)$$

For the compression process in C3,

$$r_{C3} = \frac{1}{r_{T1}} = \frac{P_{54}}{P_{53}} \quad (4.177)$$

$$T_{54} = T_{53} (r_{C3})^{\frac{(k_{He}-1)}{k_{He}e_{C3}}} \quad (4.178)$$

Power consumed in C3 is

$$\dot{W}_{C3} = 0.125\dot{m}_{He}c_{p,He}(T_{53} - T_{54}) \quad (4.179)$$

The rate of energy balance in He-HX3 reduces to

$$T_{55} = T_{54} + (T_{56} - T_{57}) \quad (4.180)$$

For the compression process in C4,

$$r_{C4} = \frac{1}{r_{T1}} = \frac{P_{58}}{P_{57}} \quad (4.181)$$

$$T_{58} = T_{57} (r_{C4})^{\frac{(k_{He}-1)}{k_{He}e_{C4}}} \quad (4.182)$$

Power consumed in C4 is

$$\dot{W}_{C4} = 0.125\dot{m}_{He}c_{p,He}(T_{57} - T_{58}) \quad (4.183)$$

The rate of energy balance in He-HX4 reduces to

$$T_{59} = T_{58} + (T_{60} - T_{61}) \quad (4.184)$$

Compression in C5 is the last step before mixing since there is no HX following.

$$r_{C5} = \frac{1}{r_{T1}} = \frac{P_{62}}{P_{61}} \quad (4.185)$$

$$T_{62} = T_{61} (r_{C5})^{\frac{(k_{He}-1)}{k_{He}e_{C5}}} \quad (4.186)$$

Power consumed in C5 is

$$\dot{W}_{C5} = 0.125\dot{m}_{He}c_{p,He}(T_{61} - T_{62}) \quad (4.187)$$



Starting from the junction of 62 and 59, helium streams mix. The rate of energy balance for the mixing process is written as

$$0.125\dot{m}_{He}c_{p,He}T_{62} + 0.125\dot{m}_{He}c_{p,He}T_{59} = 0.250\dot{m}_{He}c_{p,He}T_{63} \quad (4.188)$$

$$T_{63} = \frac{T_{62} + T_{59}}{2} \quad (4.189)$$

The rate of energy balance for the second mixing process at the junction of stations 63 and 55 yields

$$0.250\dot{m}_{He}c_{p,He}T_{63} + 0.125\dot{m}_{He}c_{p,He}T_{55} = 0.375\dot{m}_{He}c_{p,He}T_{64} \quad (4.190)$$

$$T_{64} = \frac{2T_{63} + T_{55}}{3} \quad (4.191)$$

The rate of energy balance for the third mixing process takes place at the junction of stations 64 and 51, which results with

$$0.375\dot{m}_{He}c_{p,He}T_{64} + 0.125\dot{m}_{He}c_{p,He}T_{51} = 0.500\dot{m}_{He}c_{p,He}T_{65} \quad (4.192)$$

$$T_{65} = \frac{3T_{64} + T_{51}}{4} \quad (4.193)$$

The rate of energy balance for the final mixing process yields the resultant temperature  $T_{66}$  at the HTR exit as

$$0.500\dot{m}_{He}c_{p,He}T_{65} + 0.125\dot{m}_{He}c_{p,He}T_{44} = 0.625\dot{m}_{He}c_{p,He}T_{66} \quad (4.194)$$

$$T_{66} = \frac{4T_{65} + T_{44}}{5} \quad (4.195)$$

Both streams exiting the helium regenerators flow towards the precooler to cool the incoming hot air.

### 4.3 Global Rate of Energy Balance for the Scimitar engine at Mach 5.0

A global rate of energy balance analysis of the Scimitar engine at Mach 5.0 cruise conditions is performed in this section. As it is illustrated in Figure 4.8, Scimitar Engine is treated as a stream tube where air and hydrogen fuel entering the engine

leave as CPs. Auxillary power, uninstalled thrust and heat loss terms are also included. The derivation of the formulation in this section is performed by the aid of (Fernandez-Villace and Paniagua, 2013b; Çengel and Boles, 2005; Wark, 1983).

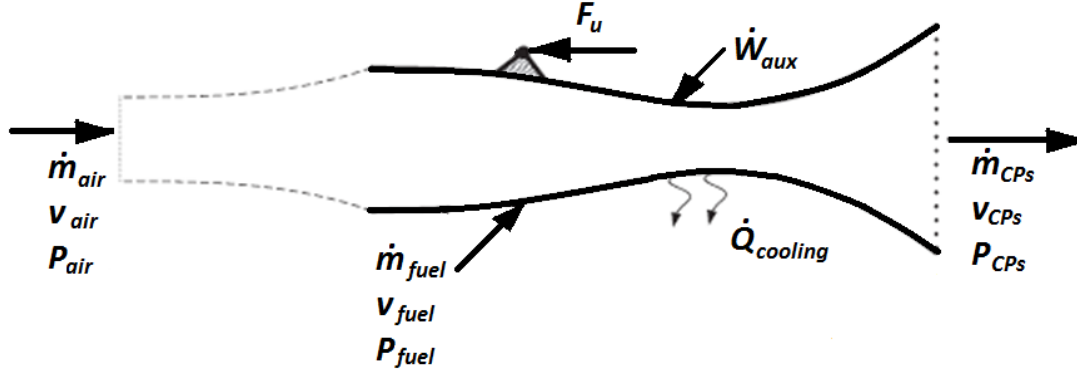


**Figure 4.8 :** Stream tube model for the global rate of energy balance of the Scimitar engine (Modified from Fernandez-Villace and Paniagua, 2013b).

In Figure 4.8 and in the following equations, subscript *air* denotes the free stream air conditions entering at the I inlet, *fuel* denotes  $H_2$  fuel entering and burned, *CPs* denotes CPs leaving the engine at the exit of C-D N, *aux* denotes auxiliary for the auxiliary power entering the engine from an additional energy source, and *cooling* denotes loss for heat from the engine.

The first law of thermodynamics for the model of thesis illustrated in Figure 4.8 at steady state can be written as

$$\underbrace{-\dot{Q}_{cooling}}_{\dot{Q}} + \underbrace{\dot{W}_{aux}}_{-\dot{W}} + \underbrace{(\dot{m}H')_{air} + (\dot{m}H')_{fuel}}_{\dot{E}_{in}} - \underbrace{(\dot{m}H')_{CPs}}_{\dot{E}_{out}} = 0 \quad (4.196)$$

where heat transfer rate is

$$\dot{Q} = \dot{Q}_{in} - \dot{Q}_{out} = 0 - \dot{Q}_{out} = -\dot{Q}_{out} = -\dot{Q}_{cooling} \quad (4.197)$$

mechanical power term is

$$\dot{W} = \dot{W}_{out} - \dot{W}_{in} = 0 - \dot{W}_{in} = -\dot{W}_{in} = -\dot{W}_{aux} \quad (4.198)$$

and open form of  $H'$  is

$$H' = h_f^0 + \Delta h + \frac{v^2}{2} = H + \frac{v^2}{2} \quad (4.199)$$

Defining  $\Delta h$  as the sensible enthalpy change in  $J/kg$ , which is the heat required to change the temperatures of air, fuel and CPs streams between the reference temperature of  $T_{ref} = T_{air} = T_{air}^0 = T^0$  and the actual temperature of each stream,  $T_{air}$ ,  $T_{fuel}$  and  $T_{CPs}$  respectively to be

$$\Delta h_{air} = h_{air} - h_{air}^0 = c_{p,air} T_{air} - c_{p,air}^0 T^0 = 0 \quad (4.200)$$

$$\Delta h_{fuel} = h_{fuel} - h_{fuel}^0 = c_{p,fuel} T_{fuel} - c_{p,fuel}^0 T^0 \quad (4.201)$$

$$\Delta h_{CPs} = h_{CPs} - h_{CPs}^0 = c_{p,CPs} T_{CPs} - c_{p,CPs}^0 T^0 \quad (4.202)$$

The rate of total static enthalpy of the air and hydrogen fuel entering and CPs leaving can be written respectively as

$$(\dot{m}H)_{air} = \dot{m}_{air} (h_f^0 + \Delta h)_{air} \quad (4.203)$$

$$(\dot{m}H)_{fuel} = \dot{m}_{fuel} (h_f^0 + \Delta h)_{fuel} \quad (4.204)$$

$$-(\dot{m}H)_{CPs} = -\dot{m}_{CPs} (h_f^0 + \Delta h)_{CPs} \quad (4.205)$$

Combining equations (4.203) - (4.205) yields

$$\begin{aligned} & (\dot{m}H)_{air} + (\dot{m}H)_{fuel} - (\dot{m}H)_{CPs} \\ &= \left[ (\dot{m}h_f^0)_{air} + (\dot{m}h_f^0)_{fuel} - (\dot{m}h_f^0)_{CPs} \right] \\ &+ \left[ (\dot{m}\Delta h)_{air} + (\dot{m}\Delta h)_{fuel} - (\dot{m}\Delta h)_{CPs} \right] \end{aligned} \quad (4.206)$$

The terms inside the first parenthesis on the right hand side in equation (4.206) is equal to the FHV  $\dot{m}_{fuel}$  in  $W$ .

Now, first defining  $\Delta \dot{E}_k$  the *increase in the kinetic power*, in  $W$ ,

$$\Delta \dot{E}_k = \left( \dot{m}_{CPs} \frac{v_{CPs}^2}{2} \right) - \left( \dot{m}_{air} \frac{v_{air}^2}{2} \right) - \left( \dot{m}_{fuel} \frac{v_{fuel}^2}{2} \right) \quad (4.207)$$

and substituting equations (4.199), (4.206) and (4.207) in equation (4.196) yields

$$\begin{aligned}
FHV\dot{m}_{fuel} + \dot{W}_{aux} \\
&= \Delta\dot{E}_k + \dot{Q}_{cooling} + \dot{m}_{CPS}(h_{CPS} - h_{CPS}^0) \\
&\quad - \dot{m}_{air}(h_{air} - h_{air}^0) - \dot{m}_{fuel}(h_{fuel} - h_{fuel}^0)
\end{aligned} \tag{4.208}$$

Stream velocity relative to the entering air velocity is

$$v' = v - v_{air} \tag{4.209}$$

Defining uninstalled thrust ( $F_u$ ), propulsive power ( $\dot{W}_p$ ) and kinetic power loss ( $\Delta\dot{E}_{k,loss}$ ), which includes the kinetic power form of the stream velocities of CPs and fuel relative to the entering air velocity, respectively as

$$\begin{aligned}
F_u = \eta_N(\dot{m}_{CPS}v_{CPS}) - (\dot{m}_{air}v_{air}) - (\dot{m}_{fuel}v_{fuel}) \\
+ (P_{CPS} - P_{air})A_{CPS} - (P_{fuel} - P_{air})A_{fuel}
\end{aligned} \tag{4.210}$$

$$\dot{W}_p = F_u v_{air} \tag{4.211}$$

$$\begin{aligned}
\Delta\dot{E}_{k,loss} = \dot{m}_{CPS} \frac{(v_{CPS} - v_{air})^2}{2} - \dot{m}_{air} \frac{(v_{air} - v_{air})^2}{2} \\
- \dot{m}_{fuel} \frac{(v_{fuel} - v_{air})^2}{2} + (1 - \eta_N)\dot{m}_{CPS}v_{CPS}v_{air} \\
- (P_{CPS} - P_{air})A_{CPS}v_{air} + (P_{fuel} - P_{air})A_{air}v_{air}
\end{aligned} \tag{4.212}$$

The first term on the right hand side in equation (4.210) is multiplied with the C-D N efficiency to account for the loss in the axial directional kinetic energy due to the flow of some parts of stream in other than the axial direction at the N exit (Fernandez-Villace and Paniagua, 2013b).

Now, let us claim that Equation (4.207) is equal to the summation of equation (4.211) and (4.212) as

$$\Delta\dot{E}_k = \Delta\dot{E}_{k,loss} + \dot{W}_p \tag{4.213}$$

Proof of this claim can be done as follows: Rewriting equation (4.213) in an open form by putting kinetic power loss term on the left hand side

$$\begin{aligned} \Delta \dot{E}_{k,loss} = & \left[ \dot{m}_{CPS} \frac{v_{CPS}^2}{2} - \dot{m}_{air} \frac{v_{air}^2}{2} - \dot{m}_{fuel} \frac{v_{fuel}^2}{2} \right] \\ & - \left[ \eta_N (\dot{m}_{CPS} v_{CPS}) v_{air} - (\dot{m}_{air} v_{air}) v_{air} \right. \\ & - (\dot{m}_{fuel} v_{fuel}) v_{air} + (P_{CPS} - P_{air}) A_{CPS} v_{air} \\ & \left. - (P_{fuel} - P_{air}) A_{air} v_{air} \right] \end{aligned} \quad (4.214)$$

$$\begin{aligned} \Delta \dot{E}_{k,loss} = & \underbrace{\dot{m}_{CPS} \frac{v_{CPS}^2}{2}}_1 + \underbrace{\dot{m}_{air} \frac{v_{air}^2}{2}}_2 - \underbrace{\dot{m}_{fuel} \frac{v_{fuel}^2}{2}}_3 \\ & - \underbrace{\eta_N (\dot{m}_{CPS} v_{CPS}) v_{air}}_4 + \underbrace{(\dot{m}_{fuel} v_{fuel}) v_{air}}_5 \\ & - (P_{CPS} - P_{air}) A_{CPS} v_{air} + (P_{fuel} - P_{air}) A_{air} v_{air} \end{aligned} \quad (4.215)$$

Calling the first five terms on the left hand side in equation (4.215) as  $Y$  yields

$$\Delta \dot{E}_{k,loss} = Y - (P_{CPS} - P_{air}) A_{CPS} v_{air} + (P_{fuel} - P_{air}) A_{air} v_{air} \quad (4.216)$$

Let us add and subtract  $\dot{m}_{fuel} \frac{v_{air}^2}{2}$  as the 6<sup>th</sup> and 7<sup>th</sup> terms to the term  $Y$

$$\begin{aligned} Y = & \underbrace{\dot{m}_{CPS} \frac{v_{CPS}^2}{2}}_1 + \underbrace{\dot{m}_{air} \frac{v_{air}^2}{2}}_2 + \underbrace{\dot{m}_{fuel} \frac{v_{air}^2}{2}}_6 - \underbrace{\dot{m}_{fuel} \frac{v_{fuel}^2}{2}}_3 \\ & + \underbrace{(\dot{m}_{fuel} v_{fuel}) v_{air}}_5 - \underbrace{\dot{m}_{air} \frac{v_{air}^2}{2}}_7 - \underbrace{\eta_N (\dot{m}_{CPS} v_{CPS}) v_{air}}_4 \end{aligned} \quad (4.217)$$

Total mass flow rate for the terms (2) and (6) and, equation (4.217) becomes

$$\dot{m}_{CPS} = \dot{m}_{air} + \dot{m}_{fuel} \quad (4.218)$$

$$\begin{aligned} Y = & \underbrace{\dot{m}_{CPS} \frac{v_{CPS}^2}{2}}_1 + \underbrace{\dot{m}_{CPS} \frac{v_{air}^2}{2}}_{2+6} - \underbrace{\dot{m}_{fuel} \frac{v_{fuel}^2}{2}}_3 + \underbrace{(\dot{m}_{fuel} v_{fuel}) v_{air}}_5 \\ & - \underbrace{\dot{m}_{air} \frac{v_{air}^2}{2}}_7 - \underbrace{\eta_N (\dot{m}_{CPS} v_{CPS}) v_{air}}_4 \end{aligned} \quad (4.219)$$

Let us subtract and add  $\dot{m}_{CPS} v_{CPS} v_{air}$  and call it the terms numbered (8) and (9)

$$\begin{aligned}
Y = & \left[ \underbrace{\dot{m}_{CPS} \frac{v_{CPS}^2}{2}}_1 - \underbrace{\dot{m}_{CPS} v_{CPS} v_{air}}_8 + \underbrace{\dot{m}_{CPS} \frac{v_{air}^2}{2}}_{2+6} \right] \\
& - \left[ \underbrace{\dot{m}_{fuel} \frac{v_{fuel}^2}{2}}_3 - \underbrace{(\dot{m}_{fuel} v_{fuel}) v_{air}}_5 + \underbrace{\dot{m}_{air} \frac{v_{air}^2}{2}}_6 \right] \\
& + \underbrace{\dot{m}_{CPS} v_{CPS} v_{air}}_9 - \underbrace{\eta_N (\dot{m}_{CPS} v_{CPS}) v_{air}}_4
\end{aligned} \tag{4.220}$$

Then, the term  $Y$  becomes

$$\begin{aligned}
Y = & \underbrace{\dot{m}_{CPS} \frac{(v_{CPS} - v_{air})^2}{2}}_{1+2+8+6} - \underbrace{\dot{m}_{fuel} \frac{(v_{fuel} - v_{air})^2}{2}}_{3+5+7} \\
& + \underbrace{(1 - \eta_N) \dot{m}_{CPS} v_{CPS} v_{air}}_{9+4}
\end{aligned} \tag{4.221}$$

Substituting equation (4.221) into (4.215)

$$\begin{aligned}
\Delta \dot{E}_{k,loss} = & \dot{m}_{CPS} \frac{(v_{CPS} - v_{air})^2}{2} - \dot{m}_{fuel} \frac{(v_{fuel} - v_{air})^2}{2} + (1 \\
& - \eta_N) \dot{m}_{CPS} v_{CPS} v_{air} - (P_{CPS} - P_{air}) A_{CPS} v_{air} \\
& + (P_{fuel} - P_{air}) A_{air} v_{air}
\end{aligned} \tag{4.222}$$

The resultant equation (4.222) is the same with equation (4.215) of  $\Delta \dot{E}_{k,loss}$  term, which proves the correctness of equation (4.213). Now, equation (4.208) can be rewritten as

$$\begin{aligned}
FHV \dot{m}_{fuel} + \dot{W}_{aux} \\
= & \underbrace{\dot{W}_p + \Delta \dot{E}_{k,loss}}_{\Delta \dot{E}_k} + \dot{Q}_{cooling} + (\dot{m} \Delta h)_{CPS} - (\dot{m} \Delta h)_{air} \\
& - (\dot{m} \Delta h)_{fuel}
\end{aligned} \tag{4.223}$$

Now, applying Scimitar engine station numbers 18 for CPs, 1 for air and 20 for fuel, and the assumptions of  $\dot{W}_{aux} = 0$  and  $\dot{Q}_{cooling} = 0$ , also substituting equations (4.203)-(4.205) in (4.208) results with

$$FHV \dot{m}_{20} = \Delta \dot{E}_k + (\dot{m} \Delta h)_{18} - (\dot{m} \Delta h)_1 - (\dot{m} \Delta h)_{20} \quad (4.224)$$

$$FHV \dot{m}_{20} = \Delta \dot{E}_k + \dot{m}_{18} (h_{18} - h_{CPS}^0) - \dot{m}_1 \left( \underbrace{h_1 - h_{air}^0}_{=0} \right) - \dot{m}_{20} (h_{20} - h_{fuel}^0) \quad (4.225)$$

Finally, the rate of global energy balance for the Scimitar engine at Mach 5.0 can be obtained as

$$FHV \dot{m}_{20} = \Delta \dot{E}_{k,loss} + \dot{W}_p + \dot{m}_{18} (h_{18} - c_{p,CPS}^0 T^0) - \dot{m}_{20} (h_{20} - c_{p,fuel}^0 T^0) \quad (4.226)$$

#### 4.4 Global Rate of Exergy Balance for the Scimitar Engine at Mach 5.0

In this section, derivation of the global rate of exergy balance for the Scimitar Engine is presented. As it is performed in the derivation of the global rate of energy balance As in section 4.3, the Scimitar engine as a whole is treated as a stream tube where the fuel hydrogen is combusted with oxygen in the entering air to produce thrust, thus propulsive power.

Substituting equation (4.197)-(4.199) to equation (4.196) and rearranging yields the global rate of energy balance as

$$\underbrace{\dot{Q}}_{-\dot{Q}_{cooling}} - \underbrace{\dot{W}}_{+\dot{W}_{aux}} + \sum (\dot{m}H)_{in} - \sum (\dot{m}H)_{out} + \sum \left( \dot{m} \frac{v^2}{2} \right)_{in} - \sum \left( \dot{m} \frac{v^2}{2} \right)_{out} = 0 \quad (4.227)$$

which can also be written as

$$\begin{aligned}
\dot{Q} - \dot{W} + \left[ \underbrace{\overbrace{(\dot{m}h_f^0)_{air} + (\dot{m}h_f^0)_{fuel}}^{in} - \overbrace{(\dot{m}h_f^0)_{CPS}}^{out}}_{FHV \dot{m}_{fuel}} \right] \\
+ \dot{m}_{air}(h_{air} - h_{air}^0) + \dot{m}_{fuel}(h_{fuel} - h_{fuel}^0) \\
- \dot{m}_{CPS}(h_{CPS} - h_{CPS}^0) \\
+ \left[ \underbrace{\dot{m}_{air} \frac{v_{air}^2}{2} + \dot{m}_{fuel} \frac{v_{fuel}^2}{2} - \dot{m}_{CPS} \frac{v_{CPS}^2}{2}}_{-\Delta\dot{E}_k = -\dot{W}_p - \Delta\dot{E}_{k,loss}} \right] = 0
\end{aligned} \tag{4.228}$$

or, it can be also written as

$$\begin{aligned}
-\dot{Q}_{cooling} + \dot{W}_{aux} + FHV \dot{m}_{fuel} + (\dot{m}\Delta h)_{air} + (\dot{m}\Delta h)_{fuel} \\
- (\dot{m}\Delta h)_{CPS} - \dot{W}_p - \Delta\dot{E}_{k,loss} = 0
\end{aligned} \tag{4.229}$$

A global rate of entropy balance between the system and its surroundings can be written as

$$\dot{S}_{gen} = \Delta\dot{S}_{system} + \Delta\dot{S}_{surr} \tag{4.230}$$

For a steady-flow system,  $\Delta\dot{S}_{system}$  is zero. Therefore,

$$\dot{S}_{gen} = 0 + \underbrace{\sum (\dot{m}s)_{out} - \sum (\dot{m}s)_{in}}_{\Delta\dot{S}_{surr}} + \frac{\dot{Q}_{surr}}{T_b} \tag{4.231}$$

Rearranging equation (4.231) by considering  $\dot{Q}_{surr} = -\dot{Q}$  and  $T_b = T_0 = T_{ref} = T_{air} = T_{air}^0 = T^0$  yields

$$\dot{Q} = -T^0 \left( \sum (\dot{m}s)_{in} - \sum (\dot{m}s)_{out} \right) - T^0 \dot{S}_{gen} \tag{4.232}$$

Substituting equation (4.232) in equation (4.228) yields





$$\begin{aligned}\bar{\psi}_k^{Ph} = \bar{\varepsilon}_k^{Ph} &= [\bar{h}_k(P, T) - \bar{h}_k(P^0, T^0)] - T^0[\bar{s}_k(P, T) - \bar{s}_k(P^0, T^0)] \\ &+ M_{w,k} \frac{v_k^2}{2} = \bar{\varepsilon}_k^{Ph,s} + \bar{\varepsilon}_k^{Kin}\end{aligned}\quad (4.237)$$

while  $\bar{s}_k$  is in J/kmol.K and the molecular weight  $M_{w,k}$  is in kg/kmol and considering  $P_0 = P_{ref} = P_{air} = P_{air}^0 = P^0$ . Stream exergy in compressible flows can also be written in J/kg, where  $s_k$  is in J/kg.K, as

$$\begin{aligned}\psi_k^{Ph} = \varepsilon_k^{Ph} &= [h_k(P, T) - h_k(P^0, T^0)] - T^0[s_k(P, T) - s_k(P^0, T^0)] \\ &+ \frac{v_k^2}{2} = \varepsilon_k^{Ph,s} + \varepsilon_k^{Kin}\end{aligned}\quad (4.238)$$

As it is seen in equations (4.237) and (4.238), *stream exergy in compressible flows*, is composed of static physical exergy and kinetic exergy terms.

Let us add and subtract  $\bar{s}_k^0$  to  $\bar{s}_k$  and  $s^0$  to  $s$  in order to yield

$$\bar{s}_k = \bar{s}_k + \bar{s}_k^0 - \bar{s}_k^0 = (\bar{s}_k - \bar{s}_k^0) + \bar{s}_k^0 \quad (4.239)$$

$$s_k = (s_k - s_k^0) + s_k^0 \quad (4.240)$$

where entropy at the reference conditions can be written as

$$\bar{s}_k^0 = \bar{s}_k(P^0, T^0) \quad (4.241)$$

$$s_k^0 = s_k(P^0, T^0) \quad (4.242)$$

Then, for each species, entropy terms can be written as

$$\begin{aligned}s_{air}(P, T) &= [s_{air}(P, T) - s_{air}(P^0, T^0)] + s_{air}(P^0, T^0) \\ &= \Delta s_{air} + s_{air}^0\end{aligned}\quad (4.243)$$

$$\begin{aligned}s_{fuel}(P, T) &= [s_{fuel}(P, T) - s_{fuel}(P^0, T^0)] + s_{fuel}(P^0, T^0) \\ &= \Delta s_{fuel} + s_{fuel}^0\end{aligned}\quad (4.244)$$

$$\begin{aligned}s_{CPS}(P, T) &= [s_{CPS}(P, T) - s_{CPS}(P^0, T^0)] + s_{CPS}(P^0, T^0) \\ &= \Delta s_{CPS} + s_{CPS}^0\end{aligned}\quad (4.245)$$

Substituting equations (4.243)-(4.245) in (4.233) yields

$$\begin{aligned}
& \dot{m}_{air} \left\{ (h_f^0 - T^0 s^0)_{air} \right. \\
& + \left[ \frac{h_{air}(P, T) - h_{air}(P^0, T^0) - T^0 (s_{air}(P, T) - s_{air}(P^0, T^0))}{\varepsilon_{air}^{Ph,s}} \right] \left. \right\} \\
& + \dot{m}_{fuel} \left\{ (h_f^0 - T^0 s^0)_{fuel} \right. \\
& + \left[ \frac{h_{fuel}(P, T) - h_{fuel}(P^0, T^0) - T^0 (s_{fuel}(P, T) - s_{fuel}(P^0, T^0))}{\varepsilon_{fuel}^{Ph,s}} \right] \left. \right\} \\
& - \dot{m}_{CPS} \left\{ (h_f^0 - T^0 s^0)_{CPS} \right. \\
& + \left[ \frac{h_{CPS}(P, T) - h_{CPS}(P^0, T^0) - T^0 (s_{CPS}(P, T) - s_{CPS}(P^0, T^0))}{\varepsilon_{CPS}^{Ph,s}} \right] \left. \right\} - \dot{W} \\
& + \left( \dot{m}_{air} \frac{v_{air}^2}{2} + \dot{m}_{fuel} \frac{v_{fuel}^2}{2} - \dot{m}_{CPS} \frac{v_{CPS}^2}{2} \right) - T_0 \dot{S}_{gen} = 0
\end{aligned} \tag{4.246}$$

Now, considering the definitions of all the chemical, static physical and kinetic exergy terms,  $\Delta \dot{E}_k$  term presented in equations (4.207) and (4.213) and neglecting the mechanical power term (i. e.,  $\dot{W} = -\dot{W}_{aux} = 0$ ), equation (4.246) can be rewritten as

$$\begin{aligned}
& \left[ \frac{\dot{m}_{air} (h_f^0 - T^0 s^0) + \dot{m}_{fuel} (h_f^0 - T^0 s^0) - \dot{m}_{CPS} (h_f^0 - T^0 s^0)}{\dot{m}_{fuel} \varepsilon_{fuel}^{Chem} = Ex_{fuel}^{Chem}} \right] \\
& + \left[ \sum_{in} \dot{m}_{in} \varepsilon_{in}^{Ph,s} - \sum_{out} \dot{m}_{out} \varepsilon_{out}^{Ph,s} \right] \underbrace{- \dot{W}_p - (\Delta \dot{E}_k)_{loss}}_{-\Delta \dot{E}_k} \\
& - T^0 \dot{S}_{gen} = 0
\end{aligned} \tag{4.247}$$

The first term in equation (4.247) is used in the calculations of the rate of exergy balance to obtain the rate of total exergy destroyed and in the performance parameters including exergy terms. Rewriting equation (4.246) by including the station numbers also results with the final form of the global rate of exergy balance as

$$\begin{aligned}
& \left[ \frac{\dot{m}_1 (h_{f,1}^0 - T^0 s_{air}^0) + \dot{m}_{20} (h_{f,20}^0 - T^0 s_{fuel}^0) - \dot{m}_{18} (h_{f,18}^0 - T^0 s_{Cps}^0)}{\dot{m}_{fuel} \varepsilon_{fuel}^{Chem} = \dot{Ex}_{fuel}^{Chem}} \right] \\
& + \dot{m}_1 \left[ (h_1 - h_{air}^0) - T^0 (s_1 - s_{air}^0) \right] \\
& + \dot{m}_{20} \left[ (h_{20} - h_{fuel}^0) - T^0 (s_{20} - s_{fuel}^0) \right] \\
& - \dot{m}_{18} \left[ (h_{18} - h_{Cps}^0) \right. \\
& \left. - T^0 (s_{18} - s_{Cps}^0) \right] \underbrace{- \dot{W}_p - (\Delta \dot{E}_k)_{loss}}_{-\Delta \dot{E}_k} - T^0 \dot{S}_{gen} = 0
\end{aligned} \tag{4.248}$$

In case there is no imbalance on the calculations,  $T^0 \dot{S}_{gen}$  is expected to be equal to the summation of the exergy destroyed in each component of the engine.

Additionally, an exergy balance for a component can be obtained from equation (4.246) as

$$\begin{aligned}
& \left[ \frac{\dot{m}_{air} (h_f^0 - T^0 s^0) + \dot{m}_{fuel} (h_f^0 - T^0 s^0) - \dot{m}_{Cps} (h_f^0 - T^0 s^0)}{\dot{m}_{fuel} \varepsilon_{fuel}^{Chem} = \dot{Ex}_{fuel}^{Chem}} \right] \\
& + \sum_{in} \dot{m}_{in} \left[ \frac{\left( h_{in}(P, T) + \frac{v_{in}^2}{2} - h_{in}^0(P^0, T^0) \right) - T^0 (s_{in}(P, T) - s_{in}^0(P^0, T^0))}{\varepsilon_{Ph}} \right] \\
& - \sum_{out} \dot{m}_{out} \left[ \frac{\left( h_{out}(P, T) + \frac{v_{out}^2}{2} - h_{out}^0(P^0, T^0) \right) - T^0 (s_{out}(P, T) - s_{out}^0(P^0, T^0))}{\varepsilon_{Ph}} \right] \\
& - \dot{W} - T^0 \dot{S}_{gen} = 0
\end{aligned} \tag{4.249}$$

where  $\dot{W}$  is the mechanical power input or output for the component. Equation (4.249) can also be written by the aid of stagnation enthalpies as

$$\begin{aligned}
& \left[ \frac{\dot{m}_{air} (h_f^0 - T^0 s^0) + \dot{m}_{fuel} (h_f^0 - T^0 s^0) - \dot{m}_{CPS} (h_f^0 - T^0 s^0)}{\dot{m}_{fuel} \varepsilon_{fuel}^{Chem} = Ex_{fuel}^{Chem}} \right] \\
& + \sum_{in} \dot{m}_{in} \left[ \frac{(h_{0in}(P, T) - h_{in}^0) - T^0 (s_{in}(P, T) - s_{in}^0(P^0, T^0))}{\varepsilon^{Ph}} \right] \\
& - \sum_{out} \dot{m}_{out} \left[ \frac{(h_{0out}(P, T) - h_{out}^0) - T^0 (s_{out}(P, T) - s_{out}^0(P^0, T^0))}{\varepsilon^{Ph}} \right] \\
& - \dot{W} - T^0 \dot{S}_{gen} = 0
\end{aligned} \tag{4.250}$$

## 4.5 Performance Parameters

In order to understand and evaluate the performance of the Scimitar engine at Mach 5.0, some performance parameters should be used. Some important performance parameters obtained from the literature and derived in the thesis are presented in the following subsections.

### 4.5.1 Uninstalled thrust ( $F_u$ )

Uninstalled thrust is used in core textbooks and studies such as (Mattingly, 2006; Fernandez-Villace and Paniagua, 2013a; Fernandez-Villace and Paniagua, 2013b).

Propulsion system with nacelle and engine is illustrated in Figure 4.9.

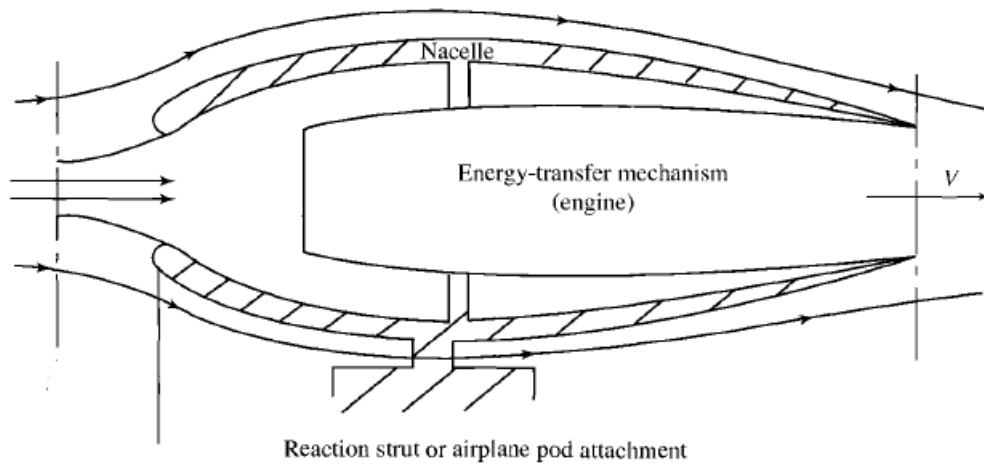


**Figure 4.9 :** Propulsion system with nacelle and engine (Modified from Mattingly, 2006).

A propulsion system is consisted of two parts namely: nacelle and engine. Different aircraft systems may be using the same engine with different nacelles. Due to this two thrust types are defined. Installed and uninstalled thrust. Uninstalled thrust neglects the effect of nacelle and focuses on the engine part of the propulsion system which increases the kinetic energy of the flow entering the engine (Mattingly, 2006).

Uninstalled thrust is given in newtons ( $N$ ) as

$$F_u = (\dot{m}_{in} + \dot{m}_{fuel})v_{exit} - \dot{m}_{in}v_{in} + (P_{exit} - P_{in})A_{exit} \quad (4.251)$$

Applying Scimitar engine station numbers 18 for CPs, 1 for air and 20 for fuel in equation (4.210) results with the uninstalled thrust is derived in newtons ( $N$ ) as

$$F_u = \eta_N(\dot{m}_{18}v_{18}) - (\dot{m}_1v_1) - (\dot{m}_{20}v_{20}) + (P_{18} - P_1)A_{18} - (P_{20} - P_1)A_{20} \quad (4.252)$$

It is utilized as a useful tool in this study as well, since equation (4.251) contains all the parameters that are evaluated in this study. Note that,  $v_{exit} = v_{aircraft}$  and  $A_{exit}$  is equal to the area of the C-D N at the engine exit.  $P_{in} = P_{atmosphere}$  at that flight altitude.

$$\frac{d(Momentum)}{dt} = Force \quad (4.253)$$

The first two terms on the right hand side of the equation (4.251) are momentum components in the rate form which are equal to the force, and the last term is the pressure thrust.

#### 4.5.2 Thrust specific fuel consumption ( $TSFC$ )

Thrust specific fuel consumption (TSFC) is an indicator of how economic an engine is. It is the rate of fuel consumed to generate a unit of thrust (Hünecke, 2003). It has units of  $kg/Ns$  or  $g/kNs$  and is defined as

$$TSFC = \frac{Amount\ of\ fuel\ consumed\ per\ unit\ time}{Thrust\ generated} = \frac{\dot{m}_{fuel}}{F_u} \quad (4.254)$$

Applying Scimitar engine station number 20 for fuel in equation (4.254) results with

$$TSFC = \frac{\dot{m}_{20}}{F_u} \quad (4.255)$$

#### 4.5.3 Specific thrust ( $F_s$ )

Specific thrust ( $F_s$ ) is an indicator of how well I air is used to create thrust. Engines with high air sucking capacity are bigger in size. Hence, specific thrust may be used as a parameter of how well an engine creates thrust when compared to its size (Hill and Peterson, 1992; Hünecke, 2003; Çolakoğlu, 2015). It is defined in Ns/kg as

$$F_s = \frac{\text{Amount of thrust created}}{\text{Total mass flow rate}} = \frac{F_u}{\dot{m}_{in} + \dot{m}_{fuel}} \quad (4.256)$$

Applying Scimitar engine station numbers 1 for entering air and 20 for fuel in equation (4.256) results with

$$F_s = \frac{F_u}{\dot{m}_1 + \dot{m}_{20}} \quad (4.257)$$

#### 4.5.4 Propulsive power

Propulsive power is the multiplication of thrust by aircraft velocity (Hill and Peterson, 1992). It has a unit of  $W$  (watts) and can be defined as

$$\dot{W}_p = F_u v_{air} \quad (4.258)$$

Applying Scimitar engine station number 1 for entering air in equation (4.211) results with

$$\dot{W}_p = F_u v_1 \quad (4.259)$$

#### 4.5.5 Net production of propellant kinetic power and the kinetic power loss

Applying Scimitar engine station numbers in equation (4.207) results with the *rate of net production of propellant kinetic energy* or the *change in kinetic power* as

$$\Delta \dot{E}_k = \dot{m}_{18} \frac{v_{18}^2}{2} - \dot{m}_1 \frac{v_1^2}{2} - \dot{m}_{20} \frac{v_{20}^2}{2} \quad (4.260)$$

which is also equal to

$$\Delta \dot{E}_k = \dot{W}_p + \Delta \dot{E}_{k,loss} \quad (4.261)$$

while kinetic power loss is obtained by applying Scimitar engine station numbers in equation (4.222) as

$$\begin{aligned} \Delta \dot{E}_{k,loss} = & \dot{m}_{18} \frac{(v_{18} - v_1)^2}{2} - \dot{m}_{20} \frac{(v_{20} - v_1)^2}{2} + (1 - \eta_N) \dot{m}_{18} v_{18} v_1 \\ & - (P_{18} - P_1) A_{18} v_1 + (P_{20} - P_1) A_1 v_1 \end{aligned} \quad (4.262)$$

#### 4.5.6 Propulsive efficiency ( $\eta_p$ )

Propulsive efficiency is defined as the *ratio of propulsive power to the rate of net production of propellant kinetic power* by (Hill and Peterson, 1992). It is given as

$$\eta_p = \frac{\text{Propulsive power}}{\text{Propellant kinetic power}} \quad (4.263)$$

$$\eta_p = \frac{\dot{W}_p}{(\dot{m}_{in} + \dot{m}_{fuel}) \frac{v_{exit}^2}{2} - \dot{m}_{in} \frac{v_{in}^2}{2}} \quad (4.264)$$

Rearranging equation (4.264) yields

$$\eta_p = \frac{\dot{W}_p}{\dot{m}_{in} \left[ \left( 1 + \frac{\dot{m}_{fuel}}{\dot{m}_{in}} \right) \frac{v_{exit}^2}{2} - \frac{v_{in}^2}{2} \right]} \quad (4.265)$$

and defining the afr as

$$f = \frac{\dot{m}_{fuel}}{\dot{m}_{in}} \quad (4.266)$$

results with

$$\eta_p = \frac{\dot{W}_p}{\dot{m}_{in} \left[ (1 + f) \frac{v_{exit}^2}{2} - \frac{v_{in}^2}{2} \right]} \quad (4.267)$$



Applying Scimitar engine station numbers 18 for CPs, 1 for air and 20 for fuel in equations (4.263), (4.266) and (4.267) result, respectively, with

$$\eta_P = \frac{\text{Propulsive power}}{\text{Kinetic power}} = \frac{\dot{W}_p}{\Delta\dot{E}_k} = \frac{F_u v_{air}}{\Delta\dot{E}_k} = \frac{F_u v_1}{\Delta\dot{E}_k}$$

$$= \frac{\dot{W}_p}{\dot{m}_{18} \frac{v_{18}^2}{2} - \dot{m}_1 \frac{v_1^2}{2} - \dot{m}_{20} \frac{v_{20}^2}{2}} \approx \frac{\dot{W}_p}{\dot{m}_{18} \frac{v_{18}^2}{2} - \dot{m}_1 \frac{v_1^2}{2}} \quad (4.268)$$

$$f = \frac{\dot{m}_{20}}{\dot{m}_1} \quad (4.269)$$

$$\eta_P = \frac{\dot{W}_p}{\dot{m}_1 \left[ (1+f) \frac{v_{18}^2}{2} - \frac{v_1^2}{2} \right]} \quad (4.270)$$

#### 4.5.7 Thermal efficiency ( $\eta_{th}$ )

Since propulsion engines are heat engines, thermal efficiency ( $\eta_{th}$ ) is an important parameter when examining their performance. It may be defined as the *rate of kinetic energy gain of air per unit fuel power consumed* (Hill and Peterson, 1992). By the aid of equation (4.265), it can be written as

$$\eta_{th} = \frac{\text{Propellant kinetic power}}{\dot{m}_{fuel} FHV} = \frac{\dot{m}_{in} \left[ (1+f) \frac{v_{exit}^2}{2} - \frac{v_{in}^2}{2} \right]}{\dot{m}_{fuel} FHV} \quad (4.271)$$

Now, defining the thermal efficiency as the *ratio of conversion of thermal power obtained from the combustion of the fuel and auxiliary power to kinetic power to that energy* and neglecting the auxiliary power in the model used in the thesis, thermal efficiency becomes

$$\eta_{th} = \frac{\text{Kinetic power}}{\text{Thermal power} + \text{Auxiliary power}} = \frac{\Delta\dot{E}_k}{FHV \dot{m}_{fuel} + \dot{W}_{aux}}$$

$$\approx \frac{\Delta\dot{E}_k}{FHV \dot{m}_{20}} \quad (4.272)$$

where  $FHV$  is obtained from the formation enthalpy  $\bar{h}_f^0$  difference of the products and the reactants at the reference temperature.

#### 4.5.8 Overall efficiency ( $\eta_o$ )

Overall efficiency is the multiplication of propulsive efficiency ( $\eta_P$ ) and thermal efficiency ( $\eta_{th}$ ) (Hill and Peterson, 1992; El-Sayed, 2008). Hence, it becomes

$$\eta_o = \eta_P \eta_{th} \quad (4.273)$$

Substituting the equations (4.270) and (4.271) in equation (4.273) results with

$$\eta_o = \frac{\dot{W}_p}{\dot{m}_{fuel} FHV} \quad (4.274)$$

Now, defining the overall efficiency ( $\eta_o$ ) as *the conversion ratio of thermal power and auxiliary power to the propulsive power* and neglecting the auxiliary power in the model of the thesis, it is obtained as

$$\begin{aligned} \eta_o &= \frac{\text{Propulsive power}}{\text{Thermal and auxiliary power}} = \frac{\dot{W}_p}{\dot{m}_{20} FHV + \dot{W}_{aux}} \\ &\approx \frac{\dot{W}_p}{\dot{m}_{20} FHV} \end{aligned} \quad (4.275)$$

#### 4.5.9 Coefficient of ecological performance (CEP)

Coefficient of ecological performance for propulsion engines is defined and used by Tanbay et. al, (2015). It is an indicator of the amount of propulsive power generated per total destroyed exergy rate in the engine.

$$CEP = \frac{\text{Propulsive power}}{\text{Rate of exergy destruction}} = \frac{\dot{W}_p}{\dot{E}x_{dest}} \quad (4.276)$$

#### 4.5.10 Exergetic sustainability index ( $\Theta_{exs}$ )

Exergetic sustainability index is introduced by (Aydm et. al, 2013). It is given as

$$\theta_{exs} = \frac{\text{Propulsive power}}{\text{Rate of exergy destruction} + \text{Kinetic power lost}} \quad (4.277)$$

$$= \frac{\dot{W}_p}{\dot{E}x_{dest} + \Delta\dot{E}_{k,loss}}$$

Exergetic sustainability index shows the ratio of the propulsive power generated per lost kinetic power and rate of exergy destruction.

#### 4.5.11 Exergy destruction factor ( $f_{exd}$ )

Exergy destruction factor is the ratio of the total exergy destruction to total exergy input to the engine and it is proposed by (Aydin et. al, 2013). Exergy destruction factor is given as

$$f_{exd} = \frac{\text{Rate of exergy destruction}}{\text{Chemical exergy supplied} + \text{Kinetic exergy at the inlet}} \quad (4.278)$$

$$= \frac{\dot{E}x_{dest}}{\dot{E}x_{fuel}^{Chem} + \dot{E}x_1}$$

#### 4.5.12 Exergy efficiency ( $\eta_{ex}$ )

Exergetic efficiency is first defined by a different name as *rational efficiency* by Clarke and Harlock (1975). The term exergetic efficiency is used by Etele and Rosen (2001) and it is defined as

$$\eta_{ex} = \frac{\text{Propulsive power}}{\text{Rate of exergy input by the combustion of fuel}} \quad (4.279)$$

$$= \frac{\dot{W}_p}{\dot{E}x_{fuel}^{Chem}}$$

This is an overall efficiency in terms of the second law of thermodynamics.



## 5. RESULTS AND DISCUSSIONS

There are many studies concentrated on the energy and exergy analysis of the turbofan and turbojet engines, however, a small amount of the Scimitar engine since it is still under designing phase. The papers regarding the Scimitar engine are the studies made by the inventors or by other researchers performed by means of computer simulations.

On the other hand, this thesis study concentrates on providing the derivations of the thermodynamic relations of the engine subcomponents obviously with the help of core textbooks about thermodynamics, gas turbines, airbreathing hypersonic flight and a few papers published about Scimitar engine.

In this chapter, data obtained from literature, results of the thesis and some discussions on the results of the analysis are presented.

### 5.1 Data Obtained from Literature for the Thesis

In this study, some values from literature are obtained and used in the analysis. Table 5.1 lists all the information taken from open literature. Differential-pressure-change based irreversibility correction factor, defined in Equation (4.39), (given as isentropic efficiencies by Fernandez-Villace and Paniagua (2013a)) of C1-C5 are shown with only one of them,  $e_{C1}$ , and for C6-C8,  $e_{C6}$ , in Table 5.1.

Polytropic efficiencies (i.e., correction factors as mentioned above in the thesis) of the turbomachinery, temperatures except for  $T_1$  and  $T_{20}$ , hydrogen line pressures of  $P_{20}$ ,  $P_{21}$ ,  $P_{22}$ ,  $P_{23}$ , mass flow rate of air and fuel, and kinetic efficiency ( $\eta_{KE}$ ) presented in Table 5.1 are obtained from EcosimPro simulation study (Fernandez-Villace and Paniagua, 2013a).

$T_1$ ,  $P_1$  are calculated with the help of the tables from (Table A.2 in Mattingly, 2006).

$T_{05}$  and  $T_{38}$  are not listed in Table 5.1, however as described in the previous chapters, they are obtained from (Jivraj et. al, 2007). Nozzle efficiency,  $\eta_N$ , and cross sectional area  $A_{exit}$  (or  $A_{18}$ ) are taken from (Marini et. al, 2013).

## 5.2 Results of the Thesis

Results of this study can be summarized as follows:

Mass flow rates, temperatures, pressures and total energy flow rates of air and CPs (for the points 09-18) are presented in Table 5.2.

Hydrogen and helium properties are presented for each station in Table 5.3.

The results of the rate of global energy balance for the Scimitar engine at Mach 5.0 is presented as follows:

$$FHV \dot{m}_{20} = \Delta \dot{E}_{k,loss} + \dot{W}_p + \dot{m}_{18} \left( \frac{c_{p,18} T_{18}}{h_{18}} - c_{p,CPs}^0 T^0 \right) - \dot{m}_{20} (h_{20} - c_{p,fuel}^0 T^0) \quad (4.226)$$

$$\begin{aligned} & \left( 119597 \frac{kJ}{kg} \right) \times \left( 4.05 \frac{kg}{s} \right) \\ &= (84578.3 kW) + (228284.3 kW) + \left( 176.65 \frac{kg}{s} \right) \\ & \times \left[ 1.45356 \frac{kJ}{kg \cdot K} \times 788 K - 265.486 \frac{kJ}{kg} \right] \\ & - \left( 4.05 \frac{kg}{s} \right) \times \left[ 13.034 \frac{kJ}{kg} - 2857.8 \frac{kJ}{kg} \right] \end{aligned} \quad (5.1)$$

$$484367.85 kW \approx 479922 kW \quad (5.2)$$

Hence, the relative percent error for the rate of global energy balance becomes

$$Error = \frac{|484367.85 - 479922|}{484367.85} \times 100 = \mathbf{0.92\%} \quad (5.3)$$

The total exergy destruction rate can be calculated from equation (4.248), which is the global rate of exergy balance equation, for the Scimitar Engine at Mach 5.0 as

$$\begin{aligned}
\dot{E}x_{fuel}^{Chem} + \dot{m}_1 [(h_1 - h_{air}^0) - T^0(s_1 - s_{air}^0)] \\
+ \dot{m}_{20} [(h_{20} - h_{fuel}^0) - T^0(s_{20} - s_{fuel}^0)] \\
- \dot{m}_{18} [(h_{18} - h_{CPS}^0) \\
- T^0(s_{18} - s_{CPS}^0)] \underbrace{- \dot{W}_p - (\Delta \dot{E}_k)_{loss}}_{-\Delta \dot{E}_k} - T^0 \dot{S}_{gen} = 0
\end{aligned} \tag{4.248}$$

Rearrangement yields

$$\begin{aligned}
\dot{E}x_{dest} &= T_1 \dot{S}_{gen} \\
&= \dot{E}x_{fuel}^{Chem} + \dot{m}_1 [(c_{p,avg} T_1 - h_{air}^0) - T_1(s_1 - s_{air}^0)] \\
&+ \dot{m}_{20} [(h_{20} - h_{fuel}^0) - T_1(s_{20} - s_{fuel}^0)] \\
&- \dot{m}_{18} [(h_{18} - h_{CPS}^0) - T_1(s_{18} - s_{CPS}^0)] - \dot{W}_p \\
&- \Delta \dot{E}_{k,loss}
\end{aligned} \tag{5.4}$$

Substituting the values in equation (5.4), the total exergy destruction rate becomes

$$\begin{aligned}
\dot{E}x_{dest} &= 473048.46 + 913.717 + 47082.02 - 911066.15 \\
&- 228284.3 - 84578.3 = \mathbf{117015.45 kW}
\end{aligned} \tag{5.5}$$

Finally, all the performance parameters calculated at Mach 5.0 flight conditions are presented in Table 5.4.

### 5.3 Discussions

Results of the analysis performed in the thesis are discussed as follows:

The engine uses an **intake I** with variable cross-sectional area that can operate both at subsonic and supersonic speeds. At Mach 5.0 configuration, the stagnation pressure of the freestream at the inlet of I is  $P_{01} = 1333 \text{ kPa}$  while the static pressure of the freestream is  $P_1 = 2.4 \text{ kPa}$ . Calculation results show that the stagnation pressure at the exit of the I as  $P_{02} = 324 \text{ kPa}$ . Hence, only 24.3% of the total pressure is recovered at the exit of the I while static (actual) pressure is increased from  $P_1 = 2.4 \text{ kPa}$  as it is decelerated.

**Table 5.1** : Information gathered from open literature.

Mass Flow Rates ( $\text{kg s}^{-1}$ )	Value
$\dot{m}_1$	172.6
$\dot{m}_{20}$	4.05
Correction Factors	Value
$e_C$	0.86
$e_{C1}$	0.94
$e_{C6}$	0.90
$e_{T1}$	0.91
$e_{T2}$	0.89
$e_{T3}$	0.88
Temperatures (K)	Value
$T_1$	222
$T_{20}$	20
$T_{34}$	844
$T_{42}$	296
$T_{49}$	371
$T_{53}$	458
$T_{57}$	559
$T_{61}$	676
$T_{75}$	75
$T_{79}$	151
$T_{83}$	284
$T_{84}$	33
Pressures (kPa)	Value
$P_1$	2.4
$P_{20}$	1800
$P_{21}$	1780
$P_{22}$	1670
$P_{23}$	1410
$P_{38}$	19440
$P_{39}$	12960
$P_{69}$	5184
Area ( $\text{m}^2$ )	Value
$A_{exit}(A_{18})$	5.38
Kinetic efficiency	Value
$\eta_{KE}$	0.9
Isentropic efficiency	Value
$\eta_N$	0.97



**Table 5.2 :** Properties of the air side.

Station	Fluid	Mass Flow Rate (kg s <sup>-1</sup> )	$c_p$ (kJ kJ <sup>-1</sup> K <sup>-1</sup> )	$k$	Pressure (kPa)	Temperature (K)	Total Energy Flow Rate (kW)
1	<i>Air</i>	172.6	1.03122	1.38786	2.4	222	192473.39
02, 03	<i>Air</i>	172.6	1.03122	1.38786	324	1298.31	192473.39
04	<i>Air</i>	172.6	1.03942	-	307.8	851.44	114152.36
05	<i>Air</i>	172.6	1.03641	1.38517	292.41	635	74991.84
06	<i>Air</i>	172.6	1.03641	1.38517	1198.84	1002.1	140660.37
09	<i>CPs</i>	172.74	1.06775	-	1078.96	1072.3	158890.48
010, 016	<i>CPs</i>	172.74	1.06402	-	1025	1033.56	151081.94
017	<i>CPs</i>	176.65	1.45356	1.2924	922.51	2752.88	659963.73
18	<i>CPs</i>	176.65	1.45356	1.2924	2.57	788	659963.73

**Table 5.3 :** Properties of hydrogen and helium.

Station	Fluid	Mass Flow Rate (kg s <sup>-1</sup> )	Pressure (kPa)	Temperature (K)	Total Energy Flow Rate (kW)
19, 20	<i>H<sub>2</sub></i>	4.05	1800	20	-11521.3
21	<i>H<sub>2</sub></i>	4.05	1780	283	3499.73
22	<i>H<sub>2</sub></i>	4.05	1670	858	37416.74
23	<i>H<sub>2</sub></i>	4.05	1410	968.88	44074.61
24	<i>H<sub>2</sub></i>	0.14	1410	968.88	1523.56
25, 26	<i>H<sub>2</sub></i>	3.91	1410	968.88	42550.9
28	<i>He</i>	103.725	19440	838.27	331924.52
29	<i>He</i>	103.725	19440	983.69	410248.1
30	<i>He</i>	92.2	19440	983.69	364664.97
31	<i>He</i>	11.525	19440	983.69	45583.12
32, 33	<i>He</i>	11.525	19440	872.44	38925.4
34, 35	<i>He</i>	69.15	19440	844	233340.48
37	<i>He</i>	92.2	19440	983.69	364664.97
38	<i>He</i>	92.2	19440	1000	372473.5
39	<i>He</i>	92.2	12960	862.75	306764
40	<i>He</i>	57.625	12960	862.75	191727.51
41	<i>He</i>	11.525	12960	862.75	38345.5
42	<i>He</i>	11.525	12960	296	4428.51
43	<i>He</i>	11.525	19440	351.76	7765.45
44	<i>He</i>	11.525	19440	843.51	37194.1
45	<i>He</i>	46.1	12960	862.75	153382
46	<i>He</i>	34.575	12960	862.75	115036.5
47	<i>He</i>	23.05	12960	862.75	76691
48	<i>He</i>	11.525	12960	862.75	38345.5
49	<i>He</i>	11.525	12960	371	8916.86
50	<i>He</i>	11.525	19440	440.89	13099.4
51	<i>He</i>	11.525	19440	845.64	37321.6
52	<i>He</i>	11.525	12960	862.75	38345.5
53	<i>He</i>	11.525	12960	458	14123.4

**Table 5.3 : Properties of hydrogen and helium (continued)**

Station	Fluid	Mass Flow Rate (kg s <sup>-1</sup> )	Pressure (kPa)	Temperature (K)	Total Energy Flow Rate (kW)
54	He	11.525	19440	544.28	19286.8
55	He	11.525	19440	848.03	37464.6
56	He	11.525	12960	862.75	38345.5
57	He	11.525	12960	559	20167.7
58	He	11.525	19440	664.3	26469.3
59	He	11.525	19440	851.05	37645.3
60	He	11.525	12960	862.75	38345.5
61	He	11.525	12960	676	27169.5
62	He	11.525	19440	803.3	34787.7
63	He	23.05	19440	827.2	72436
64	He	34.575	19440	834.14	109900
65	He	46.1	19440	837	147218
66	He	57.625	19440	838.3	184411.5
67	He	34.575	12960	862.75	115036.5
68	He	23.05	12960	862.75	76691
69	He	23.05	5184	622.6	47947.6
70	He	11.525	12960	862.75	38345.5
71	He	11.525	5184	624.8	24105.5
72	He	34.575	5184	623.3	72047.1
73	He	23.05	5184	623.3	48031.4
74	He	11.525	5184	623.3	24015.7
75	He	11.525	5184	75	-8797.17
76	He	11.525	19440	135	-5206.49
77	He	11.525	19440	607.3	23058.2
78	He	11.525	5184	623.3	24015.7
79	He	11.525	5184	151	-4248.97
80	He	11.525	19440	271.76	2977.87
81	He	11.525	19440	611.1	23285.6
82	He	11.525	5184	623.3	24015.7
83	He	11.525	5184	284	3710.37
84	He	11.525	5184	33	-11310.7
85	He	11.525	19440	59.4	-9730.75
86	He	11.525	19440	607.7	23082.1
87	He	23.05	19440	607.5	46140.3
88	He	34.575	19440	608.7	69425.9
89	He	34.575	19440	826.82	108585.8

**Table 5.4** : Performance parameters.

Performance Parameter	Units	Value Calculated in this Study	Value Reported by Fernandez-Villace and Paniagua (2013a)-(2013b)
$F_u$	kN	153.292	152-153
TSFC	g kN s <sup>-1</sup>	26.42	-
$F_s$	N s kg <sup>-1</sup>	867.77	-
$\Delta \dot{E}_k$	kW	312962.6	-
$\Delta \dot{E}_{k,loss}$	kW	84578.3	-
$\dot{W}_p$	kW	228284.3	-
$\eta_p$	-	0.729	0.675
$\eta_{th}$	-	0.646	0.66-0.743
$\eta_o$	-	0.471	0.493-0.55
$\dot{S}_{gen}$	kW K <sup>-1</sup>	527.097	-
$\dot{E}x_{dest}$	kW	117015.45	-
CEP	-	1.951	-
$f_{exd}$	-	0.247	-
$\theta_{exs}$	-	1.132	-
$\eta_{ex}$	-	0.483	0.411

However, our knowledge of ramjets tells us that this is expected since air is decelerated while static pressure increases as a result of “ram effect”, also sufficient time is crucial for more efficient “combustion” in ramjets. The losses in the I is due to the friction and shock wave.  $\eta_{KE} = 0.9$  is a value mainly used for supersonic I. The I is modeled as adiabatic and therefore stagnation temperature of  $T_{01} = T_{02} = 1298.31 K$  is the same for both sides. The key feature in the derivation of TPRs across the I with respect to  $\eta_{KE}$  is the entropy change: the entropy change between freestream condition and the actual state, and the entropy change between freestream and the fictional “a” point that expands to freestream pressure from the actual is the same. During the total energy flow rate calculation through I, an average  $c_p$  and an average  $k$  values for air is used. Average value is obtained first by using the  $k$  value at  $T_1 = 222 K$ , finding the resulting  $T_{02}$  and considering the average of  $T_1$  and  $T_{02}$  in the following iteration steps and using the corresponding  $k$  value at the average temperature until the  $T_{02}$  result converge in less than 0.1 K difference.

**Precooler** enables the use of a C by cooling the incoming air before its entering the C after the I. The precooler is consisted of two segments that employ two different mass flow rates. Constant  $c_{p,He}$  was very useful in the thermodynamic analysis of the helium side. By using constant  $c_{p,He}$  assumption, the mass flow ratios of helium

stream across the cycle could be understood just by following the thermal capacity ratios. Although not exactly the same, thermal capacity ratios are determined as they are suggested in the literature. For example in **HX1**, thermal capacity ratio with respect to hydrogen on the air side is 3, it is given for the helium side as 9. Hence, one expects 3 K drop on the air side for every 1 K temperature increase in the helium side. Results show that air temperature drops from  $T_{03} = 1298.31\text{ K}$  to  $T_{04} = 851.44\text{ K}$  by 446.87 K whereas helium temperature increases from  $T_{28} = 838.27\text{ K}$  to  $T_{29} = 983.69\text{ K}$  by 145.42 K. Temperature difference ratio of hot side to the cold side is 3.073, hence it is nearly 3 times as it is recommended in the literature (Jivraj et al, 2007). It is calculated for **HX2** as 0.99, which is nearly 1 as it is recommended again.

Compressor pressure ratio, CPR, ( $r_c = P_{06}/P_{05}$ ) greatly affects the exit temperature of the C also affecting the power consumed in the **compressor C**. **Helium turbine T1**, however, is designed to operate at an optimum level of power output by keeping T1 entrance temperature at  $T_{38} = 1000\text{ K}$  and T1 exit temperature at  $T_{39} = 863\text{ K}$ . Power consumed by the C is calculated as 65.6 MW, and power produced by T1 is calculated as 65.7 MW. Hence, no mechanical efficiency of the spool is considered. During the compression process calculations, an average  $k$  value is used in isentropic relations, and an average  $c_p$  value is used for calculations of the total enthalpy of the air through the C. Hence, calculation procedure for the C is the same as for the I.

In this study, before adapting the method of combustion process at the adiabatic flame temperature and considering the air composition, the processes in the **preburner PB** and **combustion chamber CC** were modeled as heat transfer processes without combustion previously at the initial stages of the thesis study. The results of the current consideration of combustion modelling for the combustion processes are as follows:  $\dot{m}_{24} = 0.14\text{ kg/s}$  of hydrogen fuel is combusted in PB, increasing temperature of the CPs to  $T_{09} = 1072.3\text{ K}$ . Considering air as a mixture of nonreacting ideal gases of nitrogen and oxygen, and calculating total energy flow rates with respect to the reference temperature and pressure are very useful when combustion processes are considered in the calculations. In the combustion process, calculation includes a step where every formation enthalpies and the enthalpy changes from reference state to the actual states are calculated. This is taken into account when calculating the properties of air and CPs at the entry and exit of each

component throughout the propellant cycle as a mixture of nonreacting ideal gases. During the combustion process, water vapor is formed and chemical composition of the air and fuel change to the CPs. Since the water temperature in the CPs is greater than 373 K, lower heating value (LHV) is used as FHV=-241107.56 kJ/kmol at the reference temperature of  $T_{ref} = T_{air} = T_1 = T_{air}^0 = T^0 = 222 \text{ K}$  in the calculations (Url-2).

In the **C-D N**, CPs are expanded beginning from  $T_{017} = 2752.88 \text{ K}$  and  $P_{017} = 922.51 \text{ kPa}$ . As the first calculation step, since the mass flow rate is known, throat cross-sectional area in the C-D N is determined as  $A^* = 0.136103 \text{ m}^2$  with the help of equation (4.129) when  $Mach = 1$ . Since it is known that the exit area is  $A_{18} = 5.38 \text{ m}^2$ , their ratio is found as  $A_{18}/A^*=39.5$ . Area ratio function gives the Mach number at the exit for an isentropic expansion, which can be used to find the static pressure and the temperature at the exit. However, for C-D N an isentropic efficiency term is used, which affects the results. Exit velocity and temperature for isentropic expansion are  $v_{18s} = 2426.71 \text{ m/s}$  and  $T_{18s} = 727.06 \text{ K}$ . By using  $\eta_N = 0.97$ , the results become  $v_{18} = 2390 \text{ m/s}$  and  $T_{18} = 788 \text{ K}$ , respectively, which results with the exit Mach number  $M_{18} = 4.13$ . Chemical composition and molecular weight of the combustion gases are very important in the calculation of C-D N. Treating CPs as air may lead to significant errors since  $R_u/M$  is equal to the  $R$ , which is used in the speed of sound formula.  $R$  value of air is generally given as  $R = 0287 \text{ kJ/kgK}$ , however in this study, it is  $R = 0.328 \text{ kJ/kgK}$  when CPs are considered instead of air.

Helium regenerator heat exchangers **He-HX1 – He-HX7** have matched (the same) thermal capacities which makes heat exchange calculations very simple. **T2** that provides power to five Cs in **high-temperature regenerator (HTR)** produces 28.72 MW mechanical power where power demand by the compressors **C1-C5** is 26.57 MW which shows that T2-C1-C2-C3-C4-C5 spool can operate without power deficiency problem. **T3** that provides power to three Cs in **low-temperature regenerator (LTR)** produces 14.2 MW power and power demanded by the compressors **C6-C8** is 12.4 MW. Hence, the same comment is valid for T3-C6-C7-C8 spool.

Temperature  $T_{34}$  affects  $T_{28}$  and  $T_{32}$ , which in return affects the combustion and cooling rate in the PB and precooler, respectively. The He stream leaving the HX2 at  $T_{89}$  mixes with the He stream at  $T_{34} = T_{35}$  (for Scimitar at Mach 5) which changes  $T_{28}$ . On the other hand,  $T_{28}$  is directly related to the cooling in HX1 and heating of hydrogen fuel in HX5. Temperature of hydrogen fuel at the entry of PB affects the combustion process since its enthalpy at that temperature is accounted.

The main results can be presented when compared the results of the thesis with the results of Fernandez-Villace and Paniagua (2013b) as follows:

- There is a difference of 5.4% in the propulsive efficiency (it is given as 67.5% in their study and calculated as  $\eta_p=72.9\%$  in this thesis).
- Thermal efficiency is reported as varying between 66.6 – 74.3% in their study, and it is calculated as  $\eta_{th} = 64.6\%$  in this study.
- Overall efficiency is reported varying 49.3 – 55.0%, in their study, it is calculated as  $\eta_o = 47.1\%$  in this study.
- Uninstalled thrust is reported as around 152 – 153 *kN* by Fernandez-Villace and Paniagua (2013a) according to their simulation results, and it is calculated as 153.292 *kN* in this study.
- The energy balance is calculated with an error of 0.92% as it is presented in equations (5.1) and (5.2). The reason of this error is probably the compulsory usage of the average value of  $c_{p,air}^0$  at the isentropic relations to calculate the I exit temperature and pressure, however, the usage of  $c_{p,CPs}^0$  and  $c_{p,fuel}^0$  values at the reference temperature of  $T^0 = 222\text{ K}$  during the calculations of the rate of global energy balance.
- Exergetic efficiency is calculated as  $\eta_{ex}=0.483$  for the Scimitar engine. Fernandez-Villace and Paniagua (2013b) reports this value as 0.411. There is 7.2% difference between the calculated and compared values.
- Coefficient of ecological performance for propulsion engines for the Scimitar Engine is calculated as  $CEP=1.951$ . Çolakoğlu (2015) determines  $CEP$  value in the range of 0.6-2.0 for a twin-spool turbofan engine. The reason of variance is the variation in the design parameters such as compressor pressure

ratio, by-pass air ratio and turbine inlet temperature for a turbofan engine with different rates of heat leakage from the combustion chamber. When optimum value tables in Çolakoğlu (2015) are compared, *CEP* values of 1.81 and 1.66 can be observed for the maximum turbine inlet temperature of 1800 K. Therefore, *CEP* value determined in this thesis can be considered as a meaningful result that does not contradict with the *CEP* values for the twin-spool turbofan engine in the literature.

- Exergetic sustainability index, is found as  $\theta_{exs}=1.132$  for the Scimitar engine. Aydın et. al, (2013) reports this value in the range of 0.26-0.41 for a turboprop engine with different flight modes. There is a great difference between the compared values. However, Aydın et. al, (2013) uses the ratio of useful power (shaft power, mechanical power) to the summation of the exergy destruction rate and the lost kinetic power. In this study, useful work produced by the engine is considered as propulsive power.
- Exergy destruction factor is found as  $f_{exd}=0.247$  for the Scimitar engine. Çolakoğlu (2015) reports  $f_{exd}$  value in the range of 0.12-0.18 for a twin-spool turbofan engine and Aydın et. al, (2013) reports it in the range of 0.41-0.48 for a turboprop engine with different flight modes. Therefore, exergy destruction factor found in this thesis is within the values calculated for different jet engines in the literature.





## 6. CONCLUSIONS AND RECOMMENDATIONS

As concluding remarks, in this study, a thermodynamic analysis model has been developed in order to perform an energy and exergy based performance analysis of the Scimitar engine at Mach 5.0 cruise conditions with the help of fundamental thermodynamics and compressible flow knowledge.

Thermodynamic relations regarding the engine subcomponents on the air, helium and hydrogen cycles have been derived in detail in this model.

Also, this study obviously performs the calculations using the thermodynamic relations in the developed thermodynamic analysis model for the Scimitar engine at Mach 5.0 cruise conditions.

### 6.1 Conclusions of this Study

Not only the station mass flow rates, pressures and temperatures but also some performance parameters (uninstalled thrust ( $F_u$ ), specific thrust ( $F_s$ ), thrust specific fuel consumption (TSFC), also propulsive ( $\eta_p$ ), thermal ( $\eta_{th}$ ), overall ( $\eta_o$ ) and exergetic efficiencies ( $\eta_{ex}$ ), coefficient of ecological performance ( $CEP$ ), exergetic sustainability index ( $\theta_{exs}$ ) and exergy destruction factor ( $f_{exd}$ )) for the Scimitar Engine at Mach 5.0 cruise conditions are calculated in this study.

We can conclude from the thesis that

- (i) the performance of the Scimitar Engine at Mach 5.0 is very high in terms of the energetic performance indicators ( $F_u, \dot{W}_p, \eta_p, \eta_{th}$  and  $\eta_o$ ),
- (ii) the performance of the Scimitar Engine at Mach 5.0 is high enough in terms of the exergetic performance indicators ( $\eta_{ex}, CEP, \theta_{exs}$  and  $f_{exd}$ ),
- (iii) considering the results reported in the thesis are in satisfactorily agreement with the simulation results reported in the literature, this study can be accepted as an adequately accurate model.

## **6.2 Recommendations for future Studies**

Similar thermodynamic analysis models for the cruise at the other operating modes of the Scimitar engine (turbofan and ramjet + ATR modes) at the other speeds can be derived by the aid of the model developed in the thesis.

The take-off and landing stages of the cruise in the Scimitar engine can also be modeled in the future studies similarly.



## REFERENCES

- Anderson, J.D. Jr.** (2003). *Modern Compressible Flow With Historical Perspective*, 3<sup>rd</sup> ed. New York, NY: McGraw-Hill.
- Aydın, H., Turan, Ö., Karakoç, T.H. and Midilli, A.** (2013). Exergo-sustainability indicators of a turboprop aircraft for the phases of a flight. *Energy*, 58, 550-560.
- Clarke, J.M. and Harlock, J.H.** (1975). Availability and propulsion. *Journal of Mechanical Engineering Science*, 17 (4), 223-232.
- Cohen, H., Rogers, G.F.C. and Saravanamuttoo, H.I.H.** (1996). *Gas Turbine Theory*, 4<sup>th</sup> ed. Essex: Longman Group Limited.
- Colakoglu, M., Tanbay, T., Durmayaz, A. and Sogut, O.S.** (2014). Effect of Heat Leakage on the Performance of a Twin-Spool Turbofan Engine. In Canan Kandilli, (Ed.), *7<sup>th</sup> IEESE. Proceedings of the 7<sup>th</sup> International Ege Energy Symposium & Exhibition*, (pp. 477-500). Turkey: Usak University Green Economy Research and Application Centre, June 18-20.
- Colakoglu, M.** (2015). Effect of heat leakage on the performance of a twin-spool turbofan engine. *M.Sc. Thesis*, ITU Institute of Energy, Istanbul.
- Colakoglu, M., Tanbay, T., Durmayaz, A. and Sogut, O. S.** (2016). Effect of heat leakage on the performance of a twin-spool turbofan engine. *International Journal of Exergy*, 19 (2), 173-198.
- Cumpsty, N.** (2009). *A Simple Guide to the Aerodynamic and Thermodynamic Design and Performance of Jet Engines*, 2<sup>nd</sup> ed. Cambridge University Press, New York.
- Çengel, Y.A. and Boles, M.A.** (2005). *Thermodynamics: An Engineering Approach*, 5<sup>th</sup> ed. New York: McGraw-Hill.
- Dincer, I. and Rosen, M.A.** (2007). *Exergy: Energy, Environment and Sustainable Development*. Oxford: Elsevier.
- Durmayaz, A., Sogut, O. S., Sahin, B. and Yavuz, H.** (2004). Optimization of thermal system based on finite-time thermodynamics and thermoeconomics. *Progress in Energy and Combustion Science*, 30 (2), 175-217.
- Ehyaie, M. A., Anjiridezfuli, A. and Rosen, M.A.** (2013). Exergetic analysis of an aircraft turbojet engine with an afterburner. *Thermal Science*, 17 (4), 1181-1194.
- El-Sayed, A.F.** (2008). *Aircraft Propulsion and Gas Turbine Engines*. Florida: CRC Press.

- Etele, J. and Rosen, M. A.** (2001). Sensitivity of exergy efficiencies of aerospace engines to reference environment selection. *Exergy, an International Journal*, 1 (2), 91-99.
- Fernandez-Villace, V. and Paniagua, G.** (2011). Simulation of a Variable-Combine-Cycle Engine for Dual Subsonic and Supersonic Cruise. The 47<sup>th</sup> AIAA/ASME/SAE/ASEE Joint Propulsion Conference & Exhibit, San Diego, California: 31 July – 3 August.
- Fernandez-Villace, V. and Paniagua, G.** (2013a). Numerical Model of a Variable-Combined-Cycle Engine for Dual Subsonic and Supersonic Cruise. *Energies*, 6, 839-850 doi: 10.3390/en6020839.
- Fernandez-Villace, V. and Paniagua, G.** (2013b). On the exergetic effectiveness of combined-cycle engines for high speed propulsion. *Energy*, 51, 382-394.
- Heiser, W.H., Pratt, D.T., Daley, D.H. and Mehta, U.B.** (1994). *Hypersonic Airbreathing Propulsion*, 5<sup>th</sup> ed. American Institute of Aeronautics and Astronautics, Washington.
- Hill, P.G. and Peterson, C.R.** (1992). *Mechanics and Thermodynamics of Propulsion*, 2<sup>nd</sup> ed. Massachusetts: Addison Wesley Publishing Company.
- Hünecke, K.** (2003). *Jet Engines: Fundamentals of Theory, Design and Operation*, 6<sup>th</sup> ed. Iowa: Motorbooks International Publishers and Wholesalers.
- Jachimowski, C.J.** (1988). An analytical study of the hydrogen-air reaction mechanism with application to scramjet combustion. NASA Technical Paper, 2791, Hampton, Virginia
- Jivraj, F., Varvill, R., Bond, A. and Paniagua, G.** (2007). The Scimitar precooled Mach 5 engine, The 2<sup>nd</sup> European Conference for Aerospace Sciences, Brussels, Belgium: 1 – 6 July.
- Kotas, T.J.** (1995). *The Exergy Method of Thermal Plant Analysis*. Florida: Krieger Publishing Company.
- Marini, M., Smoraldi, A., Cutrone, L., Zanchetta, M. and Varvill, R.** (2013). Analysis of Lapcat A2 vehicle scimitar engine nozzle. *Italian Association of Aeronautics and Astronautics XXII Conference*, Napoli: 9–12 September.
- Mattingly, J.D.** (2006). *Elements of Propulsion: Gas Turbines and Rockets*, 2<sup>nd</sup> ed. Virginia: American Institute of Aeronautics and Astronautics.
- Mattingly, J.D., Heiser, W.H. and Pratt D.T.** (2002). *Aircraft Engine Design*, 2<sup>nd</sup> ed. Virginia: American Institute of Aeronautics and Astronautics.
- Najjar, Y.S.H. and Al-Sharif, S.F.** (2006). Thermodynamic optimization of the turbofan cycle. *Aircraft Engineering and Aerospace Technology*, 78 (6), 467-480.
- Oates, G.C.** (1998). *Aerothermodynamics of Gas Turbine and Rocket Propulsion*, 3<sup>rd</sup> ed. Virginia: American Institute of Aeronautics and Astronautics.

- Rosen, M. A. and Etele, J.** (2004). Aerospace systems and exergy analysis: applications and methodology development needs. *International Journal of Exergy*, 1 (4), 411-425.
- Szargut, J., Morris, D.R. and Steward, F.R.** (1988). *Exergy Analysis of Thermal, Chemical, and Metallurgical Processes*. New York: Hemisphere Publishing Co.
- Tanbay, T., Durmayaz, A. and Sogut, O.S.** (2015). Exergy-based ecological optimisation of a turbofan engine. *International Journal of Exergy*, 16 (3), 358-381.
- Turan, O** (2012). Exergetic effects of some design parameters on the small turbojet engine for unmanned air vehicle applications. *Energy*, 46, 51-61.
- Turan, O., Aydin, H., Karakoc, T.H. and Midilli, A.** (2014). Some exergetic measures of a JT8D turbofan engine. *Journal of Automation and Control Engineering*, 2 (2), 110-114.
- Turgut, E.T., Karakoc T.H. and Hepbasli A.** (2007). Exergetic analysis of an aircraft turbofan engine. *International Journal of Energy Research*, 31 (14), 1383–1397.
- Turgut, E.T., Karakoc T.H., Hepbasli A. and Rosen, M.A.** (2009). Exergy analysis of a turbofan aircraft engine. *International Journal of Exergy*, 6 (2), 181–199.
- Varvill, R. and Bond, A.** (2003). A comparison of propulsion concepts for SSTO reusable launches. *Journal of the British Interplanetary Society*, 56 (3), 108-117.
- Uca, M.B., Çolakoğlu, M. and Durmayaz, A.** (2016). Energy and Exergy-based Performance Analysis of the Scimitar Engine at Mach 5.0. In Fatih Onur Hocaoglu, (Ed.), *8<sup>th</sup> IEESE. Proceedings of the 8<sup>th</sup> International Ege Energy Symposium and Exhibition* (pp. 766-773), Afyon Kocatepe University, Electrical Engineering Department, Solar and Wind Research & Application Center, Turkey, May 11-13.
- Wark, K.** (1995). *Advanced Thermodynamics for Engineers*, McGraw-Hill.
- Webber, H., Bond, A., and Hemsell, M.** (2007). The sensitivity of precooled air-breathing engine performance to heat exchanger design parameters. *Journal of the British Interplanetary Society*, 60, 188-196.
- Url-1 <<http://www.webbook.nist.gov/chemistry/fluid>>, date retrieved 14.04.2017.
- Url-2 <<http://kinetics.nist.gov/janaf/html/H-064.html>>, date retrieved 16.03.2017.
- Url-3 <<http://kinetics.nist.gov/janaf/pdf/JANAF-FourthEd-1998-Oxygen.pdf>>, date retrieved 14.04.2017.
- Url-4 <<http://kinetics.nist.gov/janaf/pdf/JANAF-FourthEd-1998-Nitrogen.pdf>>, date retrieved 14.04.2017.
- Url-5 <<http://kinetics.nist.gov/janaf/pdf/JANAF-FourthEd-1998-Hydrogen.pdf>>, date retrieved 14.04.2017.



## CURRICULUM VITAE

**Name Surname** : Muhammed Bişar UCA

**Place and Date of Birth:** Iğdır / Türkiye - 02/01/1991

**E- Mail** : bisaruca@gmail.com



### EDUCATION:

**B. Sc.** : 2014, Izmir Institute of Technology  
Mechanical Engineering

**Erasmus Programme** : 2012, Jönköping University, Sweden  
during B.Sc. Education for Mechanical Engineering

### PROFESSIONAL EXPERIENCE AND REWARDS:

July-November 2016 B/S/H Bosch and Siemens Home Appliances Group,  
Functional Development Department, Research and  
Development Engineer (Part-Time)

July 2015 - July 2016 B/S/H Bosch and Siemens Home Appliances Group,  
Technology and Innovation Department, Research and  
Development Engineer (Part-Time)

June - August 2012 M.A.N. Truck & Bus Company, Production Line and  
Mechanical Workshop (Engineering Intern)

### PUBLICATIONS, PRESENTATIONS AND PATENTS ON THE THESIS:

▪ **Uca, M.B.**, Çolakoğlu, M. and Durmayaz, A. (2016). Energy and Exergy-based Performance Analysis of the Scimitar Engine at Mach 5.0. In Fatih Onur Hocaoglu, (Ed.), *8<sup>th</sup> IESE. Proceedings of the 8<sup>th</sup> International Ege Energy Symposium and Exhibition* (pp. 766-773), Afyon Kocatepe University, Electrical Engineering Department, Solar and Wind Research & Application Center, Turkey, May 11-13.